



TECHNISCHE
UNIVERSITÄT
WIEN

VIENNA
UNIVERSITY OF
TECHNOLOGY

DISSERTATION

Harmonic Load Pull Methods

ausgeführt zum Zwecke der Erlangung des akademischen Grades
eines Doktors der technischen Wissenschaften

eingereicht an der Technischen Universität Wien
Fakultät für Elektrotechnik und Informationstechnik

von

Dipl.-Ing. Holger Arthaber

Matrikelnummer: 9525414

Hubertusgasse 1

A-2452 Mannersdorf

geb. 15. September 1975 in Wien

Wien, im März 2004

.....

1. Begutachter
O.Univ.Prof. Dipl.-Ing. Dr. Gottfried
Magerl

2. Begutachter
Univ.Prof. Dr.-Ing.habil. Robert
Weigel

Kurzfassung

Die gegenwärtige Entwicklung von Mobilfunksystemen hat es sich zum Ziel gesetzt, immer höhere Datenraten zu erzielen und komplexere Dienste zu implementieren. War man beim GSM-System noch auf ein Modulationsverfahren bedacht, welches schaltungstechnisch einfach und mit hohem Wirkungsgrad umsetzbar ist, scheint dies heutzutage kein Thema mehr zu sein. Die von UMTS verwendete Modulation erfordert hohe Bandbreiten (5 MHz) und hat auch keine konstante Amplitude. Klassische Verstärkerkonzepte weisen hierfür einen sehr schlechten Wirkungsgrad auf.

Zur Erzielung einer hohen Effizienz wird daher oft auf Verstärkerkonzepte wie Klasse F zurückgegriffen werden. Diese Konzepte erhöhen den Wirkungsgrad durch eine gezielte Formung der dynamischen Lastkennlinie. Dies wird dadurch erreicht, dass die vom Transistor erzeugten Oberwellen von der äußeren Beschaltung definiert zurückreflektiert werden.

Die Entwicklung solcher Sendeverstärker kann auf unterschiedliche Arten erfolgen. Einerseits kann der Transistor detailliert vermessen und ein Großsignalmodell erstellt werden, welches das nichtlineare Verhalten so gut wie nur möglich wiedergibt. Dies ist mit den heute verfügbaren Transistormodellen jedoch nur mit eingeschränkter Genauigkeit möglich. Auch handelt es sich um ein sehr zeitaufwendiges Verfahren welches nur bedingt in der Industrie Einsatz findet.

Eine einfachere Möglichkeit stellt der Einsatz von harmonischen Load-Pull-Systemen dar. Diese Versuchsanordnungen messen das Bauteilverhalten unter realen Betriebsbedingungen. Anstelle von festen Abschlußimpedanzen wird der Transistor mit verstellbaren Lastwiderständen versehen. Hat man den optimalen Betriebspunkt mittels Variation der Impedanzen gefunden, so besteht die Aufgabe des Schaltungsdesigners nunmehr darin, äquivalente Terminierungen für den finalen Aufbau zu realisieren – eine verhältnismäßig einfache Aufgabe. Somit kann ein gesamtes Verstärkerdesign innerhalb weniger Tage erfolgen.

Betrachtet man kommerziell verfügbare Load-Pull-Systeme, so zeichnen sich diese über programmierbare Abschlußimpedanzen, Tuner genannt, aus. Somit kann eine Vielzahl von Grundwellenimpedanzen für eine automatische Messung eingestellt werden. Mittels harmonischer Load-Pull-Systeme kann zusätzlich Einfluss auf die Oberwellen ausgeübt werden; dies ermöglicht den Entwurf von harmonisch kontrollierten Verstärkern, wie z.B. von Klasse F Verstärkern. Erfolgt jedoch bei harmonischen Load-Pull-Anordnungen die Aufteilung der Frequenzen über ein Dreifrequenzfilter, einen Triplexer, so wird durch dessen Einfügedämpfung der Variationsbereich der Abschlussimpedanzen deutlich eingeschränkt. Diese Arbeit zeigt drei alternative Verfahren auf, welche auch realisiert wurden:

- *Passives, harmonisches Load-Pull mit resonantem harmonischen Tuner:* Um den realisierbaren Bereich von Lastimpedanzen zu vergrößern, muss bspw. auf den Triplexer verzichtet werden. Die Reflexion der Oberwellen wird dabei mit verschiebbaren Resonatoren auf einer TEM-Leitung realisiert. Dabei kann für die Oberwellen nur die Phase der Reflexion verändert werden, was genau den Anforderungen von Klasse F Verstärkern entspricht. Die Grundwelle wird dabei durch einen in Serie nachgeschalteten Grundwellentuner eingestellt. Solcherart realisierte Load-Pull-Systeme zeigen einen deutlich vergrößerten Einstellbereich für die Lastimpedanzen. Die so gewonnenen Messergebnisse liegen näher an der Realität, als jene, welche mit einem passiven Triplexersystem gewonnen werden können. Auch kann das Verhalten unter breitbandiger Anregung problemlos untersucht werden.
- *Aktives, harmonisches Load-Pull für Einton:* Zur Kompensation der Verluste des Triplexers kann die Reflexion durch eine aktive Last realisiert werden. Hierfür existieren zwei verschiedene Ansätze. Eine Möglichkeit ist es, die vom Transistor kommende Welle zu verstärken und mit angepasster Phase rückzuspeisen. Die Schwierigkeiten bei dieser sehr einfachen Realisierung sind oft Laufzeitprobleme, welche einen Einsatz für breitbandige Signale einschränken. Ein weiterer sehr kritischer Nachteil ist die mögliche Oszillation der aktiven Schaltung aufgrund einer möglichen Rückkopplung. Eine Abhilfe wird in dieser Arbeit dargestellt: Um die Schwingneigung zu unterdrücken, wird die rücklaufende Welle mittels eines zur Eingangsfrequenz synchronisierten Generators erzeugt. Durch den Wegfall der Rückkopplung wird eine unbedingte Stabilität der aktiven Last erzielt. Um einen entsprechenden Reflexionsfaktor einstellen zu können, muss anhand der Messung von vor- und rücklaufender Welle der Generator in Betrag und Phase nachgeregelt werden. Durch das aktive System können Verluste kompensiert werden und auch Reflexionsfaktoren > 1 , also aktive, realisiert werden.
Erfasst man die vor- und rücklaufenden Wellen im Zeitbereich, ist es möglich, die Strom- und Spannungsverläufe innerhalb des Transistors zu ermitteln und somit die dynamische Lastkennlinie darzustellen. Der Nachteil dieser Anordnung ist jedoch, dass die Anwendung auf unmodulierte Träger beschränkt ist.
- *Aktives, harmonisches Load-Pull für Breitbandsignale:* Um die Vorteile eines aktiven Systems auch für breitbandige Signale nutzen zu können, kann das Load-Pull-System aus dem vorigen Punkt angepasst werden. Anstelle der Sinusgeneratoren werden komplexwertig modulierbare Signalgeneratoren für alle Frequenzen eingesetzt. Diese werden mit den analytisch berechneten äquivalenten Basisbandsignalen moduliert. Zur Messung der Phasen- und Amplitudenverhältnisse werden die demodulierten Signale der Grund- und Oberwellen herangezogen.
Mithilfe dieses Aufbaus kann unbedingte Stabilität der aktiven Lasten garantiert werden. Auch können Breitbandsignale verwendet werden.

Mit den verschiedenen harmonischen Load-Pull Verfahren wurde ein Klasse F Verstärker mit einem GaAs pHEMT-Transistor untersucht. Es wird gezeigt, dass ein resonanter harmonischer Tuner mit einfachen Mitteln realisiert werden kann und gänzlich ohne Spezialteile auskommt. Auch wird deutlich, dass mit Standardgeräten eines HF-Labors ein aktives harmonisches Load-Pull-System aufgebaut werden kann. Mit dem

gezeigten System ist es weiters möglich, die dynamische Lastkennlinie im Transistor zu ermitteln.

Für die Verwendung von Breitbandsignalen in aktiven harmonischen Load-Pull-Systemen zeigte sich ein sehr hoher Messgerätebedarf. Auch waren die zu verarbeitenden Datenmengen über den Messgerätebus bereits so hoch, dass die Zykluszeiten stiegen und so die Regelung für die dritte Oberwelle auf Grund der vorhandenen Phasendrift nicht mehr bewerkstelligt werden konnte. Dennoch zeigt dieses Verfahren großes Potential auf: durch entsprechende HF-Komponenten können Quellen eingespart werden und auch eine perfekte Phasenstabilität erzielt werden. So kann eine stabile Regelung, auch für die dritte Oberwelle, erreicht werden.

Ein Vergleich der Messergebnisse der verschiedenen Systeme ist nur eingeschränkt möglich. Die Ursache dafür ist in den höheren Oberwellen des Transistors zu suchen, welche durch die üblichen harmonischen Load-Pull-Anordnungen nicht behandelt wurden, das Betriebsverhalten jedoch merklich beeinflussen. Setzt man hier Transistoren ein, welche eine der Zielanwendung angepasste Transitfrequenz aufweisen, sind hier bessere Übereinstimmungen zu erwarten.

Es kann erwartet werden, dass harmonische Load-Pull-Systeme zunehmend an Bedeutung gewinnen werden; sei es einerseits für die rasche Verstärkerentwicklung als auch für die Modellverifikation.

Abstract

The development of mobile communication systems currently aims at higher data rates to implement more complex services. Whereas GSM considered modulation schemes which can be simply implemented with high efficiency this does not seem to be a topic nowadays. The applied modulation of UMTS, for example, has a 5 MHz bandwidth and a varying envelope. This results in low efficiency if classic amplifier concepts are used.

To cope with this problem new concepts like class F are required. Such concepts increase efficiency by specifically forming the dynamic loadline. This can be achieved by reflecting the harmonic frequencies back to the transistor

The development of such class F amplifiers can be done in different ways. One possibility is the use of a large-signal model based on exact measurements. However, the reproduction of the transistor's nonlinear behavior is not perfect with the methods available at present. Developing suitable large-signal models is also a time-consuming task and, therefore, not often used in industry.

A much simpler way is the application of harmonic load-pull systems. Such setups allow to measure the behavior of the transistor under real operating conditions. Harmonic load-pull uses variable terminations for all frequencies to find the optimum loads. Realizing an amplifier based on load-pull results requires only the design of equivalent terminations. Thus an amplifier design can be finished within some days.

Commercially available load-pull systems feature programmable terminations, called tuners. This allows the use of many different fundamental impedances in an automated setup. By using harmonic load-pull systems it is further possible to control the terminations at the harmonic frequencies, allowing the design of class F amplifiers. If the necessary frequency splitting is done by a triplexer, a three-frequency filter, the tuning range is obviously reduced due to the losses of the triplexer. This thesis realizes three alternative methods which deal with this problem:

- *Passive harmonic load-pull with resonant tuner:* One solution for increasing the tuning range is to omit the lossy triplexer. The harmonic frequencies are reflected by resonators along a TEM-line. For the harmonic frequencies only the phase of the reflection can be varied – this is exactly what is required for class F designs. The fundamental matching is done by a standard tuner, connected in cascade. Harmonic load-pull systems of this kind show a larger tuning range at all frequencies. The gained measurement results are closer to real designs than those gained by passive triplexer setups. Furthermore, the system allows the application of broadband signals.
- *Active harmonic load-pull for single-tone:* By using active loads the insertion losses

of the triplexer can be compensated. Two approaches can be chosen. One idea is to amplify and phase-shift the wave coming from the transistor and then return it back to the device. This method cannot be used for broadband signals because of delay times of the active load. Also critical is the possible oscillation of the active circuit because of the introduced feedback. An improvement is shown within this thesis. By using synchronized RF sources to generate the reflected signal no feedback loops exist; the active load becomes unconditionally stable. For setting the reflection coefficient the sources are controlled in amplitude and phase by means of forward and backward travelling wave measurements. The active loads do not compensate losses only; reflection coefficients > 1 can be realized also.

If the measurement of the forward and backward travelling waves is done in time-domain it is also possible to calculate the intrinsic voltages and current. This allows to display the dynamic loadline. The disadvantage of this setup is its limitation to unmodulated signals.

- *Active harmonic load-pull for broadband signals:* To take advantage of the benefits of an active system for broadband signals the single-tone system can be adapted. Instead of using CW sources this setup requires baseband-modulatable generators. The modulation signals are analytically calculated and created by separate baseband-arbitrary-generators for each frequency. For the measurement and control of the reflection coefficients, the fundamental as well as the harmonic signals were demodulated.

This setup guarantees unconditional stability of the active loads and supports the use of broadband signals.

The different harmonic load-pull setups were used to investigate a class F amplifier based on a GaAs pHEMT. It will be shown that a resonant harmonic tuner can be realized by very simple means. It comes clear that such a system can be realized with standard equipment of an RF laboratory. Furthermore, it is possible to calculate the dynamic loadline inside the transistor.

For using broadband signals in active harmonic load-pull setups a high demand for measurement instruments turned out. The amount of data which needed to be transferred over the instrument bus was very high. Thus, the achievable cycle times were too long to allow a successful control of the third harmonic because of the existing phase-drifts. Nevertheless, this method shows high potential: by using dedicated RF components it is possible to reduce the number of required sources as well as to establish perfect phase stability. This would allow for a stable control of the third harmonic frequency.

A comparison of the different harmonic load-pull results is possible in a limited way only. The reason for this can be found in the unconsidered higher order harmonic frequencies. These are not treated by the different setups in the same way and influence the behavior significantly. Using transistors with a lower transit frequency would give a better matching.

It can be expected that harmonic load-pull systems will gain importance for rapid development of high efficiency amplifiers as well as for model verification.

Acknowledgment

This thesis was supported by some people and companies which I would like to thank explicitly.

Special thanks go to my supervisor Prof. Dr. Gottfried Magerl for his very exact and detailed review of this work. His quick response to questions and problems allowed me to finish this thesis within the initial time schedule.

I would like to thank my colleague Dr. Markus Mayer for his ideas and fruitful discussions on harmonic load pull. Thanks also go to Dipl.-Ing. Michael Gadringer for often showing me a way out when I was stuck in algorithms.

The realization of the automated tuner would have been much harder without a 3D field simulator. My thanks go to the Ansoft Corporation Germany, which supported this work with a free time limited license.

I also wish to thank Dr. Wolfgang Konrad of Siemens Austria for providing additional signal generators which were used for the active load pull system within this thesis. I am also thankful to the Austrian office of Rohde&Schwarz, which supported this work by providing a baseband generator for the measurements. Both companies' free instrument rental enabled the realization of the equipment-intensive setup for the broadband active load pull system.

I would also like to thank the Austrian Council for Research and Technology Development which helped financing much of the equipment used for this thesis.

Contents

1	Motivation	1
2	Class F Amplifiers	4
2.1	Achievable Efficiency and Output Power	6
2.2	The importance of input matching	9
2.3	The role of the extrinsics	9
2.4	Effect of non perfect short circuits and opens	9
2.5	Summary	10
3	Load-Pull Setups and Tuning Elements	11
3.1	Fundamental Load-Pull	12
3.1.1	Power Measurement Issues	13
3.1.2	Applicable Tuner Types	15
3.1.3	Summary	20
3.2	Harmonic Load-Pull	21
3.2.1	Applicable Tuner Types	23
3.3	Summary	25
3.4	Active Loads	26
3.5	Prematching, Active Prematching	27
3.6	Conclusion	28
4	Realization of a “Harmonic Tuner”	29
4.1	Required Impedances, VSWRs,	30
4.2	Selection of the Transmission Line Type	33
4.3	The Slabline	36
4.4	The Resonator	37
4.5	Prototype (Proof of Principle)	38
4.5.1	Construction of the Prototype	39
4.5.2	Findings of the Prototype	42
4.6	Final design (3D-Field-Simulator supported)	44
4.6.1	Selection of Connector Type	44
4.6.2	Coaxial to Slabline Transition	48
4.6.3	Slabline – Impedance	48
4.6.4	Slabline – Measurements	49
4.6.5	Slider with Resonating Stub	50
4.6.6	Handle	59

4.7	Performance of the Initial Design	60
4.8	Design Iteration / Tuner Modeling	64
4.9	Final Realization	67
4.10	Electromechanical System for Automation	68
4.11	Performance of the Harmonic Tuner	68
4.12	Summary	75
5	Realization of Harmonic Load-Pull Setups	76
5.1	Transistor used for Measurements	76
5.2	Test Fixture Considerations	77
5.3	TRL Calibration / Errorbox Extraction	80
5.4	Deembedding of the Transistor's Extrinsic Elements	84
5.4.1	Triplexer	85
5.5	Passive Harmonic Load Pull with Triplexer	90
5.5.1	System Setup	90
5.5.2	System Calibration	91
5.5.3	Achievable Tuning Range	93
5.5.4	Setting of Fundamental Match and Bias Point	95
5.5.5	Measurement Results	96
5.5.6	Summary	98
5.6	Passive Harmonic Load Pull with "Harmonic Tuners"	98
5.6.1	System setup	98
5.6.2	System calibration	99
5.6.3	Achievable Tuning Range	100
5.6.4	Measurement Results	101
5.6.5	Summary	103
5.7	Active Harmonic Load Pull (Open Loop, Single Tone)	103
5.7.1	Measurement Setup	104
5.7.2	Calculating the Intrinsic Waveforms	105
5.7.3	Amplitude and Phase Extraction	107
5.7.4	Phase Stability of Generators	108
5.7.5	System Calibration	110
5.7.6	Achievable Tuning Range	111
5.7.7	Control Algorithm	111
5.7.8	Measurement Results	112
5.7.9	Excursus: Time Domain Measurement Results for Inverted Class F	113
5.7.10	Summary	115
5.8	Active Harmonic Load Pull (Open Loop, Broadband)	117
5.8.1	System setup	117
5.8.2	Equivalent baseband signals for harmonic frequencies	118
5.8.3	Calculation of Reflection Coefficient	122
5.8.4	System calibration	124
5.8.5	Achievable Tuning Range	126
5.8.6	Control Algorithm	126
5.8.7	Measurement Results (Single-Tone)	127
5.8.8	Measurement Results (Broadband)	128

CONTENTS

iii

5.8.9 Summary	130
6 Summary	131
A Equipment Used	134

List of Figures

1.1	Transformation of different load-circles by extrinsic elements	2
1.2	Active load realization with a loop	2
1.3	Active load realization with second path	3
2.1	Performance of an amplifier depending on condcution angle	4
2.2	Ideal class F amplifier schematic	5
2.3	Waveforms of a class F amplifier using terminations at $2f_0$ and $3f_0$	5
2.4	Ideal class F voltage and current waveforms	6
2.5	Efficiency dependence on harmonic loads	10
3.1	Fundamental load-pull setup	12
3.2	Different ways to measure load-pull output power	13
3.3	Load-pull setup for calculation of losses	13
3.4	Dependence of losses on the the setting of an ideal tuner	14
3.5	Photos of typical slidescrew tuners	15
3.6	Photograph of a boxed automatic tuner	17
3.7	Photograph of a double slug tuner	18
3.8	Photos of typical stub-tuners	19
3.9	Tuning patterns of an electronic and mechanical tuner	20
3.10	Harmonic load-pull with triplexer	21
3.11	Harmonic load-pull with harmonic tuner	22
3.12	Photograph of a sliding-short	23
3.13	Photograph of manual harmonic tuners	24
3.14	Active load realization types	26
3.15	Active prematching	28
4.1	Figure: Relationship between $ \Gamma $, VSWR, Z_{\min} and Z_{\max}	31
4.2	Model of two lossless tuners connected in series	31
4.3	Realizable Impedance of two Tuners connected in series	32
4.4	Achievable tuning impedance of two tuners conneted in series	33
4.5	Different types of transmission lines	34
4.6	Slabline and troughline dimensons	36
4.7	Slabline impedance	37
4.8	Photograph of the partly assembled prototype	41
4.9	Photograph of the finally assembled prototype (without resonator)	41
4.10	Photograph of the prototype's inner conductor and slider	42

4.11	Photograph of the prototype's resonator mounted on slider	42
4.12	APC7-connector and 7mm airline	45
4.13	3D-Structure for coaxial to slabline transition simulation	46
4.14	Different Coaxial to Slabline Transitions, S-Parameters	47
4.15	Different Coaxial to Slabline Transitions, Loss	47
4.16	Coaxial to Slabline Transmission Dimensions	48
4.17	Worst case coaxial to slabline transition performance for $f = 0 \dots 15$ GHz .	49
4.18	Theoretical and real slabline impedance	49
4.19	Realization of slabline with with APC-7 connectors	50
4.20	Measured S-parameters of empty slabline with transitions to airline/APC-7	51
4.21	Slabline Slider Dimensions	51
4.22	Simulation geometry for slider analysis	51
4.23	Simulation results of slider analysis	52
4.24	Area for E-field simulation of slotted slider	52
4.25	E-field animation of slotted slider for $f = 15$ GHz	53
4.26	Slider with resonator, dimensions	54
4.27	Simulation geometry for resonator analysis	54
4.28	Field simulator results for slotted and solid slider with resonator	55
4.29	Thickness variation of the resonator	56
4.30	Thickness variation of the resonator (detail)	56
4.31	Length variation of the resonator	57
4.32	Slider with resonator including small gap, dimensions	58
4.33	Slider with resonator and small gap, simulation results	58
4.34	Slider with resonator and small gap, simulation results (detail)	58
4.35	Simulation geometry for handle analysis	60
4.36	Resonator with handle, simulation of different handle materials	61
4.37	Resonator with handle, simulation of losses of different materials	61
4.38	Resonator with slotted slider and Teflon handle	62
4.39	Slotted resonator with handle, comparison of measurement and simulation .	62
4.40	Simulation environment for overall performance estimation	63
4.41	Simulation results for overall performance estimation (based on measurements)	63
4.42	Electrical model of the slider	64
4.43	Electrical model of the slider with resonator	64
4.44	Model performance and optimized design	65
4.45	Photograph of the redesigned slider	66
4.46	Redesigned slider with handle, comparison of measurement and simulation .	66
4.47	Simulation results for overall performance estimation (redesigned slider) . .	66
4.48	Final realization of slabline to 7mm airline transition	67
4.49	Final realization of the slider with resonator and handle	68
4.50	Photograph of the realized harmonic tuner (front)	69
4.51	Photograph of the realized harmonic tuner (back)	69
4.52	Reflection coefficient $\Gamma_{\text{Port}2}$ dependency on slider position	70
4.53	Reflection coefficient $\Gamma_{\text{Port}2}$ dependency on slider position	72
4.54	Transmission coefficient S_{21, f_0} dependency on slider position	73
4.55	Measurement setup for checking reproducibility	73
4.56	Reproducibility test of harmonic tuner, phase error of $2f_0$ and $3f_0$	73

4.57	Reproducibility test of harmonic tuner, $\Delta\Gamma_{f_0}$	74
5.1	Available power gain of IAF 2.1 mm transistor	77
5.2	DC-IV plot of IAF 2.1 mm transistor	77
5.3	Transistor test fixture	78
5.4	Testfixture detail: bonded transistor	79
5.5	Connexion Rosenberger PCB testfixture	80
5.6	TRL calibration kit	81
5.7	Verification of TRL-errorboxes, transmission measurement	82
5.8	Verification of TRL-errorboxes, reflection measurement	83
5.9	Reference planes of the setup	83
5.10	Model of the IAF 2.1 mm pHEMT	84
5.11	Schematic used for calculating S-parameters of drain extrinsic model	85
5.12	Triplexer realizations	86
5.13	Triplexer based on directional filters, schematic	87
5.14	Photogrpah of the triplexer	88
5.15	Triplexer transmission measurement	89
5.16	Triplexer losses	89
5.17	Passive harmonic load pull with triplexer, block diagram	90
5.18	Passive harmonic load pull with triplexer, calibration	92
5.19	Passive harmonic load-pull, tuning range at triplexer input	93
5.20	Passive harmonic load pull, tuning range at fixture and intrinsic transistor	95
5.21	Results of fundamental load pull (intrinsic, at Γ_E reference plane)	96
5.22	Results of second harmonic load pull	97
5.23	Passive harmonic load pull with harmonic tuner, block diagram	98
5.24	Passive harmonic load pull with harmonic tuner, calibration	99
5.25	Passive harmonic load pull with harmonic tuner, tuning range	100
5.26	Singleton P_{OUT} and PAE dependence on harmonic phases	101
5.27	WCDMA P_{OUT} and PAE dependence on harmonic phases	102
5.28	WCDMA ACP1 and ACP2 dependence on harmonic phases	103
5.29	Active harmonic load-pull setup (singleton)	104
5.30	Signal flow-chart of active load-pull setup	106
5.31	Signal flow-chart two-port	107
5.32	Decomposition of measured signal into single frequencies	107
5.33	Test setup to measure phase drift of locked generators	109
5.34	Phase deviation of the generators over time	109
5.35	Measured phase drift within one and five seconds (PDF)	110
5.36	Active harmonic load-pull (singleton), calibration	110
5.37	Active harmonic load pull (singleton), tuning range	111
5.38	Singleton P_{OUT} and PAE dependence on harmonic phases	113
5.39	PAE and P_{out} dependence on harmonic phases	114
5.40	Intrinsic voltage magnitude dependence on harmonic phases	114
5.41	Intrinsic current magnitude dependence on harmonic phases	115
5.42	Comparison of measured and simulated intrinsic dynamic load line	116
5.43	Comparison of measured and simulated intrinsic voltage and current over time	116

5.44	Active harmonic load pull for broadband signals, block diagram	118
5.45	Required nonlinearity for baseband processing	119
5.46	Spectrum of a nonlinear distorted broadband-signal	121
5.47	Test setup for verification of equivalent baseband signals	122
5.48	Comparison of different Γ -estimators	123
5.49	Calibration of time delays	124
5.50	Active harmonic load pull for broadband signals, calibration	125
5.51	Active harmonic load pull (broadband), tuning range	126
5.52	Singleton P_{OUT} and PAE dependence on harmonic phases, $ \Gamma_{2f_0,3f_0} = 1$.	127
5.53	Singleton P_{OUT} and PAE dependence on harmonic phases, $ \Gamma_{2f_0,3f_0} < 1$.	128
5.54	Broadband P_{OUT} and PAE dependence on harmonic phases	129
5.55	Comparison of forward and backward waves of active load	130

List of Tables

2.1	Class F voltage and current ratios for maximum efficiency [1]	8
2.2	Reported performance of class F amplifiers	8
3.1	Performance of different slidecrew tuners	16
3.2	Performance of automatic slidecrew tuners	17
3.3	Performance of double slug tuners	18
4.1	Slabline geometries for typical impedances	36
4.2	Bulk conductivity of non-magnetic materials	39
4.3	Coaxial Line Geometries used for Transition Simulation	46
4.4	Simulated materials for mechanical handle	60
4.5	Required movement range for resonators	67
5.1	Taconnic CER-10 properties	78
5.2	Parameters of TRL-calibration kit for $f = 900 \text{ MHz} \dots 7 \text{ GHz}$ parameters	81
5.3	Parameters of IAF-2.1mm transistor model	85
5.4	Achievable Γ of passive load-pull system (at triplexer input)	94
5.5	Results of third harmonic load-pull	97
5.6	Achievable Γ of passive harmonic load-pull system with harmonic-tuner (at tuner input)	100
5.7	Achievable Γ of active singletone load-pull system (at coupler input)	112
5.8	Achievable Γ of active broadband load-pull system (at coupler input)	126
5.9	Result variation for different Γ -magnitudes	128

List of Abbreviations

ACP	Adjacent Channel Power
ACPR	Adjacent Channel Power Ratio
APC-7	Amphenol Precision Connector 7 mm
CW	Continous Wave
DC	Direct Current
DUT	Device Under Test
EM	Electro-Magnetic
FDD	Frequency Division Duplex
FEM	Finite Element Method
FET	Field Effect Transistor
GPIB	General Purpose Instrument Bus
HCA	Harmonic Controlled Amplifier
HEMT	High Electron Mobility Transistor
HFSS	High Frequency Structure Simulator
PCB	Printed Circuit Board
PDF	Propability Density Function
PLL	Phase Locked Loop
PTFE	Polytetrafluoroethylene (Teflon)
RF	Radio Frequency
SA	Spectrum Analyzer
SMA	Sub-Miniature Type A
SOLT	Short Open Load Thru
TDR	Time Domain Reflectometry
TEM	Transversal Electro-Magnetic
TRL	Thru Reflect Line
UMTS	Universal Mobile Telecommunications System
VNA	Vector Network Analyzer
VSWR	Voltage Standing Wave Ratio

List of Symbols

$A(t)$	amplitude of complex baseband signal
a_n	Taylor series coefficient
BW	bandwidth
$b_n(t)$	basis function of signal space
$\underline{b}(t)$	equivalent complex baseband signal
c_0	speed of light ($2.998 \cdot 10^6 \frac{m}{s}$)
D	distance between slabline's sidewalls
d	radius of slabline's center conductor
f	frequency
f_0	fundamental frequency, center frequency
k_n	amplitude of real basis function
\mathbf{k}_n	complex amplitude of basis function
$n(t)$	noise signal
P	power
R	geometry factor of slabline
$s(t)$	general time signal
Z	impedance
ϵ_0	free space permittivity ($8.854 \frac{pF}{m}$)
Γ	reflection coefficient
λ	wavelength
$\Phi(t)$	phase of complex baseband signal
μ_0	free space permeability ($1.256 \frac{\mu H}{m}$)

Chapter 1

Motivation

For the design of an RF transistor amplifier it is necessary to provide the correct impedance matching at its input and output. This is absolutely no problem when dealing with small signal amplifiers where the required matching can be gained from vector network analyzer (VNA) measurements. As soon as power levels increase, other design methods need to be chosen. Now it is the designer's intention to realize a specific loadline at the intrinsic transistor. The loadline-design gains importance when designing high efficiency amplifiers, like class F.

The required loads for such amplifiers can be found by two ways. One possibility is to generate a transistor model which allows to do the circuit design entirely by an RF simulation software. The development of the required nonlinear large-signal model is a time-consuming process. Also currently published models do not perfectly reflect the behavior of the amplifier. Especially the accuracy for predicting adjacent channel power ratios is often insufficient. To overcome these problems, load-pull setups can be used. These measurement systems enable the user to test a transistor under real operating conditions, allowing to find the optimum loads by trial and error. A transistor model is not required and, hence, design times are much shorter.

Load-pull systems allow to vary the impedance which is connected to the device under test. For the setting of the load manual, electro-mechanical and electronic systems exist on the market. A typical setup for a load pull system is depicted in figure 1.1 (bias tees and additionally required measurement equipment is not shown). Commercially available tuners are usually two-port devices whose amplitude transformation ratio as well as their phase shift can be varied. Therefore, the tuner is terminated with a $50\ \Omega$ impedance in order to realize a tuning range which is centered around the origin. The losses of the setup are symbolized by an extra element. Also shown in figure 1.1 is the transformation of the tuning range: Having a tuner with a reflection coefficient $|\Gamma| < 1$ and low losses could lead for example to an external tuning range as indicated by the solid line in the right hand side Smith Chart in figure 1.1. All realizable reflection coefficients lie inside the solid circle. If we analyze the reflection coefficient seen by the intrinsic transistor (left hand side Smith Chart in figure 1.1) it turns out that the tuning range is reduced. This happens due to the transformation of the extrinsic elements of the transistor and of the transformation of the testfixture as well. Hence, the intrinsic tuning range is always smaller than the one seen outside in the $50\ \Omega$ system. It is also shown by the dashed line in the Smith Charts of figure 1.1 that a small increase in the losses can result in a dramatically reduced intrinsic

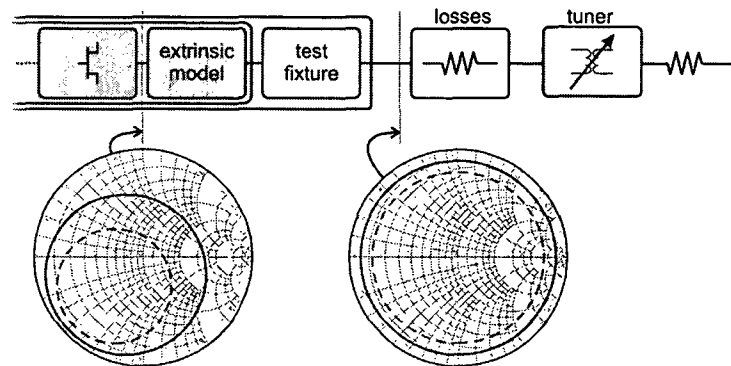


Figure 1.1: Transformation of different load-circles by extrinsic elements

tuning range.

A small tuning range becomes very critical when using harmonic load-pull setups for the design of highly efficient power amplifiers. Because the influence of the extrinsic elements increases at the harmonic frequencies of the amplifier, the tuning range becomes smaller and smaller with increasing frequency. A class F amplifier for example requires short circuits and opens at the harmonic frequencies – this cannot be realized because of the losses within the setup.

To overcome the problem of the insertion losses active systems can be used. Such systems simulate the behavior of a load by active elements. This makes reflection coefficients $|\Gamma| > 1$ possible in order to allow a perfect compensation of the losses. Hence, an ideal short circuit or open can be realized at the reference plane of the intrinsic transistor. An active load is typically realized by one of two types. Figure 1.2 shows a setup which uses a circulator to split the forward and backward travelling wave. Of course, a coupler can

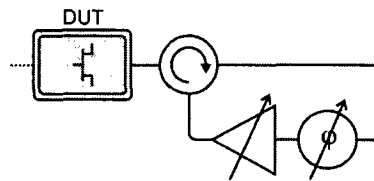


Figure 1.2: Active load realization with a loop

also be used instead of the circulator. This setup allows to use narrowband-modulated signals – it is not useful for broadband applications because of the delay times caused by the setup. A disadvantage of the system is its poor stability. Because of the fact that the circulator is not perfect a small portion of the loop amplifier's output signal is fed back into its input. Attention must be paid also on the out of band behavior of the circulator. Hence, filters are required – but this still does not guarantee the stability at the frequency of interest.

Another solution for an active load, which guarantees unconditional stability, is given by using a copy of the input signal to generate the backward travelling wave (figure 1.3).

For the application in harmonic load-pull systems frequency doublers and triplers are

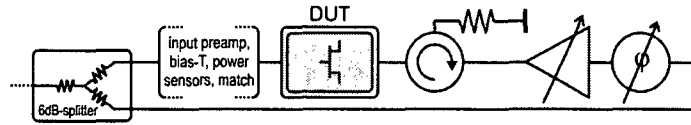


Figure 1.3: Active load realization with second path

needed in order to generate the required backward travelling waves. This limits the setup to the use of single-tone signals.

This thesis will show different ways to improve the performance of harmonic load-pull setups. Additionally it shall be tried how different systems can be compared to each other. A simple passive mechanical harmonic tuner will be investigated. Further it shall be shown that an active system can be set up by standard RF measurement equipment. Finally an extension of active systems to broadband signals will be discussed.

Chapter 2

Class F Amplifiers

To improve the efficiency of RF amplifiers new concepts were developed over time. The idea behind all these concepts is to 'pull' the dynamic loadline towards the axes to prevent regions of high losses. Increasing the efficiency of a standard class A or class B amplifier can be done for example by setting the bias point into the pinch-off region. The disadvantage of this class C amplifier is that an increased drive power is needed to get the transistor conductive. The more the transistor is driven into pinch-off the more the conduction angle (the relative turn-on-time during a cycle) is reduced. The effect onto drain efficiency, output power and gain is depicted in figure 2.1. It can be seen that the drain efficiency

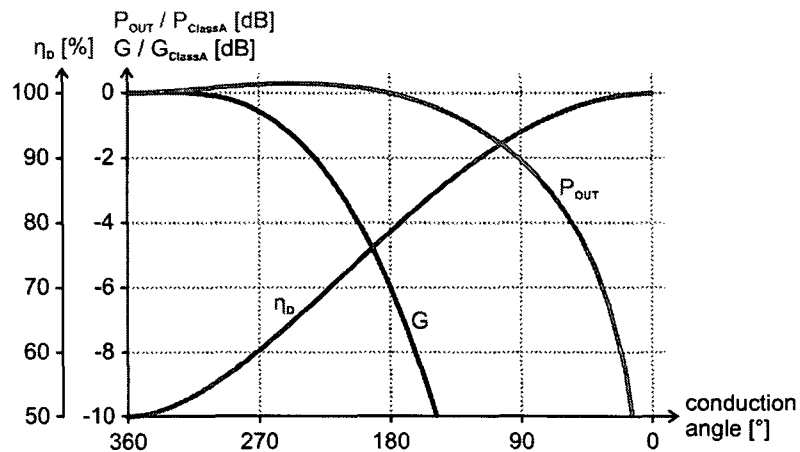


Figure 2.1: Performance of an amplifier depending on conduction angle

increases from 50% in class A (360° conduction angle) to 78.5% in class B (180° conduction angle) and up to 100% in class C (conduction angle = 0°...180°). Because the output power as well as the gain constantly decrease (until 0 at 0° conduction angle) a reasonable application is not given for extreme class C operation. Also linearity is a problem for class C operation as small input signals do not lead to an output signal. A more detailed description of these classic amplifier concepts can be found in [2, section 3.3] and [3, section 3.3 – 3.6].

A much better solution to improve efficiency is given by the class F amplifier [4]. This

amplifier operates in a class B bias condition but it is not restricted to an output network for the fundamental frequency only. The idea is to terminate the harmonic frequencies in such a way that the voltage and current waveforms become rectangularly and half-sinusoidally shaped. This requires an output matching as shown in figure 2.2. According to the Fourier decomposition of the desired signals it is necessary to short circuit all even harmonic frequencies and to leave all odd harmonics open (indicated by the impedances Z_E and Z_O in figure 2.2). However, the termination of all harmonic frequencies is neither

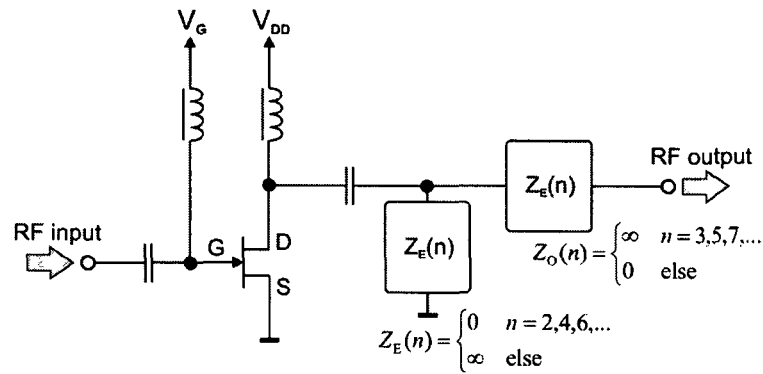


Figure 2.2: Ideal class F amplifier schematic

possible nor does the device provide enough gain at higher frequencies. The theoretical analysis (section 2.1) turns out that terminating the first three frequencies (fundamental + 2 harmonics) seem to be a good trade-off between complexity and realizable efficiency improvement. The resulting waveforms are depicted in figure 2.3. Having an unlimited number of harmonics would result in a perfectly L-shaped loadline. Figure 2.3 indicates

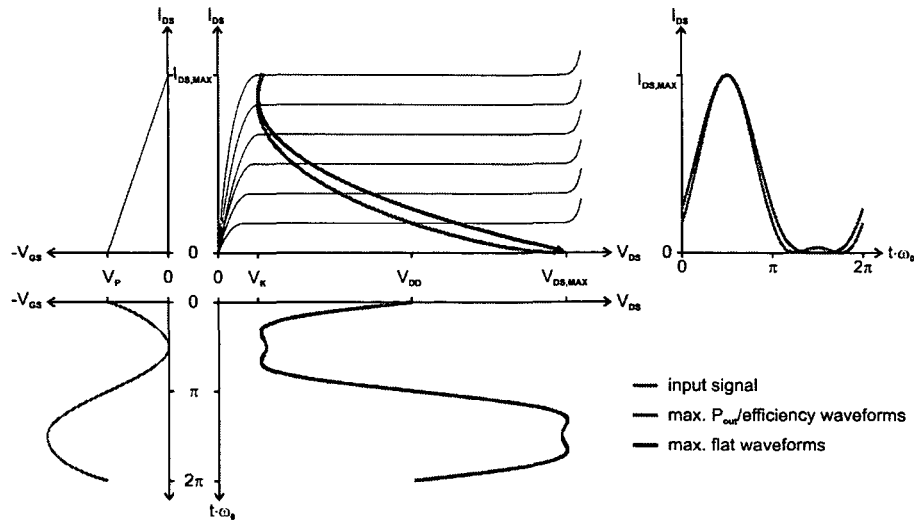


Figure 2.3: Waveforms of a class F amplifier using terminations at $2f_0$ and $3f_0$

two different waveform sets. The original idea [4] took use of maximally flat waveforms to fit the signal traces in the allowed voltage/current ranges. A more recent publication [1] shows that the maximum efficiency is reached for a less-flat waveform. For the class F amplifier the maximum efficiency goes along with the maximum output power [1].

By exchanging the even and odd order harmonic terminations it is also possible to realize an inverted class F amplifier. In this mode the current waveform becomes rectangularly shaped, the voltage signal is half-sinoidal.

For the theoretical analysis of both concepts a simplified FET model will be used (already shown in figure 2.3). This model represents an intrinsic transistor and does not take any extrinsic elements into account. Furthermore, the device is assumed to be perfectly linear which gives a constant transconductance g_m . For the analysis of the class F concept the maximum current $I_{DS,MAX}$ is assumed to be $I_{ds}(V_{gs} = 0 \text{ V})$. Of course, the gate voltage can also be slightly positive for a real FET – this is not taken into account here. V_P denotes the pinch-off voltage (the voltage, were $I_{ds}=0$). V_K defines the knee-voltage; from this drain voltage on the transistor acts like a current source. $V_{ds,max}$ is the maximum allowed voltage before forward breakdown occurs. Here, the breakdown voltage V_{gs} was assumed to be constant.

2.1 Achievable Efficiency and Output Power

For the calculation of the drain efficiency of a class-F amplifier it is necessary to understand which frequencies contribute to the output waveforms. Therefore, the ideal waveforms of the drain voltage v_{ds} and the drain current i_{ds} (depicted in figure 2.4, where θ denotes the current phase) are split into their Fourier-coefficients. It turns out that the drain

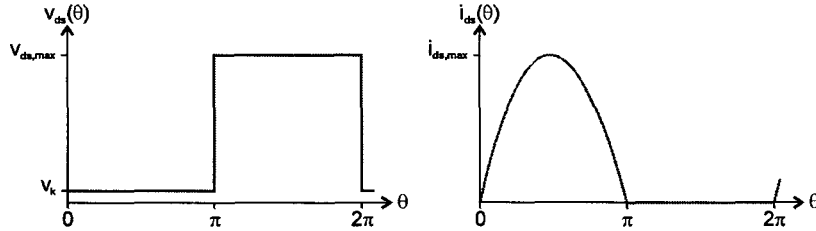


Figure 2.4: Ideal class F voltage and current waveforms

voltage (formula 2.1) consists only of odd harmonics whereas the drain current (equ. 2.2) is composed of even harmonics only.

$$v_{ds}(\theta) = \frac{V_k + V_{ds,max}}{2} - \frac{2(V_{ds,max} - V_k)}{\pi} \cdot \sum_{n=1}^{\infty} \frac{1}{2n-1} \sin((2n-1)\theta) \quad (2.1)$$

$$i_{ds}(\theta) = \frac{I_{ds,max}}{\pi} + \frac{I_{ds,max}}{2} \sin(\theta) - \frac{2I_{ds,max}}{\pi} \cdot \sum_{n=1}^{\infty} \frac{1}{(2n-1)(2n+1)} \cos(2n\theta) \quad (2.2)$$

To analyze the expected efficiency the power-integral $\int_{\theta=0}^{2\pi} v_{ds}(\theta) i_{ds}(\theta) d\theta$ has to be calculated. This leads to the multiplication of two infinite sums. These partial sums always have a product term like $\sin((2n-1)\theta) \cdot \cos(2m\theta)$ inside. The integration from

$\theta = 0 \dots 2\pi$ shows that almost all combinations cancel out. Therefore, the power at the fundamental frequency as well as the consumed DC-power can easily be calculated and are given in equations 2.3 and 2.4.

$$P(f = f_0) = \frac{1}{2\pi} (V_{ds,max} - V_k) I_{ds,max} \quad (2.3)$$

$$P(f = DC) = \frac{1}{2\pi} (V_{ds,max} + V_k) I_{ds,max} \quad (2.4)$$

Calculating the drain efficiency – which is defined as the ratio of RF output power over consumed DC power – gives:

$$\eta_D = \frac{P(f = f_0)}{P(f = DC)} = \frac{V_{ds,max} - V_k}{V_{ds,max} + V_k} \quad (2.5)$$

Equation 2.5 shows that a drain efficiency η_D of 100% is theoretically possible if the knee voltage V_k vanishes. This can also be seen in figure 2.4: Power is only lost during times where both, the drain voltage and current, have a value larger than zero. Setting $V_k = 0$ V forces the product $v_{ds} \cdot i_{ds} = 0$ W all the time.

The output power of the ideal class F amplifier (equ. 2.3) is 1.05 dB higher than for class A:

$$P_{\text{Class F}} = \frac{4}{\pi} \cdot \frac{(V_{ds,max} - V_k) I_{ds,max}}{8} = \frac{4}{\pi} P_{\text{Class A}} \quad (2.6)$$

The gain is reduced by 5 dB compared to the class A amplifier. This results from a +1 dB higher output power but a –6 dB reduction due to the class B bias condition.

Using the results for the fundamental frequency of the Fourier series of v_{ds} (equ. 2.1) and i_{ds} (equ. 2.2) allows to calculate the required load impedance:

$$Z_{L, \text{Class F}} = \frac{\widehat{v}_{ds, f_0}}{\widehat{i}_{ds, f_0}} = \frac{4}{\pi} \cdot \frac{V_{ds,max} - V_k}{I_{ds,max}} = \frac{4}{\pi} Z_{L, \text{Class A}} \quad (2.7)$$

Of course, these results are only useful for a theoretical treatment of the class F concept. When moving the focus more onto a practical realization it is important to remember that a real transistor is not capable of delivering power at an infinite number of harmonic frequencies. Also the harmonic matching becomes harder to accomplish with an increasing number of harmonics. Furthermore, amplifiers typically use RF-transistors which are operated as close as possible to f_T to keep the costs down. Thus it is necessary to analyze the circuit performance under the use of fewer harmonics:

Having a limited number of harmonic frequencies results in deviations of $v_{ds}(\theta)$ and $i_{ds}(\theta)$ from their ideal rectangular- and half-sinusoidal-shape. Therefore, overlapping between the drain voltage and the drain current waveforms occurs resulting in a reduced drain efficiency.

To determine the maximum efficiency, the drain voltage 'available' harmonic amplitudes must be adapted in order to produce the maximum output power. The waveform swing must range from the knee voltage V_K up to the maximally allowed drain voltage $V_{ds,max}$ [1] in order to realize high output powers and high efficiency. The same must be done for the current. But in contrary to the voltage, a maximally flat drain current i_{ds} does not give the best results. A slight ripple in the current waveform is required in order to maximize the output power and efficiency (improvement of about 6...8% as compared to

maximally flat case). Finding the optimum combinations of the harmonic frequencies, the maximum efficiency of a class-F amplifier depending on the number of available harmonics can be calculated and is shown in table 2.1. For the sake of simplicity the knee voltage was neglected ($V_K = 0$ V); voltage and current amplitudes are given in relation to their DC-parts. The maximum efficiency dynamic load-line for three harmonics is shown by the red trace in figure 2.3.

no. of harmonics	1	2	3	4	5	∞
P_{out}	0.1250	0.1250	0.1443	0.1443	0.1508	0.1592
η_D	50.0%	70.7%	81.7%	86.6%	90.4%	100.0%
$\hat{v}_{\text{ds},f_0}/V_{\text{dc}}$	1	1	1.1547	1.0824	1.2071	1.2732
$\hat{i}_{\text{ds},f_0}/I_{\text{dc}}$	1	1.4142	1.4142	1.5000	1.5000	1.5708
$\hat{i}_{\text{ds},2f_0}/I_{\text{dc}}$	—	0.3540	0.3540	0.3890	0.3890	0.6667
$\hat{v}_{\text{ds},3f_0}/V_{\text{dc}}$	—	—	0.1667	0.1667	0.2323	0.4224
$\hat{i}_{\text{ds},4f_0}/I_{\text{dc}}$	—	—	—	0.0556	0.0556	0.1333
$\hat{v}_{\text{ds},5f_0}/V_{\text{dc}}$	—	—	—	—	0.0607	2.5133

Table 2.1: Class F voltage and current ratios for maximum efficiency [1]

Comparing the theoretically realizable performance of table 2.1 shows that having control of the second harmonic can improve the amplifier's efficiency from 50% up to 71%. Adding a third harmonic gives a further 11%-increase to 82%. From now on, using more harmonic frequencies improves the output power and drain efficiency in very small steps. So, a reasonable decision is the termination up to the third harmonic.

Of course, all these observations are done from a theoretical point of view. They should help for understanding the concept of class-F amplifiers. When applied for microwave frequencies the extrinsic elements and nonlinearities have to be considered. Also, low impedance shorts and high impedance opens as required for class-F operation can only be realized approximately at microwave frequencies. So the efficiency values given above must be seen as an upper theoretical limit. Due to nonlinear effects and non-considered assisting higher order harmonics, the measurements can also give higher efficiency values in measurements. Table 2.2 gives a brief survey of published class-F amplifier results

f_0 [GHz]	P_{out} [dBm]	PAE [%]	G [dB]	Device	Reference, Year
0.5	43	74	17	LDMOS	Grebenikov 2000 [5]
1.8	23	90	18	HBT	Mallet 1996 [6]
1.8	21.1	84	14.6	MESFET	Barataud 1999 [7]
1.75	24.5	71	11	FET	Duvanaud 1993 [8]
10	27.8	75.8	8.8	HFET	Saunier 1992 [9]

Table 2.2: Reported performance of class F amplifiers

2.2 The importance of input matching

This effect has also been verified several times in literature. For example, an active harmonic load/source-pull measurement of a medium-power MESFET [10] shows a drain efficiency improvement of 6...18% by adding input second harmonic tuning.

During the measurements performed within this thesis it further turned out that some particular settings of the input tuner allow class F operation whereas other settings can be used for inverted class F designs only [11]. Due to the lack of harmonic tuning at the transistor input this effect could not be further investigated. The input setting was therefore kept constant for all measurements. The effect of the input harmonic terminations is covered by device level harmonic balance simulations in [12]. This paper clearly illustrates the effect of different input networks onto the dynamic loadline as well as on the output power and the efficiency.

2.3 The role of the extrinsics

So far the theory for class F amplifiers uses an ideal transistor for all calculations. For the realization with a real transistor further effects have to be considered. Besides all non-linear effects which degrade the achievable performance, the role of the extrinsic elements must not be forgotten. The extrinsic elements represent all passive and linear elements outside the active area of the semiconductor. These elements include e.g. the bond wire inductance, the package capacitances, ... The extrinsic elements can be primarily seen as a transformation which is quasi lossless, especially for power transistors. The transformation ratio increases at higher frequencies due to the inductor-capacitor combination in the extrinsic circuit.

The externally required loads for a class F amplifier are, therefore, different from the intrinsic ones and can be calculated by two ways. On the one hand the extrinsic elements can be determined and used for calculating the required loads. On the other hand harmonic load-pull measurements can be done. The latter one allows to find the required external terminations without the knowledge of the extrinsic elements.

2.4 Effect of non perfect short circuits and opens

Because an ideal short or an ideal open cannot be realized, it is important to know what performance degradation has to be expected from imperfect terminations at the harmonic loads. An investigation of this problem for a class F amplifier is given in [13]. In this work the power added efficiency was simulated for different harmonic loads. Figure 2.5 shows the results for a power transistor which requires a $3.64\ \Omega$ load seen by the transistor. The blue trace indicates the efficiency over the impedance of the 2nd harmonic load, the third harmonic was kept constant at a quasi open. The red line shows the efficiency depending on the 3rd harmonic, the second harmonic was quasi short circuited. It turns out that performance improvement is negligible if the third harmonic termination is $> 35\ \Omega$. The same applies for second harmonic loads $< 4\ \Omega$. Therefore, the following rule of thumb is given in [13]: For class F amplifiers a load $> 10 \cdot Z_{\text{fundamental}}$ acts as an open resp. a load $< \frac{1}{10} \cdot Z_{\text{fundamental}}$ acts as a short.

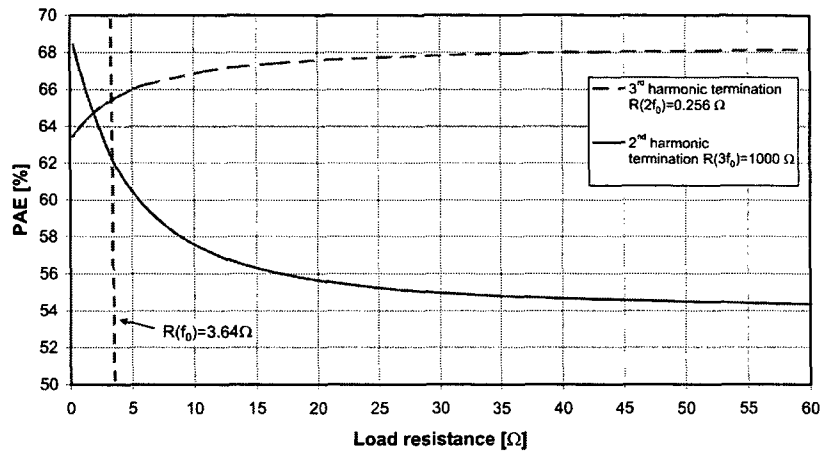


Figure 2.5: Efficiency dependence on harmonic loads [13]

2.5 Summary

The ideal class F amplifier allows to operate a transistor perfectly linear and with high efficiency due to waveform shaping. The determination of the appropriate externally connected loads requires either knowledge of the extrinsic elements or the use of a harmonic load-pull system. It can be shown that even a non-perfect termination is sufficient for class F operation.

Chapter 3

Load-Pull Setups and Tuning Elements

Load-Pull defines a type of a measurement where the load at the output side of the device under test (DUT) is varied ("pulled"). The pulling is done by variable loads, so called tuners, which allow the adjustment of the reflection coefficient in magnitude and phase. The DUT is typically a transistor which is optimized for certain parameters like output power, power added efficiency, noise figure . . . This is quite a typical application in industry. The great benefit of load-pull in this case is that the amplifier designer gets rid from the need for a nonlinear large-signal model of the transistor. The development of a nonlinear model is a time-consuming and difficult process, also the accuracy is often not satisfying. Model parameters available from the transistor manufacturer can of course be used for small signal designs. However, driving the transistor into its nonlinear regions requires more precise models than provided. By using load-pull measurements the amplifier designer gets knowledge of an optimum load without the need for a transistor model. The transistor is seen as a black-box which has to be supplied with a certain loading. Knowing this value it is an easy job to realize the final amplifier. Designing amplifiers this way can reduce development times down to some days.

Besides the amplifier design, load-pulling can also be used for the verification of large-signal nonlinear transistor models [14][15][16], an application rather found at universities than in the industry. The use of a load-pull system enables the verification with a huge number of different loads within short time. Without a load-pull system many printed circuit boards would be needed to do this job. Due to the possibility of using harmonic tuning as well, a transistor model can be tested for different operation modes ranging from the small signal class A case to harmonic terminated concepts like class F. Passive harmonic systems also allow to use modulated signals as well. Hence, the dependency of parameters like adjacent channel power (ACP) can also be observed with a load-pull setup.

Furthermore, the application is not limited to transistors only. Load-pull, especially harmonic load pull, is an emerging type of measurement. Due to its high potential more and more universities as well as companies use it in their labs.

Setups for load-pull application can be realized in many different ways: manual or automatic tuners can be used, an active or passive realization can be used, harmonics can be included for the load-pull or not, . . . This chapter's intention is to give an overview on the different setups. It will list the block diagrams of different setups and will also

comment on their advantages and disadvantages. Besides that, the commonly used tuning elements will also be introduced.

It is important that nearly all which is said here about load-pulling can also be applied for the input side of a DUT. This so called source-pulling should not be labeled as being unimportant. For example, when designing a highly efficient amplifier, it has a big influence on the achievable efficiency. A certain load at the source can for example favour the operation of a transistor in class F, whereas another load gives better results for inverted class F operation of the same device. To have comparable results, the load-pull methods which were realized within thesis use constant input matching.

3.1 Fundamental Load-Pull

The simplest setup is to use a single tuner at the output of the device under test (figure 3.1).

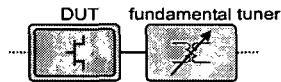


Figure 3.1: Fundamental load-pull setup

This tuner is typically a two-port device and it allows the cascaded connection of additional measurement equipment like power meters or spectrum analyzers. Since almost all tuners for frequencies $f < 20$ GHz are based on TEM transmission lines the biasing (the DC-supply) can be done at the tuner's port which is opposite to the DUT. This has the benefit that the connection of the tuner to the device under test has low losses. This is an important factor to maintain a large tuning range. For each load-pull setup it should be strived for minimum insertion losses of the components.

The different tuners which can be used for fundamental load-pull have one thing in common: all frequencies besides the one of interest are terminated undefined. By knowing nothing about the harmonic frequencies it could happen for example that the transistor is operated unintended in a highly efficient class F mode. But it is also possible to have a harmonic setting which lowers the efficiency. Hence, having a transistor with a high enough gain at harmonic frequencies could lead to different load-pull results if one and the same device is measured with different fundamental load-pull setups or different tuners. Commonly used automated tuners, when set to high reflection at the fundamental frequency, also have a good reflection at the harmonics due to their construction principle (see section 3.1.2 for an example). This is always a problem of fundamental load pull and it is even hard to address: inserting a low-pass filter before the tuner would even not help, because the incoming wave is reflected with an undefined phase also. Using a frequency splitter to terminate the harmonics would give the same results, as long as the same test fixture is used. This can be used for model testing but it is not applicable for the exact prediction of an amplifier's behavior which is based on the load-pull measurements but does not use a frequency splitter to terminate the harmonics.

So attention has to be paid when having load-pull data in hands: What value was used for the harmonic terminations? Which input matching was used (also at harmonic frequencies)? Without this information it is not possible to reproduce measurements.

3.1.1 Power Measurement Issues

When using a manual tuner special attention has to be paid to the measurement of the output power. There are two possible pitfalls which should be known in advance: Let us assume output power measurement according to figure 3.2a.

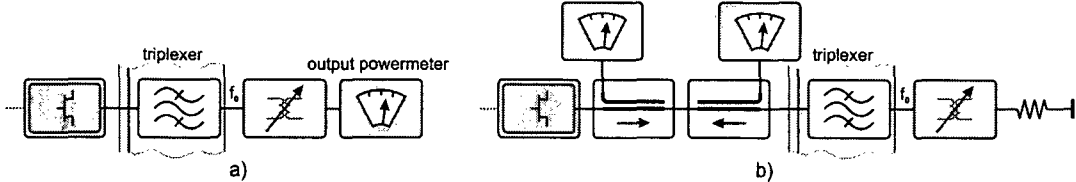


Figure 3.2: Different ways to measure load-pull output power

If the fundamental tuner is varied its input matching S_{11} and S_{22} will be changed. Of course, the tuners transfer parameters $S_{21} = S_{12}$ also change. This is not a problem for the power measurement as long as the insertion loss keeps constant. This can be assumed to be true for most of the commercially available tuners. But even having an ideal (loss-less) tuner, losses in the setup can lead into problems. To demonstrate this, a measurement setup according to figure 3.3 was simulated. The setup includes the extrinsic

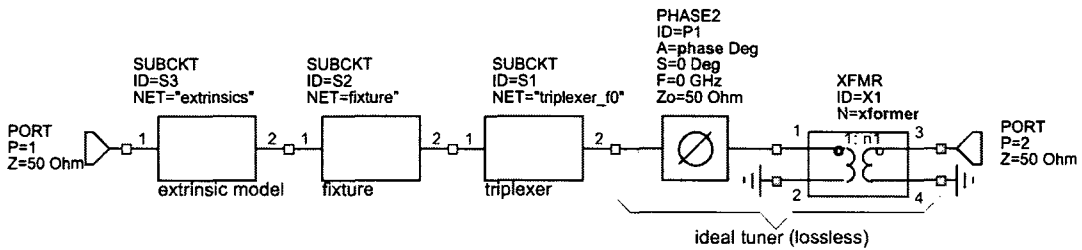


Figure 3.3: Load-pull setup for calculation of losses

elements of the transistor as well as the effects of the test fixture (compare section 5.2 for details about these blocks). Hence, port 1 can be seen as being directly connected to the intrinsic transistor. Now it was chosen to insert a triplexer (a filter which separates the fundamental from the harmonic frequencies, compare section 5.4.1) with an insertion loss of ≈ 0.8 dB. Figure 3.3 only shows the input and the fundamental frequency output port of the triplexer. The reason for inserting a triplexer could be the need of a defined termination of the harmonic frequencies with e.g. a 50Ω load. Then an ideal tuner (represented by a phase shifter and a transformer, both lossless) is connected. Further the amount of lost power $= 1 - (S_{11}^2 + S_{21}^2)$ of the entire setup in figure 3.3 is calculated. This is done for several settings of the transformation ratio of the tuner 'xformer' and different phase shifts 'phase'. The result is given in figure 3.4. It is clearly obvious that the overall system loss (from the intrinsic transistor at port 1 to the powermeter on port 2) depends on the chosen parameter set. For high transformation ratios it turns out that the loss is higher than 50% which equals to > 3 dB deviation of the powermeter's reading compared to the value measured with a lossless triplexer. This can be simply explained: Due to the

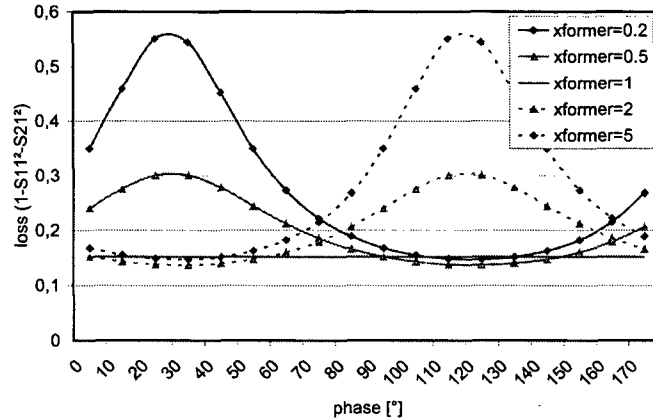


Figure 3.4: Dependence of losses on the the setting of an ideal tuner

high reflection at both ends at the setup (the extrinsic elements on one side and a highly mismatched tuner on the other side) the output wave of the DUT starts circulating in this structure. Now, the lossy triplexer is passed through very often and with each reflection at the transformer at port 2 only a small portion of the wave is coupled out to port 2. Therefore, the overall loss increases dramatically. This is an important fact to consider when using load-pull setups: If the fundamental tuner is operated at high reflection values the measured power must be corrected. This can be done with a few calculations as long as the S-parameters of the used elements (including the tuner) are known. This is not a problem when using an automated tuner at positions which have been calibrated by a vector network analyzer measurement before. Using an uncalibrated manual tuner can lead to totally wrong results here. Anyhow, to enable the application of manual tuners with a tolerable error, the insertion loss of the system has to be very small and the tuner's mismatch must not be too high. It is recommended to do a simulation like the one above before tuning to have an idea on the variation range of the overall loss.

To overcome this problem an alternative would be to use a directional coupler connected to the device under test (figure 3.2b). This eliminates the problem of the unknown loss but introduces another one. Again, when having a high reflection coefficient at the fundamental tuner, the transistor's output wave starts circulating inside the structure. So the measured power in forward direction (at the directional coupler) becomes typically higher than the power which would be measured at port 2. This is nothing unphysical – the effect is comparable to a laser resonator: inside the resonator there is a high energy density but only a small portion is coupled out at the output. So it becomes necessary to measure the backward travelling wave as well in order to calculate the difference. Because the power measurement is now done before the main lossy element, the result is even more accurate. What could also be problematic is if the power levels of the forward and backward traveling waves have about the same value. Because the 'real' output power is defined by the difference $P = P_{\text{forw.}} - P_{\text{rev.}}$ a small measurement uncertainty of the two measured power levels could lead to a high inaccuracy of the calculated difference. Of course this can only happen in a setup with extremely low losses and highly reflective tuners. Within this

thesis this never turned out to be a problem due to the moderate input mismatch setting of the fundamental tuner.

3.1.2 Applicable Tuner Types

The only requirement which a suitable tuner has to fulfill primarily is the possibility to vary its reflection coefficient over a large range at the frequency of interest. The insertion loss of the tuner is often of minor importance as long as it is quasi constant – of course low losses are required to achieve a high VSWR at its input. Hence, a very simple realization could be a transmission line with a mismatch on it. By allowing to vary the magnitude of the mismatch (e.g. by moving a metallic object closer to the inner conductor of a TEM transmission line) and the phase (e.g. by changing the mismatch position along the line) a tuner can already be realized. This describes the principle of a slidescrew tuner.

Manual Slidescrew Tuners

Coaxial slide screw tuners provide a convenient method of matching a wide range of impedances to a 50 ohm transmission line system. These tuners typically consist of a coaxial slot line or a slabline section (compare section 4.2) with a sliding carriage upon which one or two adjustable micrometer screws are mounted (figure 3.5). These micrometer screws

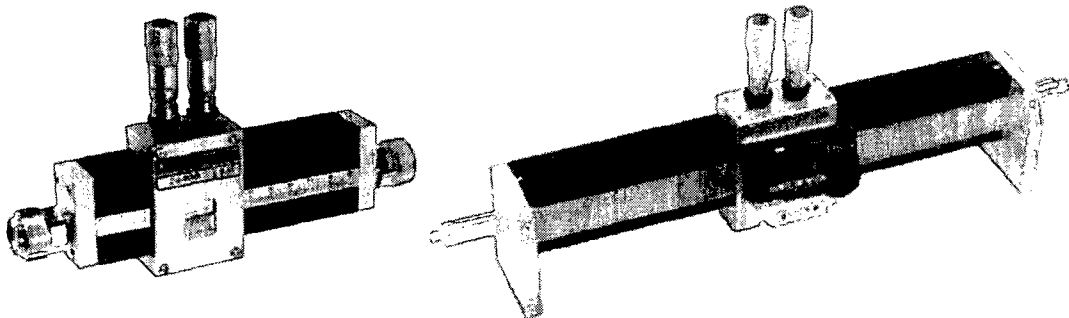


Figure 3.5: Photos of typical slidescrew tuners [17]

control a variable reactance element whose magnitude is changed by varying its depth of insertion into the coaxial line and whose phase is varied by sliding the carriage along the line. The lowest usable frequency results from the necessity that the carriage can be moved $\geq \frac{\lambda}{2}$. This ensures to realize all possible phases of the reflection coefficient at the ports of the tuner. Many tuners normally also provide scale and vernier to allow a readout of the carriage position as well. This is needed when a certain setting has to be restored. Some slidescrew tuners provide digital readouts for higher accuracy – especially required at higher frequencies. The often used second reactance element is not needed by the underlying principle. On the one hand it allows to realize higher reflection coefficients within the same frequency range, on the other hand it is possible to extend the usable frequency downwards while maintaining the achievable VWSR. In normal operation, only one probe is required for setting a reflection coefficient within the tuning range. Slidescrew tuners are also available as waveguide models for higher frequencies.

To have an idea on commercially available models in terms of power handling, bandwidth, matching range, ... the data of some slidescrew tuners is listed in table 3.1 (data taken from [17] and [18]).

model	$f_{\min} \dots f_{\max}$	VSWR / $ \Gamma $	P_{\max} . (peak)	connector
Maury 1643N	0.8 ... 2.5 GHz	25 : 1 / 0.92	50 (500) W	type N
Maury 8041B	12 ... 34 GHz	6 : 1 / 0.71	25 (250) W	3.5 mm
Focus MMT-5004	3 ... 50 GHz	15 : 1 / 0.88	not listed	2.4 mm

Table 3.1: Performance of different slidescrew tuners

The specified VSWR / $|\Gamma|$ (reflection coefficient) must be seen as the guaranteed minimum for the entire frequency range. Within a narrow band, for example, the Focus MMT-5004 achieves a VSWR of 40 : 1 which corresponds to $|\Gamma| = 0.95$. This tuner was also the only with an insertion loss specification: 0.2 ... 0.9 dB depending on the frequency.

It should be noted explicitly here, that a set reflection coefficient is only valid for one frequency. The termination at other frequencies is not defined. Having set a certain Γ at e.g. 2 GHz requires a different position of the carriage and the tunable reactance at 2.1 GHz. The following example will show an estimate for the error introduced by assuming the tuner's input matching to be constant for neighboring frequencies. Assume the following scenario for a calibration at $f_a = 2$ GHz and a measurement at $f_b = 2.01$ GHz. Due to the setup of the system (the often required test fixture, cables, a possible triplexer and the slidescrew tuner), the carriage might be located up to 1 m of equivalent free space distance¹ away from the device under test. This gives a delay time of 6.67 ns for the round trip DUT – tuner's carriage – DUT. Referencing this to the wavelengths of f_a and f_b this gives a $360^\circ \cdot ((2 \cdot 1 \text{ m}) \cdot f_a / c_0) = 120^\circ$ -phase shift at 2 GHz and a 144° -phase shift at 2.01 GHz. The variation of the variable reactance's magnitude is typically negligible for such small frequency differences. However, the error of $\Delta\varphi = 22^\circ$ is too high for almost all applications.

If the user wants to use a slidescrew tuner for load-pulling with UMTS-signals ($BW \approx 5$ MHz) at $f = 2$ GHz the same calculation would lead to $\Delta\varphi = \pm 6^\circ$ at the edges of the spectrum. This is typically accepted for an amplifier design but might be too inaccurate for model verification for example. Hence, it is recommended to keep the cabling lengths as short as possible to reduce the phase deviation. Having a compact setup also reduces the insertion losses and, therefore, widens the tuning range.

Automatic Slidescrew Tuners

The slidescrew tuner principle is also very well suited for automation. The variable reactance is realized as a metallic or dielectric element whose distance to the center conductor of the transmission line can be set with a stepping motor. The carriage is also moved by a stepping motor. This tuners typically come as a closed box with two RF ports and a connector for the motors. An exemplary tuner is shown in figure 3.6. The tuner has adjusting screws to allow for height adjustment. This is a critical point when setting up a tuner system, especially when bulky units are connected together. A misalignment of the

¹Measurement cables slow down the wave due to $\epsilon_r > 1$. This compares to a longer distance in an air-filled cable.

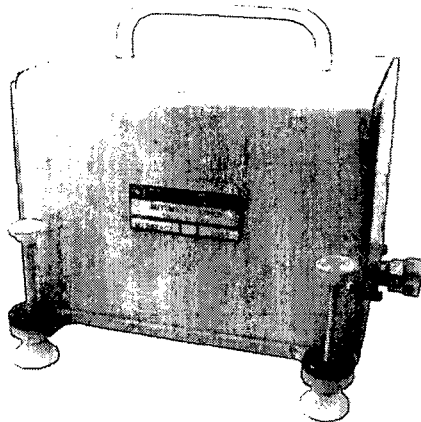


Figure 3.6: Photograph of a boxed automatic tuner, based on slidescrew principle

connectors plane is then hard to detect. It introduces additional reflections into the setup and can shorten connector life dramatically.

The performance of some commercially available tuners is listed in table 3.2 (data taken from [17],[18] and [19]).

model	$f_{\min} \dots f_{\max}$	VSWR / $ \Gamma $	$P_{\max.}$ (peak)	connector
Maury MT982A02	1.8 ... 18 GHz	15 : 1 / 0.88	50 (500) W	APC-7
Focus CCMT-5002-2C	2 ... 50 GHz	10 : 1 / 0.82	not listed	2.4 mm
Athena AFT-633-18	0.63 ... 18 GHz	12 : 1 / 0.85	50 W	APC-7

Table 3.2: Performance of automatic slidecrew tuners

When shipped to the customer typically no calibration data comes along with the tuners. This would not be possible, because the tuner's properties already vary significantly if the frequency is slightly changed (see section 3.1.2). It would be required to have a perfect model of the tuner available which can be fitted by a finite number of measurements. Because of the residual error of the used models it is required to characterize the tuners for each frequency and each motor setting separately.

For the realized load-pull setups within this thesis the Maury Microwave MT982A02 model was used. This tuner's maximum insertion loss is 0.4 dB and it has for example a step resolution of the carriage of $9 \mu\text{m}$ (corresponds to 0.4° @ $f = f_{\max} = 18 \text{ GHz}$). A statement about the repeatability was not found. In order to keep the reproducibility high, a desired motor position is always approached from the same direction. This is done to reduce the play of the construction. Measurements turned out that the repeatability error at $f = 2.1445 \text{ GHz}$ was smaller than 0.01 in magnitude and less than 1° in phase². The tuner software which can also be bought from Maury Microwave allows a calibration based on a model. But the model is only used to estimate the motor positions to obtain

²For this measurement the tuner was connected to a vector network analyzer and calibrated. Without opening the connectors several – randomly chosen – positions were measured and compared to the calibration.

certain reflection coefficients. Each position is then set and measured in order to keep high accuracy.

Manual Double Slug Tuners

When using manual tuners a very cheap realization is a double slug tuner. In contrary to the methods described before it uses two fixed mismatches which can be separately moved along a slotted, air-filled coaxial transmission line. Figure 3.7 shows a photograph of such a tuner. Depending on the required VSWR, the mismatches are typically sleeves either

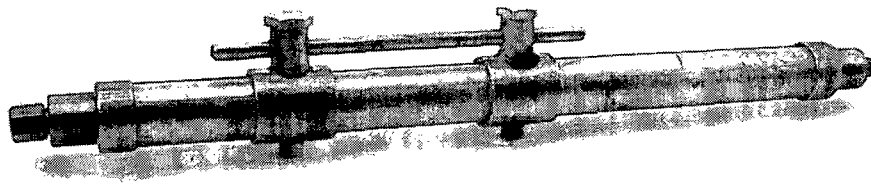


Figure 3.7: Photograph of a double slug tuner

made of a dielectric material like Teflon or a metal for achieving higher reflection. The magnitude of the reflection coefficient almost entirely depends on the distance between both mismatches. The tuner can be seen as a loosely coupled resonator along the line. Depending on the ratio of resonator's resonant wavelength and the wavelength actually used, the resonator can either act as a thru or an open. Of course, the resonator's wavelength is set by the distance of both mismatches. To have control of the phase both sleeves (resp. the resonator) need to be moved along the line. Therefore the tuner (figure 3.7) has a connection rod between both mismatches in order to allow maintaining a certain distance between them while moving both of them.

Hence, for an ideal double slug tuner a variation in the distance between both mismatches varies the reflection coefficient's amplitude – but also influences the phase. By moving both sleeves the phase is controlled without influencing the magnitude.

These tuners are available for frequencies up to ≈ 6 GHz. The performance data of commercial products is listed in table 3.3.

model	$f_{\min} \dots f_{\max}$	VSWR / $ \Gamma $	$P_{\max.}$ (peak)	connector
Microlab/FXR SF-10N ¹⁾	0.3 ... 1.7 GHz	2 : 1 / 0.33	500 (5000) W	type N
Microlab/FXR SF-31N ²⁾	1 ... 5 GHz	10 : 1 / 0.82	not listed	3.5 mm

1) using air-dielectric slugs, 2) using metal-dielectric slugs

Table 3.3: Performance of double slug tuners

The repeatability of these tuners is typically bad, because they do not have scales on them. The insertion loss of the tuners listed in table 3.3 is guaranteed to be ≤ 0.2 dB (all data taken from [20]).

Stub Tuners

Another type of mechanical tuner uses multiple short circuited stubs (typically two or three) to achieve matching over a large frequency range.

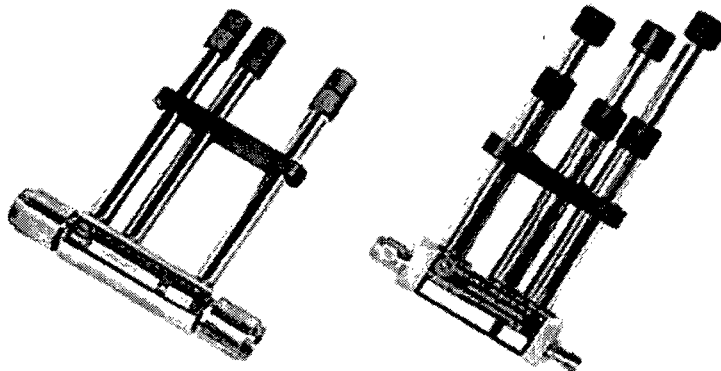


Figure 3.8: Photos of typical stub-tuners [17]

Because stub tuners are specified by the stub spacing and the stub travel, no performance data in terms of achievable VSWR can be given here. Typical power ratings in the frequency range $f < 6$ GHz are 25 ... 100 W, the insertion loss is about 0.2 dB. Maximum usable bandwidths of triple-stub models are e.g. 2 ... 18 GHz (all data taken from [17] and [20]).

Because these tuners do not allow a decoupled setting of magnitude and phase their application for load-pulling is of minor interest.

Automatic Electronic (Solid-State) Tuners

For the sake of completeness electronic tuners have also to be mentioned. These tuners use a set of switched PIN-diodes (typically in microstrip circuits) to achieve a limited number of reflection coefficients. Due to the diodes their application is limited to low power levels. For harmonic load-pull setups, the used power must be set even lower to prevent wrong measurement results due to intermodulation effects caused by the tuner's diodes. Because of the given physical distribution along microstrip lines solid state tuners generate sets of reflection coefficients which cannot be distributed uniformly in the Smith Chart. Figure 3.9 shows the comparison of an electronic-tuner (left) to an automated slidescrew tuner (right) at $f = 2$ GHz.

These tuners are perfectly suited for noise measurements because of the low power needed and they allow fast setting times. A new reflection coefficient can be set within microseconds (limited by the switching speed of the used diodes only). This allows a very fast measurement at many different loads. Solid-state tuners from Maury Microwave have a tuning range up to a VSWR of 10 : 1 (corresponds to $|\Gamma| = 0.82$). They are available in the frequency range from 0.3 ... 40 GHz (banded), provide 369 different states and have an extremely high repeatability (< -50 dB residual error vector). Electronic tuners generally have the highest repeatability of all tuner types because no mechanical parts are used.

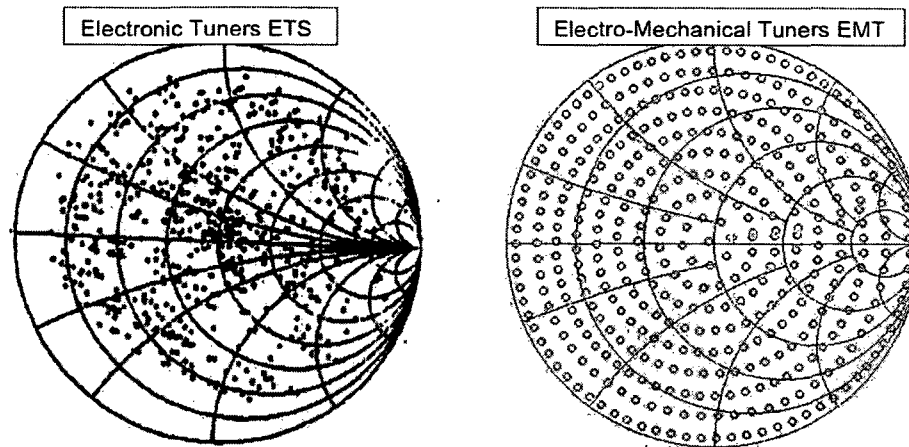


Figure 3.9: Tuning patterns of an electronic and mechanical tuner at $f = 2$ GHz [21]

Information on the allowed power levels as well as intermodulation was not available due to referring to a preliminary data sheet from [17].

Another disadvantage besides the very low power handling is their high insertion loss of about 10...12 dB. This reduces the accuracy when using an electronic tuner for noise measurements.

3.1.3 Summary

Passive load-pull measurements are a simple tool for finding an appropriate matching for an amplifier. A transistor can be tested under real conditions with different input signals. Optimization of the termination can be done with respect to many parameters like output power, efficiency, adjacent channel power / intermodulation and so on. There is neither need for the circuit designer to have knowledge about the extrinsic transistor parameters nor a large-signal nonlinear intrinsic model. This shortens amplifier design times down to some days.

Fundamental load-pulling can either be done with manual as well as automated tuners. Manual tuners allow a cheap realization when the goal of load-pulling is finding the optimum load. If a plot of a certain parameter over the reflection coefficient is needed (e.g. for analyzing the influence of component tolerance) this becomes a time-consuming job. Also, exact measurements are often not possible because the actual value of the reflection coefficient is usually not known which might lead into erroneous power meter readings (see section 3.1.1). The need for 'parameter over Γ '-plots and the need for more accuracy leads to the application area of automated tuners. Of course such systems are definitely more expensive than manual ones but ease up the measurement.

Typical VSWR-values which are achieved by commercial products range from 2 : 1 to 25 : 1. The latter VSWR corresponds to $|\Gamma| = 0.92$ ($Z = 2.1 \Omega$). It is important to realize that this is not the load seen by the intrinsic transistor in a load-pull setup, this is the load at the tuner's input. Due to the losses of the setup and the transformation applied by the extrinsic circuit of the device under test (compare chapter 5.5.3) the achievable $|\Gamma|$ is further reduced. Therefore, tuners with higher VSWR are often needed. This can either

be realized by prematching (see section 3.5) or by using active loads (see section 3.4).

It is further important to know that all tuners introduced have an undefined reflection coefficient besides the frequency of interest. This unintentionally introduces waveform-shaping: The transistor might be operated in class F mode for example. If the harmonic termination is not taken into account an amplifier realized on the basis of fundamental load-pull measurement might give a completely different performance to what was measured during load pull. To overcome this problem and even to exploit waveform shaping for achieving higher efficiency, harmonic load pull is needed. By measuring the second and third harmonics the error due to the non-investigated higher harmonics is reduced extremely.

3.2 Harmonic Load-Pull

The idea of harmonic load-pull is quite old. In the year 1979 a system allowing independent control of the fundamental and the second harmonic frequency was already set into operation [22]. The setup used a vector network analyzer for the measurement of the manually set terminations. This publication also introduced an active tuner.

For having control of the included harmonic frequencies – which is required to operate transistors in highly efficient modes – additional tuners are needed. These tuners – typically two are used for the second and third harmonic – have different requirements than a fundamental tuner: it is only required to change the phase of the reflection coefficient but not its magnitude. The tuner should reflect as much energy as possible. This introduces another type of tuning element: the sliding short (explained later on).

Having a look at the block diagram of the setup (figure 3.10) shows a further element, a triplexer. This is a filter which allows to separate the fundamental frequency from the

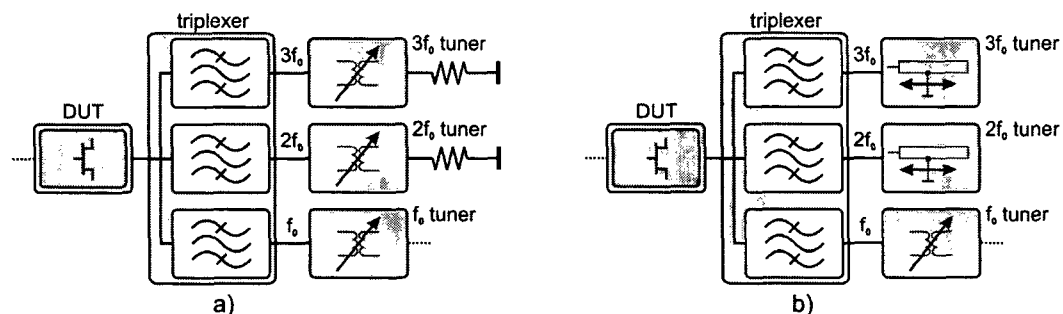


Figure 3.10: Harmonic load-pull with triplexer

harmonics to allow independent tuning. Of course, more and less frequencies can be used for a harmonic load-pull setup. Having a look at the theory of class F amplifiers (chapter 2) turns out that using the second and third harmonic is a good trade-off between amplifier complexity and efficiency improvement.

Figure 3.10a) shows the realization with impedance matching tuners which are terminated with $50\ \Omega$. Even a short or an open could be used here which would lead to a kind of prematching. As shown in figure 3.10b) the use of sliding shorts is possible as well. Sliding shorts typically achieve higher reflection than impedance matching tuners (see section

3.2.1).

Due to the triplexer's insertion loss which is usually 0.5 dB or higher (data from [18]) the tuning range shrinks. Also the transformation due to the extrinsic elements of the transistor is even more critical at the harmonic frequencies due to its lowpass behavior. This means that much attention has to be paid to a high reflection factor at the third harmonic. If the achievable $|\Gamma|$ which is seen by the inner transistor is still too low there are some ways for a further improvement:

- **Prematching tuners for the harmonic frequencies:** This can be done very easily by inserting a manual impedance matching tuner between the triplexer and the actual tuner. By knowing the S-parameters of the entire setup (transistor's extrinsic elements, test-fixture, cables, triplexer, ...) an appropriate setting of the added tuner can be calculated and set with the help of a VNA. This allows the improvement for a specific setup but requires a new setting if anything is changed in the setup. So, if possible, an automatic prematching tuner should be preferred (compare section 3.5). This enables the user to realize high $|\Gamma|$ for all phases and allows for changes in the setup.

When measuring power devices a prematching tuner might still give a too low performance due to the insertion loss of the triplexer: Assume an ideal prematching tuner with $|\Gamma| = 1$ and a triplexer insertion loss of 0.5 dB (which is a very good value). The combination of both elements limits the reflection coefficient to $|\Gamma| = 0.94$ (corresponds to $Z = 1.55 \Omega$). Because the ratio of the harmonic impedances to the fundamental ones should be about one order of magnitude, a resistance of 1.55Ω is not acceptable for even medium power transistors (a fundamental output impedance of 10Ω is found for 1 W-devices already). Please note, that the transformation due to the extrinsic elements was not taken into account yet – this would give even worse ratios.

Since triplexers with lower insertion loss are not reported in literature, even the use of pre-matched tuners is quite often not good enough.

- **Harmonic tuners instead of a triplexer:** As already indicated before, the triplexer seems to be the limiting element within a harmonic load-pull setup. Hence, a setup without a triplexer promises to be a solution. Such a setup is achieved by using tuners which are resonant at the harmonic frequencies in-between DUT and the fundamental tuner (figure 3.11). This so called harmonic tuner allows to move

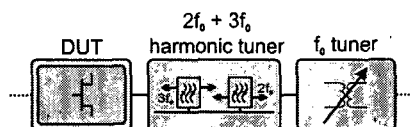


Figure 3.11: Harmonic load-pull with harmonic tuner

resonators along its transmission line to allow changing the phase. Due to the resonant behavior the mutual influence of the harmonic tuner and the fundamental tuner can be kept quite low. Only a small correction has to be applied to the fundamental tuner's setting when changing the harmonic phases. These tuners typically achieve

$|\Gamma| = 0.92 \dots 0.95$ for frequencies $f = 2 \dots 5$ GHz (data taken from [23]). The performance is comparable with the results of a prematching tuner. The advantage is the less complex setup and the easily manufactured resonators. The disadvantage is a worse decoupling of the tuner settings.

- **Active loads:** In the same way as for the fundamental wave, active loads can also be used at harmonic frequencies. Again they can compensate for all losses as long as they use sufficiently powerful amplifiers. Realizing $|\Gamma| = 1$ as 'seen' by the transistor is not a problem. Of course, there are certain issues to be aware of: Depending on the realization of the active load the probability for oscillation is often very high and hard to control. Existing systems are further limited to the use of smallband signals. Section 3.4 gives more details on active loads.

Nevertheless, it should be possible to realize a setup which ensures stable loads and enables application for broadband signals. Section 5.8 of this thesis will introduce such a system.

Comparing these three methods active loads seem to be the only useful solution at a first glance. This is true when high reflection coefficients need to be exactly realized (e.g. for model verification or precise prediction of amplifier behavior). If the driving factor to use harmonic load-pull is to design an amplifier it is also possible to use the original setup with triplexers (figure 3.10) or harmonic tuners (figure 3.11). Of course the values measured during the harmonic load-pull do not reflect what the device is really capable of doing – but tendencies are possible to extract. So it is possible to come to a statement like: 'using harmonic terminations with a phase of x°/y° at $2f_0/3f_0$ guarantees an ACP of xx dB or even better' – still, the real value is not known.

3.2.1 Applicable Tuner Types

Besides the tuners already known from fundamental load pull, two additional types were introduced for harmonic load-pull: the sliding short and the harmonic tuner. Common to both tuners is that they only allow to vary the phase but not the magnitude. The value of $|\Gamma|$ is as high as possible by the tuner's construction:

Sliding-Shorts

Manual sliding shorts are found in two different realizations. One type uses a slotted outer conductor that allows adjustment of the short's position while not increasing overall dimensions. The other type which is often used for higher frequencies is adjusted by a handle extending from the mouth of the stub (figure 3.12) Models are available of different

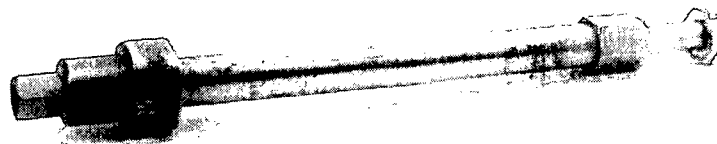


Figure 3.12: Photograph of a sliding-short

manufacturers (e.g. [17] and [20]) for frequencies³ $f = 0.2 \dots 40$ GHz (banded) but do not state which reflection coefficient can be achieved. Measurements of the depicted sliding-short (Microlab/FXR SO-6MF, $f = 1.5 \dots 6$ GHz) showed a $|\Gamma| > 0.95$ (corresponds to VSWR = 39 : 1) for the entire frequency range (tested at >10 different positions). Power rating is specified to be 100 W average and up to 5 kW peak.

Sliding-shorts are also found in automated versions, like the Maury MT999A: frequency range is $f = 0.8 \dots 7.5$ GHz, power handling is 10 W average and 500 W peak. The guaranteed VSWR is 50 : 1 (corresponds to $|\Gamma| = 0.96$).

Using sliding shorts has the advantage of a higher reflection coefficient. The disadvantage is that there is no second port to measure the harmonic power for example. Adding for example a directional coupler to a sliding short typically limits its performance to what can be achieved with two port impedance-matching tuners.

Manual Harmonic Tuners

These tuners provide a high reflection coefficient at the designed frequency by a resonator which can be positioned along a transmission line. The design goal is a high reflection at the harmonic frequency while reducing the influence on the fundamental wave as far as possible to allow independent tuning. These tuners are available both in manual and automated versions.

A manual harmonic tuner's design is comparable to a slidescrew-tuner whose variable reactance element is replaced by a resonator with a high coupling to the inner conductor of the transmission line. These tuners are available also in combination with a slidescrew element as well as stand alone. Figure 3.13 depicts a set of a tuner with a $3f_0$ -resonator and a tuner with a $2f_0$ -resonator combined with a slidescrew-element (MHMT-308 and MHMT-308-3H, made by [18]).

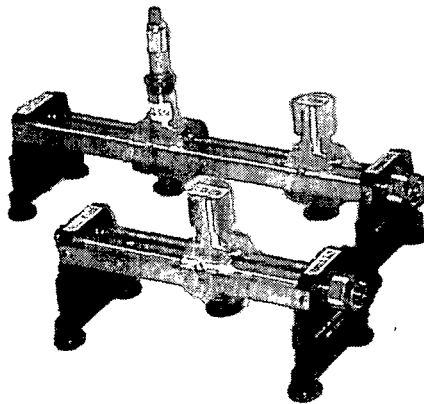


Figure 3.13: Photograph of manual harmonic tuners [18]

The performance data for this customer specific designs (possible $f_0 = 0.8 \dots 3$ GHz) are: fundamental VSWR up to 20 : 1, VSWR of the harmonic resonators at $2f_0$ and $3f_0$

³The frequency of a sliding short tuner is specified by a positioning range $> \frac{\lambda}{2}$ of the short. This ensures all phases $0^\circ \dots 360^\circ$ being realizable at the input port.

is $\approx 40 : 1$ resp. $|\Gamma| \approx 0.95$, bandwidth of the harmonic resonators = 8%, insertion loss (frequency dependent) = 0.1 ... 0.9 dB.

Automated Harmonic Tuners

The automation can be done again by using stepper motors to move the position of the resonators. Harmonic tuners are typically boxed two-port units with an additional connector for the control of the motors. The performance data of a customer specific design of a so called 'bi-Harmonic Combo Tuner' (which integrates the fundamental and the harmonic tuners in a single unit) by Focus Microwave [18] are: $f_0 = 5.25$ GHz, $VSWR_{f_0} = 15 : 1$, $VSWR_{2f_0} = 80 : 1$ ($|\Gamma| = 0.975$), $VSWR_{3f_0} = 35 : 1$ ($|\Gamma| = 0.94$), decoupling harmonics-fundamental > 2 dB, bandwidth ≈ 500 MHz.

Automated harmonic tuners are also available from Athena Microwaves [19]. The company claims to provide resonator based models with $VSWR > 100 : 1$ for frequencies up to 18 GHz. Neither further details nor measurement results are provided.

3.3 Summary

Harmonic load-pull is an ideal extension of fundamental load pull in several ways: By having a defined load also at the harmonic frequencies (usually the second and third ones are used) the influence of non-considered higher order harmonic frequencies is dramatically reduced. Because transistors selected for amplifiers typically have a transit frequency which is as small as possible to just fulfill the amplifier requirements (this is a matter of device price). Therefore, the available power gain at the fourth and higher order harmonics is often so small that it can be neglected. This allows to give a very good prediction on the final performance of an amplifier when doing load pull. Having control of the lower order harmonics is a necessary prerequisite also to allow the design of highly efficient amplifiers like class F.

Unfortunately, harmonic load-pull brings some additional problems along. Because of the need for an independent control of the reflection coefficient at different frequencies, frequency-selective components need to be used. This can either be a triplexer with standard tuners or a triplexer-less setup with resonant harmonic tuners. Thus, the system's frequency becomes fixed now. A fundamental load-pull system, in contrary, can be used for a large bandwidth depending on the specification of the used tuner. Changing the center frequency requires either a replacement of the triplexer respective the harmonic resonators depending on the setup. Automated measurement are limited to a certain frequency range (up to 8% relative bandwidth with commercially available models).

It turns out also, that the tuning range for the harmonic frequencies need to be higher than for the fundamental frequency in order to allow realistic design of class F amplifiers. Due to the insertion loss of the triplexer the tuning range shrinks and limits the application to transistors which require a not too low output resistance. Hence, ideal conditions are found for devices with an output power up to some Watts depending on the technology. Typically the realizable mismatch of the tuner systems is not as high as desired. An alternative is the use of harmonic tuners which do not need triplexers due to their resonant behavior – but the improvement is often too small. Again, the need comes up for an active system to overcome these problems.

In contrary to a passive system, where broadband test signals can be used, harmonic load pull might introduce some restrictions here. Using active loads in an open loop design (compare 3.4) typically limits the range of signals to CW signals. Whereas using closed loop designs allows the use of narrowband modulation it introduces severe stability problems also. This thesis proposes a harmonic load-pull system which guarantees stable loads as well as allows the use for broadband modulation (see section 5.8).

It is also important to note, that designing class F amplifiers absolutely requires appropriate source matching as well to allow highly efficient operation. Since this thesis focuses on the problems and improvements of the harmonic load-pull measurement setup this effect will not be taken into account. Nevertheless, most of the topics discussed for the output side apply for the input side also.

3.4 Active Loads

As already mentioned in the preceding sections, active loads are a solution to overcome problems introduced by insertion loss. This section will give a brief survey on the topic, more details are given in sections 5.7 and 5.8, which both realize active tuner setups.

To understand the active load principle it is required to look at a passive termination in the following way: As long as a load is a linear element its behavior can be described with a complex number, the reflection coefficient Γ , for each frequency. Independent on how the load is realized internally the reflected wave of the load is related to the incoming wave by the reflection coefficient. This means that the termination of the forward travelling wave and the generation of an appropriate backward travelling wave behaves the same way as a passive load. This can be realized in two ways (figure 3.14).

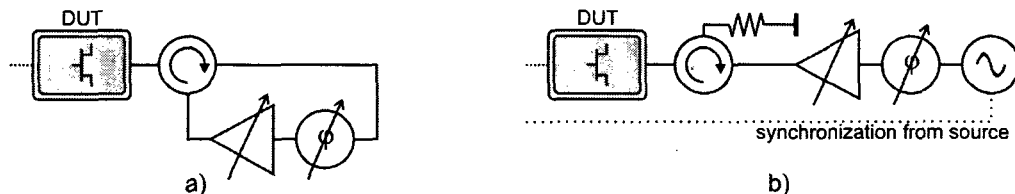


Figure 3.14: Active load realization types

The most intuitive way (figure 3.14a) would be using a circulator (to split forward and backward travelling wave) and apply a variable amplifier and phase shift on the incoming wave before feeding it back into the circulator [7][24]. If the circulator is ideal, the complex gain of the combination amplifier and phase shifter becomes equivalent to the Γ -value of a passive load. By setting a higher gain at the amplifier it is also possible to realize $|\Gamma| > 1$ to compensate for losses in the remaining setup. Of course a directional coupler can also be used instead of the circulator.

Due to the closed loop design new problems arise. Because of a circulator/coupler showing undefined behavior outside its designated frequency band, a high portion of the amplifier's output is fed back into the phase shifter and hence to the input of the amplifier. The loop might start to oscillate! This can also occur inside the frequency band. If high gains of the loop amplifier are needed a small feedback (due to a realistic, imperfect

circulator) can also run the loop into oscillation. This is the major problem of such a design. Filters and often a little bit of 'black-magic' is needed to provide stability for all frequencies (from DC up to the frequency limit of the loop amplifier).

Another restriction which has to be taken into account is the applicability to broadband modulation signals. Section 3.1.2 already showed that a load-pull setup with an electrical length of $l = 1$ m leads to a phase error of $\pm 6^\circ$ for a signal at 2 GHz with a bandwidth of 5 MHz. Because the realization of a closed loop active load requires many components which need to be connected to each other, it happens quite easy that the electrical length of the setup is extended by 2 m or more. This, of course, triples the phase deviation and the corner frequencies at least – the system becomes to inaccurate. Therefore this design allows narrowband modulation only and can be hardly used for UMTS signals.

An alternative realization of an active load is depicted in figure 3.14b). To prevent oscillation the loop must be opened. This can easily be achieved by using an input signal for the amplifier derived from the load-pull setup's input source. If applied for the harmonic frequencies, the input signal is usually generated by frequency doublers and triplers [25] or locked RF sources [26][27]. Both limit the range of signals to CW. A possible solution to extend the application to broadband signals is proposed in section 5.8 of this thesis.

Common for both setups is that additional measurement equipment is needed in order to measure the forward and backward waves to set the gain and phase. Doing an initial calibration of active load systems is often too inaccurate because the components have a gain and phase variation on the used power levels. Especially an open loop design has to track the parameters of the forward travelling wave to generate the requested reflection coefficient. The measurement equipment is not shown in figure 3.14 but is usually a directional coupler and a sampling oscilloscope (very often found in literature is the use of an Agilent Microwave Transition Analyzer, which is a sampler in principle).

Also important to know is that the used amplifier needs to have an output power which is high enough to realize the desired Γ . To achieve $|\Gamma| = 1$ the amplifier must have the same output power as the device under test. Thinking of a realistic setup with insertion losses which have to be compensated the required output level becomes even higher. If the amplifier is further used for modulated signals an additional back-off has to be used to maintain linearity. This can become quite expensive if power levels of 50 W or more are needed. So it is often tried to realize a passive load for the fundamental while using active loads for the lower power harmonic frequencies.

3.5 Prematching, Active Prematching

Another technique to improve the reflection factor is the use of prematching. This can be done by connecting two tuners in series. As a result the impedance transformation ratios are multiplied and allow to realize higher reflection at the input. The first tuner transforms the possible Γ -values of the second tuner into a smaller area which is located closer to the border of the Smith Chart. An exemplary calculation is given in section 4.1. Commercially available prematching tuners integrate two standard tuners in a single unit. A VSWR $> 100 : 1$ ($|\Gamma| = 0.980$) is a typical result. Commercial models are available which guarantee a VSWR $> 150 : 1$ ($|\Gamma| = 0.987$) for frequencies below 10 GHz. But still, having even small insertion losses within the setup leads to an extreme reduction of the achievable VSWR which would require active loads again.

As already stated in section 3.4, the output power needed by the loop amplifier is higher than the one of the device. An improvement can be achieved by active prematching.[28] The idea is shown in figure 3.15 (an open loop design would also be possible). By finding

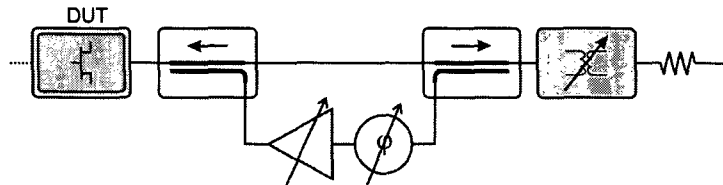


Figure 3.15: Active prematching

the optimum trade-off between low insertion loss of the directional coupler and its coupling value it is possible to achieve reflection coefficients with $|\Gamma| \gtrsim 1$ while requiring an amplifier with less output power than the device under test. The active loop has to support only the small amount of energy because the passive tuner provides the predominant part of it. Such systems are commercially available and will be built to user needs. Of course the same restrictions and problems as for active loads occur.

3.6 Conclusion

The basic ideas of fundamental and harmonic load-pull have been presented within this chapter. The problem of generating comparable results due to undetermined loads at the harmonic frequencies was discussed. This and the need for the design of class F amplifiers led to harmonic load-pull systems.

The analysis of insertion loss effects revealed that the use of active loads is often the only way to achieve high reflection coefficients. By using closed loop active loads it is possible to do measurements with smallband modulated signals only. The bandwidth of such systems is usually too small because of the delay times introduced by the setup. Hence, the application of 5 MHz wide signals like WCDMA is not possible. Also precautions have to be taken in order to keep the loops stable, which is often quite difficult.

An alternative to overcome loop stability problems is the use setups without loops. Such systems are limited to the use of continuous wave signals. To overcome this restriction this thesis will propose a new measurement setup to show how broadband active load-pulling with open loops can be done.

Chapter 4

Realization of a “Harmonic Tuner”

As already shown in the preceding chapter (compare section 3.2) there are two possibilities for performing harmonic load pull. One of them, the active harmonic load pull, uses active components (compare section 3.4) to overcome the impedance limitations introduced by the triplexing filter. Firstly this needs a much more complicated setup than a passive one; secondly there are limitations with respect to broadband signal excitation, power, . . . The alternative solution is a passive only concept by the use of "harmonic tuners" (compare section 5.6).

One of the motivations of this thesis is to show that a harmonic tuner can be realized quite easily without the need for special tools. The performance of this tuner should be comparable to commercially available ones with the exception that it will be designed to a small frequency range (meaning if the center frequency would change from e.g. 2.1445 GHz to 2.3 GHz, new resonators would be needed). Also it was not the intention to perfectly remove the influence of the harmonic tuner onto the fundamental frequency f_0 ; this work only aims on minimizing the mutual coupling as required for typical measurements (see section 4.1). All these constraints are chosen in order not to restrict the range of typical applications of the tuner.

A harmonic tuner has the following ideal properties:

- the fundamental frequency is passed loss-free through the harmonic tuner, thus $|S_{21}| = 1$ for $f = f_0$. The phase of S_{21} is not affected by variation of the harmonic terminations.
- the harmonic frequencies are perfectly reflected by the tuner, thus $|S_{11}| = 1$ at $2f_0$, $3f_0$, . . . The phase of all harmonic frequencies can be controlled separately without mutual influence to other harmonics.

For realizing the harmonic tuner it is of course necessary to move away from the ideal behavior to a realistic one. Also further parameters depending on the targeted measurements have to be defined. Therefore, the following guidelines have been taken into account:

- The fundamental frequency for the application is $f_0 = 2.1445$ GHz (UMTS FDD frequency). The resonator's usable bandwidth should be as high as possible. A

bandwidth $BW > 50$ MHz (to cover 10 UMTS carriers) is preferable. The absolute minimum is of course

- Main focus should be put on a high reflection coefficient at the harmonic frequencies rather than to minimizing mutual influence. First tests have shown that a reflection coefficient for the harmonic frequencies of $|\Gamma_{2f_0,3f_0}| > 0.95$ (corresponds to $1.3\Omega/1950\Omega$) should be possible to realize. According to ‘the factor 10 rule’ (see chapter 2.4) this requires a realizable fundamental impedance of $Z_{f_0} = 10 \cdot (1.3\Omega/1950\Omega) = 13\Omega \dots 195\Omega$, resulting in a requirement of $|\Gamma_{f_0}| > 0.59$ of the complete system (harmonic tuner combined with fundamental tuner). For the planned system setup this requires an input mismatch for the fundamental frequency f_0 of the harmonic tuner of $|\Gamma_{f_0}| < 0.57$. See section 4.1 for the computation of this value. Thus, the design goals of the harmonic tuner were set to $|\Gamma_{2f_0,3f_0}| > 0.95$ ($2f_0 = 4.289$ GHz, $3f_0 = 6.4335$ GHz) and to $|\Gamma_{f_0}| < 0.57$.
- For not constraining the tuning range for the fundamental frequency f_0 by the cascaded fundamental tuner, the input mismatch as well as the loss of the harmonic tuner at $f = f_0$ should be minimized (defined by the power balance $|S_{11}|^2 + |S_{21}|^2 \lesssim 1$). See section 4.4 for more details.
- The tuner should be entirely dismountable. Especially the interchanging of the resonators should be possible without the need for soldering.
- The tuner should be easy to produce: No need for special tools or special parts; the tuner should be producible in the mechanical department of our institute.
- The tuner shall be made of standard materials: Special coatings, absorbers, ... should be avoided.

4.1 Required Impedances, VSWRs, ...

Inserting a harmonic tuner between the DUT (device under test) and the fundamental tuner requires that the performance of the fundamental tuner will ideally not be degraded. For a practical setup the amount of acceptable degradation has to be determined; allowing some influence on the fundamental frequency f_0 by the harmonic tuner of course eases up its design.

This chapter will deal with the calculation of the acceptable VSWR of the harmonic tuner for the frequency f_0 . To do this, the relationship between the reflection coefficient Γ , the load impedance Z and the VSWR (voltage standing wave ratio) shall be recapitulated (formula 4.1 and 4.2), with the reference Impedance set to $Z_0 = 50\Omega$.

$$\Gamma = \frac{Z - Z_0}{Z + Z_0}, \quad Z = Z_0 \cdot \frac{1 + \Gamma}{1 - \Gamma} \quad (4.1)$$

$$\text{VSWR} = \frac{1 + |\Gamma|}{1 - |\Gamma|}, \quad |\Gamma| = \frac{\text{VSWR} - 1}{\text{VSWR} + 1} \quad (4.2)$$

This relationship can also be represented in a graph (figure 4.1). Please note that two solutions for the impedance, Z_{\min} and Z_{\max} are given value of $|\Gamma|$ or VSWR . The reason

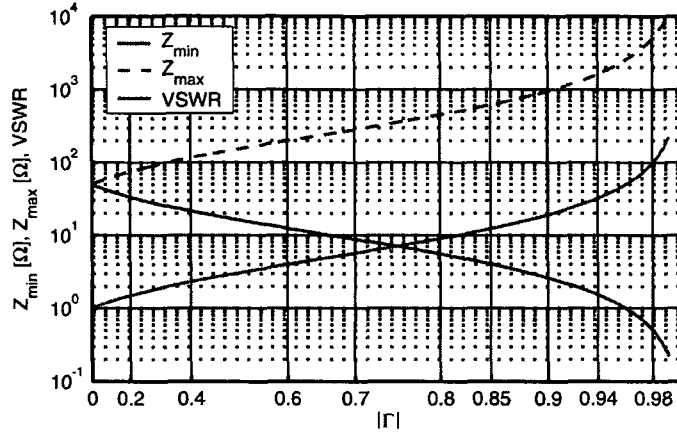


Figure 4.1: Figure: Relationship between $|\Gamma|$, VSWR, Z_{\min} and Z_{\max}

for this is that gamma only defines the radius of a circle in the Smith Chart. Z_{\min} and Z_{\max} , therefore, indicate the minimum and maximum realizable real impedance (corresponds to the intersection of the $|\Gamma| = \text{constant}$ circle with the horizontal axis in the Smith Chart).

Calculating the reflection coefficient of two tuners connected in series, requires a mathematical model. As measurements on commercially available tuners as well as on the realized prototype have shown that the tuners have very low loss, meaning $|S_{11}|^2 + |S_{21}|^2 \lesssim 1$. Hence, the tuner can be modeled as an ideal transformer with variable transformation ratio and a phase shifter (of course with different values for each frequency). Further simplification of the calculation can be achieved by neglecting the phase shifters (this does not give wrong or inaccurate results, as explained afterwards). This leads to a model according to figure 4.2 for the in series connection of two tuners; the harmonic tuner (HT), which is at the DUT side, and the fundamental tuner (FT).

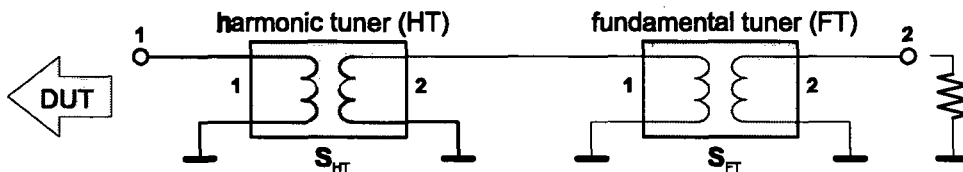


Figure 4.2: Model of two lossless tuners connected in series

Why does this lead to a reduced tuning of the entire setup? Let's assume that the harmonic tuner has a winding ratio of 1:2 (transforming a $50\ \Omega$ impedance on port 2 into $12.5\ \Omega$ on port 1, as transformation of resistances is proportional to the square of the winding ratio). If the fundamental tuner also has a winding ratio of 1:2, the $50\ \Omega$ load is transformed into a $12.5\ \Omega$ one in between both tuners and by the harmonic tuner further down into a $3.125\ \Omega$ impedance on the DUT side. This is exactly what happens inside a prematching tuner: the cascade of two tuners for further increasing the achievable reflection coefficient. But what would happen if the harmonic tuner would have a ratio

of 2:1 (thus, uptransforming the impedance)? The two tuners would perfectly cancel out and an impedance of $50\ \Omega$ would be seen from the DUT side (This would be a combination where a prematching tuner does not make sense at all).

Therefore, the influence of the harmonic tuner on the fundamental wave can only be canceled out by a fundamental tuner with the same transformation ratio. To further enable load pulling at the fundamental frequency, the harmonic tuner must have a higher VSWR than the harmonic tuner at f_0 to achieve an overall transformation to higher- as well as to lower impedances. But a tuner also needs to influence the phase. Assuming a variable phase shift between the two tuner blocks results in achievable impedances like given in the blue contour in figure 4.3. It can be seen from the graph that the fundamental

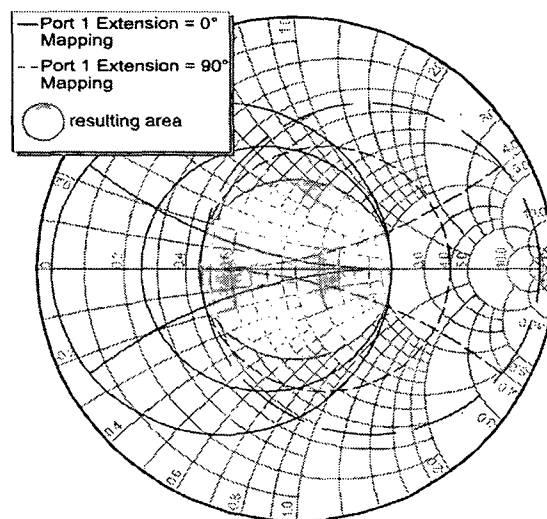


Figure 4.3: Realizable Impedance of two Tuners connected in series

tuner chosen for example has a higher transformation ratio (from 3:1...1:3) than the harmonic one (about 2:1...1:2) and can, therefore, result in extremely small impedances (prematching case, overall transformation 1:6) as well as in impedances larger than $50\ \Omega$ (overall transformation of 1:1.5). Further extending port 1 of the complete setup by a 90° -delay line (resp. a $\frac{\lambda}{4}$ -transformer) gives the opposite picture (see red contour in figure 4.3); now an overall transformation ratio ranging from 1.5:1...1:3 becomes possible. The ratio of 1:3 is again the prematching case, giving now an extremely high impedance.

Now it becomes quite clear that a harmonic tuner that influences the fundamental frequency f_0 results in a prematching behavior for the actual fundamental tuner. Depending on the phase-shift between the two tuners as well as on the phase-shift on port 1 of the harmonic tuner, only impedances within the green area in figure 4.3 can be realized in case of unknown phase-shifts. Of course much higher reflection coefficients can be realized if the phase-shifts are favorable – but only the green area can be guaranteed all the time. It is not possible to arrange the phase-shifts within a tuner system for realizing a higher VSWR without changing the desired reflection factor at the fundamental or at the harmonic frequencies – there is unfortunately no degree of freedom left, which would allow this .

Since it was the design goal to realize a harmonic tuner with a reflection coefficient for the harmonic frequencies of $|\Gamma| > 0.95$ (which is equivalent to an impedance range of $1.28\ \Omega \dots 1950\ \Omega$), the fundamental frequency tuning range should be a tenth of this: $12.8\ \Omega \dots 195\ \Omega$. This ensures that a low resp. a high impedance at the harmonic frequencies is quasi equivalent to a short resp. open (see chapter 2.4). Figure 4.4 shows a graph, which shows the minimum achievable impedance of the series connection of harmonic tuner and the fundamental tuner. Knowing that the VSWR of the fundamental tuner is 1:15 (a

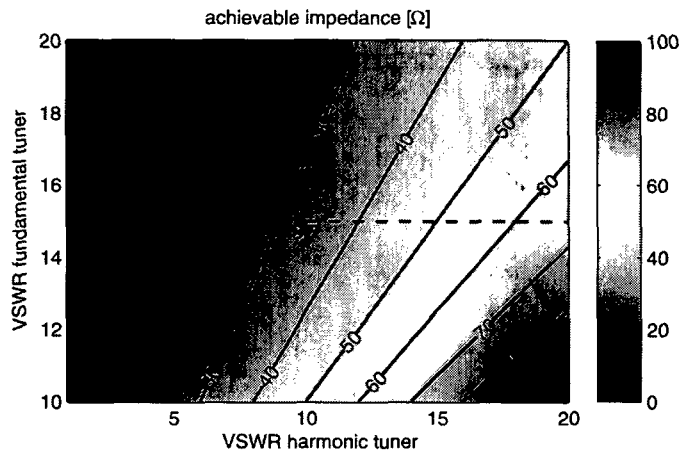


Figure 4.4: Achievable tuning impedance of two tuners conneted in series

Maury Microwave MT982A02 [17] tuner), assuming a required impedance of $12.5\ \Omega$ results in a maximum VSWR of 1:3.7 of the harmonic tuner. This corresponds to a reflection coefficient of $|\Gamma| \leq 0.574$ (equals $-4.815\ \text{dB}$). This is the design guideline which must be necessarily fulfilled for the realization of the harmonic tuner.

4.2 Selection of the Transmission Line Type

To realize such a type of tuner, resonators for each harmonic frequency have to be used. Because of the application of such tuners – the design of harmonic controlled amplifiers – there is no need to change the magnitude of the reflection coefficient and, therefore, the coupling of the resonators need not to be changed. What is important for tuning is the variation of the phase of the harmonic terminations. Hence, a structure allowing to move the position of the resonators respectively the phase of the harmonic terminations is needed. Thus a line has to be used which can be accessed from outside (for mechanical movement of the resonators). Closed structures like a coax cannot be used. The decision for an appropriate transmission line was made from the following choices:

- **Slotted Coax** (figure 4.5a): This structure provides good shielding (a closed coax is self-shielding). An application for a harmonic tuner would require air as dielectric to allow mechanical movement along the structure. Further, a resonating element which fits inside the structure is required, which cannot be accomplished easily. If the mantle is opened wider to allow placement of the resonator outside, a troughline or a

wire above ground should be preferred due to their much easier fabrication. Slotted coaxial lines find their application for standard tuners because this type of tuners only needs a reflective element (e.g. a dielectric ring in an air filled slotted coax which can be easily manufactured) with no distinct resonance. Other applications include E-field sensing along the line for VSWR determination. The characteristic impedance is given in [29].

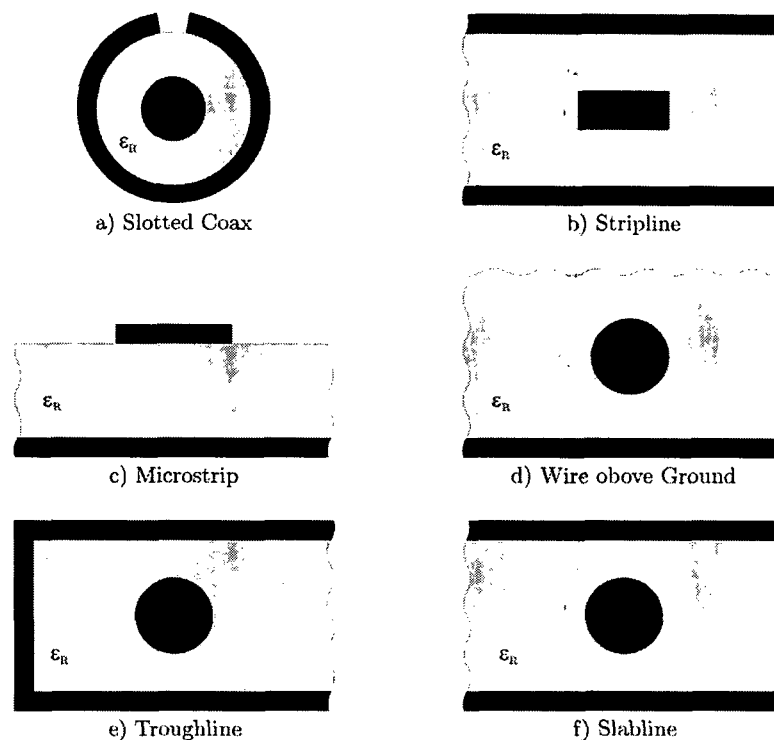


Figure 4.5: Different types of transmission lines

- **Stripline** (figure 4.5b): The stripline configuration is often used in microwave circuits due to its excellent shielding. An application for harmonic tuners would be possible but requires transitions from a rectangular cross section to a round one at the connectors. This requires milling as well as turning of the conductor¹. Also sliding contacts are easier to manufacture for a round cross section². It is, therefore, not used for the harmonic tuner in this thesis in terms of keeping the construction as simple as possible. Impedance formulas for zero thickness as well as finite thickness

¹The realized harmonic tuner will have an airline interface for the connectors. This requires a round center conductor. Of course, a rectangular cross section can also be connected to a connector but requires soldering in contrary to an airline connector. See section 4.6.1 and 4.6.2 for details about the airline and the connectors.

²To achieve high reflection for the harmonic frequencies a strong coupling between the transmission line and the resonator is required. To get rid of the need for small mechanical tolerances (e.g. to keep coupling constant/high for a capacitively coupled resonator) a sliding contact will be used for the realised tuner. See section 4.6.5 for details on the resonator.

microstrip lines are given by [30].

- **Microstrip** (figure 4.5c): The greatest benefit of the microstrip structure is that it can be accessed from outside, even when using a dielectric. In contrary to the other structures – where air filling is necessary for harmonic tuner application – this makes positioning of the conductor quite easy. If produced on a copper plated microwave substrate it is important to use materials with a small loss tangent in order to minimize the insertion loss. For better performance an air dielectric can be used. Shielding is not optimal because of only one ground plane. Impedance formulas are given in a lot of papers; worth mentioning is [31], which bases on an excellent analytical formulation of the problem. Formulas including dispersion effects are given in [32], the necessary corrections for finite conductor thickness are found in [33].
- **Wire above ground** (figure 4.5d): When using a microstrip or a wire above ground transmission line the latter one is preferable for tuners using sliding contacts. Since this structure is quite similar to a microstrip line the same problems in terms of shielding occur.
- **Troughline** (figure 4.5e): Depending on the distance of the center conductor to the left ground plane in figure 4.5e the major part of the electric field is concentrated on the left hand side in the figure. Therefore shielding is quite good (of course depending on the extension of the upper and lower sidewalls). Due to its round conductor the transition to an airline interface is easy to accomplish. A troughline would be a good solution for tuners. Formulas for the characteristic impedance are found in [34], more accurate ones are [35] (both papers give formulas for the slabline also).
- **Slabline** (figure 4.5f): Increasing the distance of the center conductor of a troughline to the left sidewall leads to a so called slabline. Again, the shielding is quite good if the sidewalls are wide enough. Also the round center conductor allows a simple transition to an airline interface. The benefit of this structure, in contrary to a troughline, is the accessibility of the center conductor from both sides. It is suitable for harmonic tuners and will, therefore, be used for the realization. The first formulas for impedance calculation are given in [34], more accurate ones can be found in [35] (both papers give formulas for the troughline also).

Finding a trade-off between good shielding properties and good accessibility of the center conductor led to the selection of the slabline structure for the harmonic tuner. Due to its symmetric geometry the E-field in the middle of the slabline (in a plane parallel to the sidewalls) is zero; therefore, placing of a resonator within this plane should not influence the slabline’s behavior for frequencies beside the resonance³. Also a mechanical handle for moving the resonator could be placed in this plane.

³Of course, this would be true for an infinitely small resonator structure only. Due to the relatively small electric field, a finite thickness of the resonator should not result in too much changes of this ideal behavior.

4.3 The Slabline

The characteristic impedance of an ideal⁴ slabline can be analytically approximated by a "zero order" logarithmic term minus a "second order" correction term, given by [35]:

$$Z_0 = Z_{fs} \cdot \left[\underbrace{\frac{1}{2\pi} \ln \left(\frac{2}{\pi R} \right)}_{\text{zero order term}} - \underbrace{\frac{0.2153R^4}{1 - 5.682R^4}}_{\text{second order term}} \right] \quad (4.3)$$

$$Z_{fs} = \sqrt{\frac{\mu_0}{\varepsilon_0}} = 376.730 \Omega \quad (4.4)$$

with the geometry factor $R = \frac{d}{2D}$, $0 < R < 0.5$ (geometry shown in figure 4.6a). Z_{fs} denotes the free space impedance (free space permeability $\mu_0 = 1.257 \mu\text{H/m}$, free space permittivity $\varepsilon_0 = 8.854 \text{pF/m}$). The "second order" correction term amounts to about 0.3Ω for $Z_0 \approx 50 \Omega$ and can be neglected for a rough estimation of the slabline impedance. Further improving the accuracy requires using a "fourth order" correction term [35], which gives an accuracy of about $1 \text{m}\Omega$ for $Z_0 \approx 50 \Omega$. Off-center displacements of the conductor can be taken into account by a "third order" correction term. The equations given by [35] are kept this general that they can also be applied for trough lines.

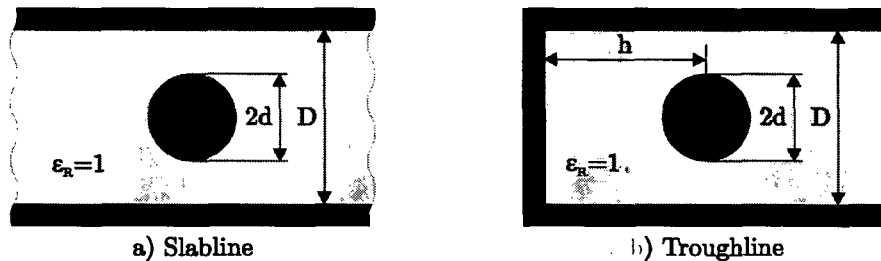


Figure 4.6: Slabline and troughline dimensions

The slabline impedance for different geometries is depicted in figure 4.7. Formula 4.3 is further solved for typical impedance values and the corresponding geometry factor R is given in table 4.1.

slabline impedance Z_0 [Ω]	slabline geometry R
25	0.4024
50	0.2743
75	0.1820
100	0.1201

Table 4.1: Slabline geometries for typical impedances

⁴no dielectric losses, perfectly polished surfaces (no surface roughness), perfect conductors (no field penetration)

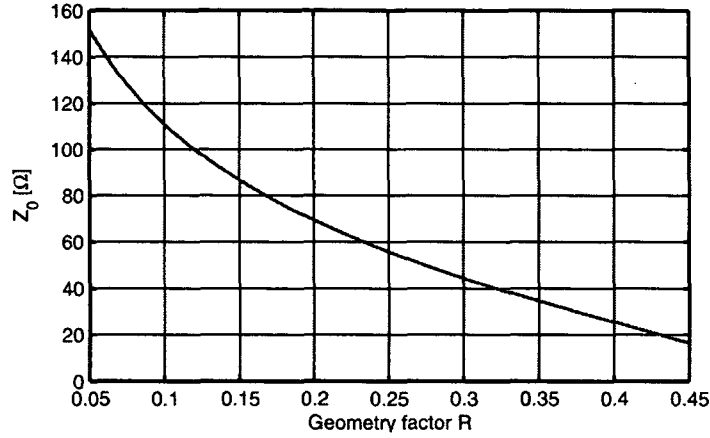


Figure 4.7: Slabline impedance

For the realization of the slabline the geometry factor was set to $R = 0.2743$ to achieve $Z_0 = 50 \Omega$.

Because it is not possible to realize an infinite ground plane it is necessary to get an estimate on how a finite ground plane would influence the behavior of the slabline. This can be approximated by inserting a third ground wall – which is connected to the both existing ones – and look at the change of the characteristic impedance. The now generated transmission line corresponds to a troughline (figure 4.6b). Assuming $\frac{h}{D} = \frac{3}{4}$ gives a characteristic impedance according to formula 4.3 [35]:

$$Z_0 = Z_{fs} \cdot \left[\frac{1}{2\pi} \ln \left(\frac{2}{\pi R} \tanh \left(\frac{3\pi}{4} \right) \right) - \frac{0.0005068R^2 + 0.1714R^4 - 0.322R^6}{1 - 1.822R^2 - 6.559R^4 + 11.80R^6} \right] \quad (4.5)$$

For the chosen slabline geometry $R = 0.2743$ this results in $Z_0 = 49.01 \Omega$ (which corresponds to a mismatch of $|\Gamma| = -40$ dB). It becomes quite clear now that a limited ground plane does not severely affect the design. Thinking about the resonators – which will be stubs perpendicular to the conductor (compare section 4.4) – a maximum length for the second harmonic stub at $f = 2f_0 = 4.289$ GHz is estimated by $\frac{\lambda}{4} = \frac{c_0}{4 \cdot 2f_0} \approx 17.5$ mm. Assuming a slabline conductor diameter of $2d = 5$ mm gives a conductor height $h \approx 6.8$ mm for the tested troughline configuration ($\frac{h}{D} = \frac{3}{4}$). Therefore, the resonator length will determine the slabline dimension for achieving proper shielding.

4.4 The Resonator

After defining the type of the transmission line, a realization must be chosen for the resonator. On the one hand, the resonator should have a large bandwidth to allow load pull measurements of wideband amplifiers or at different center-frequencies. On the other hand the bandwidth must be limited to reduce the influence onto the other harmonic resonator or onto the fundamental frequency. The decision for the resonator’s type of construction was made by considering the following options:

- **Crystal resonator:** This element would allow a precise selection of the harmonic frequencies without the need for tuning. The main drawback for the desired application is its extremely small bandwidth. Harmonic load pull measurement would, therefore, be limited to single carrier operation. Hence, a crystal oscillator was not used.
- **LC-circuits:** With an LC-resonator lower Qs are achieved, thus allowing the application for broadband signals. Tuning to a center frequency can also be achieved by the use of adjustable capacitors. Similar to the crystal resonator, a sliding contact to ground is needed. An application for the harmonic tuner would be possible but requires an additional contact to ground respectively to the slabline’s sidewalls. The design of the resonator might lead into problems due to very limited space between the slabline’s sidewalls. The requirement for an additional small RF-circuit board was also a reason for discarding this idea.
- **Cavity resonators:** Due to the need of an extra mechanical construction (with tight tolerances) and a sliding ground contact this possibility was dismissed. The benefit of cavity resonators is the possibility to tune the resonance within a small range.
- **$\frac{\lambda}{4}$ -stub with open end:** As a very simple alternative a stub can be mounted on the slider. By choosing an appropriate length of about $l = \frac{\lambda}{4}$ the open end will be transformed into a short at the transmission line and will, therefore, work as a good reflection. By varying the stub thickness a change of the bandwidth should be achievable. The mechanical construction requires only soldering a rigid cable perpendicular onto the slider. Tuning can be done by step by step cutting of the wire length. Also an additional contact to the sidewalls of the slabline is not necessary. The only drawback is that the resonant frequency must be tuned with the resonator mounted inside the slabline. Taking the resonator outside would change the field configuration and thus the resonant frequency. Nevertheless, this configuration will be used for the sake of mechanical simplicity.

Especially the resonator needs a prototype realization. The influence of the reflection factor on the fundamental frequency f_0 as well as on the other harmonic frequency has to be analyzed. Also the bandwidth and the achievable reflection factor have to be determined.

4.5 Prototype (Proof of Principle)

Because of the fact that the Microwave Group at the Institute for Electrical Measurements and Circuit Design did not have a license for a full 3D-simulator a prototype had to be realized. With this prototype the harmonic tuner was undergone some fundamental tests to see if the concept would work. After measuring the prototype it can be decided either to stop the project or to invest money in a field simulator for a further optimization of the final design. This section will explain the harmonic tuner prototype and will outline the most important measurement results. The results are listed quite briefly because the prototype harmonic tuner’s only purpose was to proof that the idea would work. More detailed measurements, performance data as well as construction drawings will be given for the finally realized tuner only.

4.5.1 Construction of the Prototype

Before realizing a prototype some decisions have to be made: First of all a material must be chosen, also connectors as well as the transition from the connectors to the slabline has to be planned. The following text will explain how these decisions have been made:

- **Material:** The selection of the material to be used was made under several criteria:
 - **Conductivity:** To minimize losses of the harmonic tuner, a material with a high bulk conductivity is needed.
 - **Non-magnetic:** The material has to be non-magnetic. Magnetic materials could lead to problems with the resonator movement.
 - **Machinability:** The material should provide excellent milling/turning properties.
 - **Solderability:** For the assembly of the sliding resonator as well as for the mounting of the connectors, the material should be solderable.

Having a look at different non-magnetic materials’ bulk conductivity in table 4.2 and excluding noble materials, copper turns out to be the optimum candidate. Taking, however, into account that copper highly tends to oxidize leads to an exclusion of copper. The next possibility, alumina, cannot be used because it is not solderable. Therefore, the choice fell onto brass which has still a high bulk conductivity. Stainless steel, which is ranked last in table 4.2 should only be used when being plated with a high conductivity layer of e.g. silver.

material	bulk conductivity [S/ m]
silver	$61 \cdot 10^6$
copper	$58 \cdot 10^6$
gold	$41 \cdot 10^6$
aluminium	$35 \cdot 10^6$
brass	$15 \cdot 10^6$
stainless steel	$1 \cdot 10^6$

Table 4.2: Bulk conductivity of non-magnetic materials

- **Slabline:** As the slabline’s characteristic impedance is defined by the ratio $R = \frac{d}{2D}$, either the center conductor diameter or the ground-plate distance has to be defined. The selection fell onto the determination of the center conductor: The diameter is limited in both directions because of the following reasons:
 - A too small conductor diameter would result in the need for very precise manufacturing and assembling. This is because the milling/turning tolerances and assembly displacements remain the same for smaller parts; therefore, the relative error becomes higher and higher. This would result in a non 50Ω characteristic impedance of the slabline and maybe in increased losses. Also, a non parallel alignment of the two ground-plates and the center conductor would result in an increasing or decreasing impedance along the slabline

- Using a too thin conductor becomes mechanically too instable and would tend to sag between its mounting points, i.e. both connectors. Also, the conductor could be bent much easier by mistake. Again this would result in a non $50\ \Omega$ impedance, which might be varying up and down along the slabline due to a bent center conductor.
- Having a too large diameter would favor the propagation of higher-order modes (non TEM-modes) in the slabline. This could lead to increased losses as well as mismatches.
- A too thick conductor has more weight. Due to the planned mounting of the center conductor between the connectors without any additional fixations, this could give to much load on the connectors, possibly resulting in breaking the connectors.

After empirically testing the bending strength of different brass rods it turned out that a diameter of about $2d > 3\text{ mm}$ should be thick enough for convenient handling and mechanical robustness for a slabline length of $\approx 15\text{ cm}$. Placing a sliding contact on the center conductor required a larger diameter due to the mechanical construction of the slider. Hence, the center conductor diameter was defined to be $2d = 5\text{ mm}$, which is also a standard diameter of commercial available brass rods (and therefore reduces the need for turning the center conductor to target diameter, which is mechanically complicated due to its extreme aspect ratio). The construction is depicted in figures 4.8 and 4.9. As shown in figure 4.8 the tuner’s slabline walls are made of a $10\text{ cm} \times 5\text{ cm} \times 1\text{ cm}$ blocks, supplemented with the 15 mm long transition elements on both sides. To ensure that the walls are mounted parallel with the calculated distance of 9.11 mm , both slabline walls are combined by end parts on both sides which allow an accuracy of adjustment of about $\pm 0.1\text{ mm}$. Assembling was done by inserting two 9.11 mm -blocks on both sides of the inner conductor to ensure correct distance and parallelism.

The center conductor was made of a $5\text{ mm}\varnothing$ brass bar stock material. Hence, there was no need for turning of the $\varnothing 5\text{ mm}$ -region of the center conductor. This made manufacturing much easier, because achieving a constant diameter along a small, long rod requires a very exact adjustment of the drilling machine in order to prevent cone-shaping of the conductor (also a curved conductor could result, if the brass rod is not perfectly kept in position with additional guiding rolls during machining). Thus only the ends of the rod need to be machined for the transition.

- **Connectors:** For the sake of simplicity SMA flange-connectors with soldering tabs were used (Radiall R124.510.000, square flange jack receptacle with a 2.54 mm long, $1.27\text{ mm} \times 0.13\text{ mm}$ tab contact). The ends are further slotted with a 0.2 mm circular saw to enable fitting onto the connector’s tab. The left part of figure 4.10 shows the center conductor’s slot at the end to house the SMA connector’s tab. Because of the small inner conductor diameter of the SMA connector of 1.27 mm a transition to the 5 mm slabline becomes necessary.
- **Connector to slabline transition:** Because of having no license for a 3D-EM simulator at this time a very simple approach for the transition was chosen. The

50 Ω -slabline ($2d = 5$ mm, $D = 9.11$ mm) will be reduced towards its ends to 50 Ω -slabline with $2d = 1.27$ mm and $D = 2.31$ mm to fit the SMA connector’s dimension (see figures 4.8 and 4.9).



Figure 4.8: Photograph of the partly assembled prototype

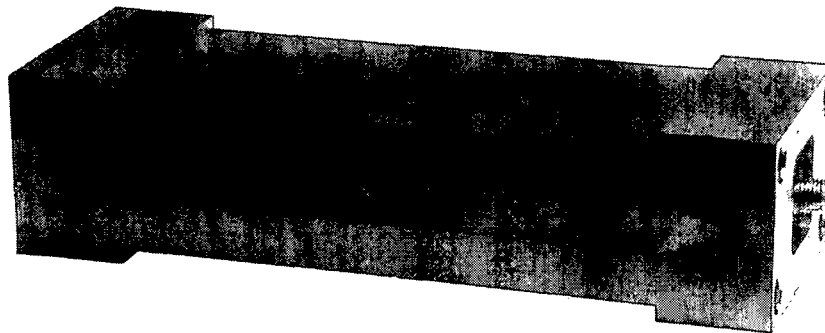


Figure 4.9: Photograph of the finally assembled prototype (without resonator)

- Slider with resonator:** For the reflection of the harmonic frequencies a resonator tuned to $f = 2f_0$ resp. to $f = 3f_0$ is necessary. For a high reflection coefficient a galvanic coupling of the resonator to the slabline’s conductor was chosen. To accomplish this, a slider was manufactured (see figure 4.10). The slider consists of a brass sleeve with spring contacts at each end (manufactured by multiply slotting the sleeve with a 0.2 mm circular saw at both ends). The slider’s geometry was empirically designed in order to achieve smooth gliding on the slabline’s inner conductor. The outer diameter of the brass sleeve was kept as small as possible (≈ 6 mm at the ends when assembled with inner conductor, ≈ 5.8 mm unassembled due to displacement of the contacts), to reduce its influence of the behavior of the slabline. The resonating $\frac{\lambda}{4}$ -stub was realized by a standard copper wire, soldered perpendicular onto the slider (see figure 4.11). Attention was paid to use as little solder as possible.

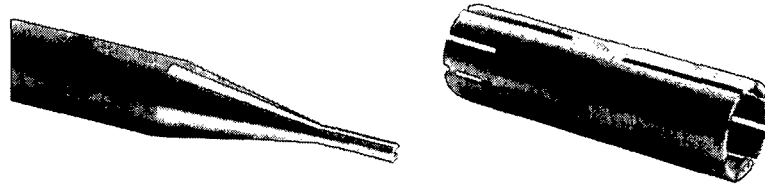


Figure 4.10: Photograph of the prototype’s inner conductor (left) and the slider (right)

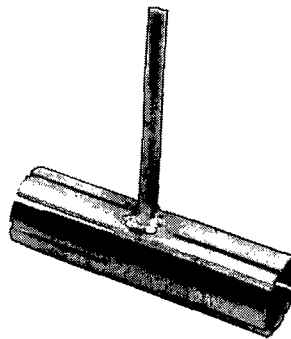


Figure 4.11: Photograph of the prototype’s resonator mounted on slider

4.5.2 Findings of the Prototype

It should be stated firstly that the prototype was used for evaluating the concept of a harmonic tuner. Some ideas – especially concerning the design of the sliding resonator – were investigated.

- **Loss of slabline:** It was not quite clear if the surface roughness (from milling the slabline walls) is low enough to ensure negligible damping of the travelling waves. Therefore, the insertion loss of the tuner (including both coax-slabline transitions) was measured two times. Firstly the structure was assembled how it came from the milling machine. Secondly, the center conductor as well as the sidewalls were ground and polished until the surface became mirroring. No performance increase could be observed. \implies no further steps have to be done for the final design.
- **SMA to slabline transition:** Further the resonator’s S_{11} was measured for different slider positions. It turned out that the realizable reflection coefficient was dependent on the resonator’s position and repeated with $\frac{\lambda}{2}$ -increments of the position (without any degradation depending on the distance to the connector; also an indicator that the slabline is quasi lossless). This was a clear indicator for a mismatch/losses in the region of the coaxial connector to the 5/9.11 mm-slabline transmission. To detect the position of the mismatch, a broadband vector network analyzer measurement was carried out to allow equivalent time domain reflectometry (TDR). This showed that the problem was exactly located at the SMA connector’s plane (where the coaxial mode ends). Therefore, the soldering joint to the slabline conductor was overworked in order to remove excessive solder and have perfect roundness. This resulted in

a slight performance increase but still not in optimum values. It seemed that the problem might be the small gap between the slabline’s conductor front and the SMA connector. This could not be perfectly filled with solder due to the construction of the SMA connector. \implies some re-engineering is required here.

- **Slider with resonator:** It was the most critical point to check if the reflection coefficient is as high as required. Tests with different resonator lengths have shown that the reflection coefficient was always higher than 0.97 (slider positioned in order to minimize influence of transition mismatch). No repeatability problems could be observed which shows that the contact has good quality. Further the ease of tuning was tested: this can be quite simply accomplished by piecewise cutting the length of the resonator when placed inside the slabline with a wire cutting tool. The bandwidth proved to be high enough that the desired frequency can be achieved within minutes. If the wire was cut a little bit too short by accident, putting some solder onto the wire’s end proved to be a good corrective. The high bandwidth also pointed out that there might arise problems with the necessary influence onto the fundamental wave. \implies maybe some rework necessary.
- **Connectors:** Beside the problem of the mismatch it would be preferable to have a connection system which does not require soldering. It has proven to be quite unhandy to unsolder the connectors each time another slider should be placed on the line. Also the reproducibility suffers from the solder connection. Further it turned out that a small connector (corresponds to small airline dimensions for the transition) is quite tricky in terms of centering between the slabline walls. Measurements have shown that a small displacement of ± 0.2 mm does not increase the losses ($|S_{11}|^2 + |S_{21}|^2$ remained constant) but of course influences the slabline’s impedance and, therefore, the mismatch of the coax-slabline transition. \implies a connector system with larger dimensions should be used; screw-mounting would be preferable.
- **Mechanical displacements:** To have an idea on the required tolerances for machining the harmonic tuner, some test with respect to mechanical tolerances were made. Changing the distance between the slabline walls by ± 0.1 mm did not show a significant change in the $|S_{11}|$ of the tuner (this was done by multiple disassembling and reassembling of the slabline without the 9.11 mm-blocks, so parallelism was also not guaranteed). Also the need for positioning exactness of the resonator was tested: It turned out that tilting the stub towards the center conductor of $\approx 10^\circ$ did not result in a degradation of the achievable reflection coefficient. On the contrary, a tilt toward the slabline’s ground wall of $\approx 5^\circ$ showed a small shift of the resonating frequency (due to the change in the capacity) and, therefore, a degradation of the reflection coefficient at the desired frequency. Tests have shown that the tilt should be $< 2^\circ$ to have negligible influence ($|\Gamma|$ still > 0.96). \implies no further steps with respect to machining and assembly tolerances have to be made for the final design. (assuming a larger connector system)

4.6 Final design (3D-Field-Simulator supported)

Because of the very promising results gained from the prototype measurements, a licence for a three-dimensional field simulator was obtained to further investigate and improve the tuner’s behavior before the final mechanical realization. The choice fell on the product "HFSS" (high frequency structure simulator), release 9.0, from Ansoft Corporation [36]. HFSS is a full 2D/3D electromagnetic field solver based on the finite element method (FEM). It consists of an AutoCAD-compatible 3D modeler with the ability to parametrize the entire geometry. It allows the calculation of all fields, port parameters, near- and far field antenna patterns. Optional capabilities allow parametric simulation, sensitivity analysis as well as optimization of parameters.

By the use of a 3D EM simulator the following questions should be answered:

- Behavior of the slabline under real conditions
- Selection of the connector type
- Optimizing the coaxial to slabline transition
- Performance of the resonator
- Application of a mechanical handle to the resonator

The listed topics will be addressed in more detail in the following subsections.

4.6.1 Selection of Connector Type

As already mentioned in section 4.5.2, a connector system with larger dimensions should be used to overcome tolerance problems when assembling the harmonic tuner. Of course a commercially available connector should be used, which reduced the range of products to the following three types:

- 7/16 or similar type connector: This range of connectors features the application in high power broadcast applications. Large connector dimensions are required in order to withstand the high currents. Due to their large diameter of the inner conductor (7 mm for the 7/16-system) the transition to the 5 mm \varnothing conductor of the slabline can be easily realized without tolerance problems due to misalignment. These connectors have a maximum usable frequency of $f = 8$ GHz, reproducibility is not guaranteed. Only designs which require soldering are available. Adapters to other connection systems are available but not very common. This connector type is, therefore, not recommended for the application.
- N-type connector: This widely used connector would be a good choice due to its large inner conductor. The inner connector is typically soldered – also precision designs supporting the standardized 7 mm airline interface (figure 4.12b) exist. Maximum usable frequency is $f = 18$ GHz, adapters to other connection systems are standard products. Application of precision N-type connectors with airline interface for the harmonic tuner would be possible.

- APC-7 connector: This Amphenol precision connector (APC), standardized by IEEE-STD. 287 (also named RPC-7, PC-7, GPC-7, Prefix AA, ...) is a hermaphroditic (sexless) coaxial connector with very high reproducibility (higher than precision-N). Again, this connector is available in solder designs as well as screw-design for the 7 mm airline interface (figure 4.12). Maximum usable frequency is $f = 18$ GHz, adapters to other connection systems are standard products. Application of APC-7 for the harmonic tuner can be recommended.

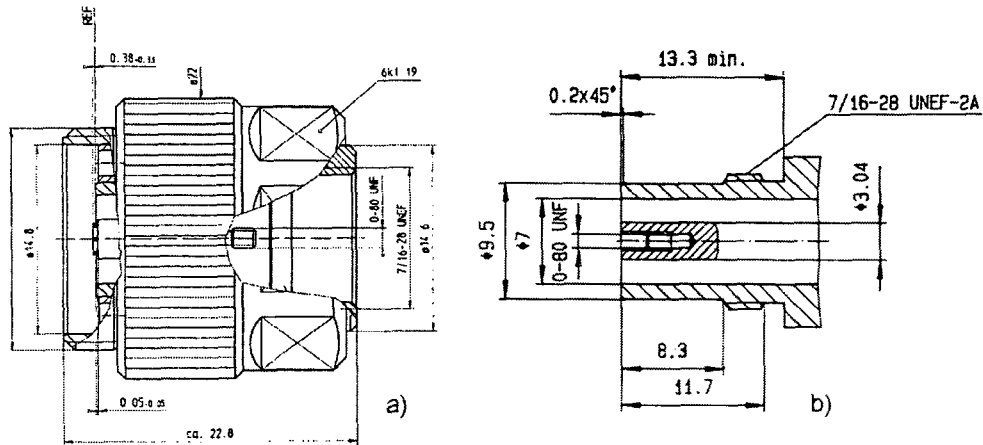


Figure 4.12: APC7-connector (a) and 7mm airline (b) [37]

Finally it was decided to realize the harmonic tuner with 7mm airline interfaces on both ends. This allows mounting of precision N-type as well as APC-7 connectors. Since the harmonic tuner will be connected in series with an existing APC-7 connectorised fundamental tuner, the choice fell onto the APC-7 connectors. These connectors give very high reproducibility, do not require soldering and can be changed to an N-type connector within one minute if required. The connector used was an APC-7-compatible RPC-7 connector (Rosenberger precision connector [37]). The connector and the standardized 7mm airline interface are shown in figure 4.12.

For additionally checking this decision, 3D field simulations for different connector resp. transition types were performed: For comparison a 7 mm PTFE-coax, a 7 mm airline and a 3 mm airline – all with 50Ω impedance – were simulated. To calculate for the required dimensions the impedance formula for a coaxial line (formula 4.6) can be reversed.

$$Z_0 = \frac{Z_{fs}}{2\pi\sqrt{\epsilon_r}} \ln\left(\frac{R_o}{R_i}\right) \quad (4.6)$$

with R_o , R_i giving the outer and inner diameter and Z_{fs} denoting the free space impedance (see formula 4.4). The properties of the three connector types (resp. the type of the coaxial transmission line inside the connector) are shown in table 4.3 Now, the transitions from all three line types to a slabline (9.11 mm / 5.0 mm) were calculated with the 3D field simulator. For the simulation a structure according to figure 4.13 was realized. The structure shows only one quarter of the transition due to its symmetry (this can also be used

connector's line type	dielectric	ϵ_r	R_o [mm]	R_i [mm]
7 mm airline	air	1	7.00	3.04
3 mm airline	air	1	3.00	1.30
7 mm Teflon-filled coax	Teflon	2.1	7.00	2.09

Table 4.3: Coaxial Line Geometries used for Transition Simulation

for speeding up simulation by inserting perfectly H-planes into the simulation ($\mu_r = \infty$). All brass parts (coaxial ground and slabline ground) are brown colored; the air inside is shown in light blue. Each transition was optimized for having a good input matching (see

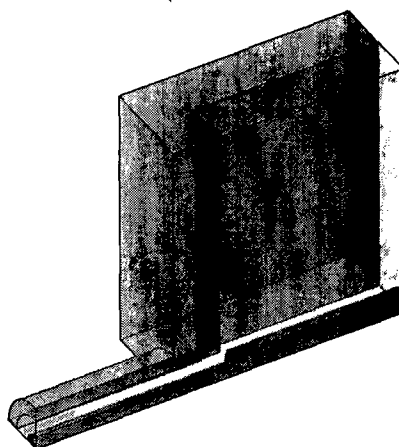


Figure 4.13: 3D-Structure for coaxial to slabline transition simulation

chapter 4.6.2 for details on the optimization). The results are given in figure 4.14 and 4.15. It can be seen from figure 4.14 that all three types have a return loss better than 24 dB which is high enough for the intended application⁵. The oscillating behaviour of the curves in the region 0 . . . 7 GHz is due to the allowed tolerances in the 3D field simulator. If higher accuracy is required, the meshing of the field simulator must be refined more and more until the S-parameters of the result become stable enough. Since this would exponentially increase the memory requirements as well as the simulation duration an acceptable trade-off between accuracy and simulation complexity was chosen for each simulation. Nevertheless, figure 4.14 shows that the 7 mm airline has the lowest insertion loss. To probe further, figure 4.15 shows the loss of the transition. Since all energy which is sent into a lossless two-port must be either reflected or transmitted, meaning $|S_{11}|^2 + |S_{21}|^2 = 1$. If this equation results in values less than 1, the missing part $1 - (|S_{11}|^2 + |S_{21}|^2)$ equals to the relative power loss, ranging from 0 (lossless) to 1 (perfectly matched, energy entirely lost). The loss is a much more important design criterion for the harmonic tuner than the input matching. This is the case because a slight mismatch at the fundamental wave can be compensated

⁵In the final harmonic tuner design sliders will be put on the slabline which are expected to produce a mismatch of about -15 dB or even worse. Therefore, a return loss of the coaxial to slabline transition of better 20 dB or better is definitely sufficient.

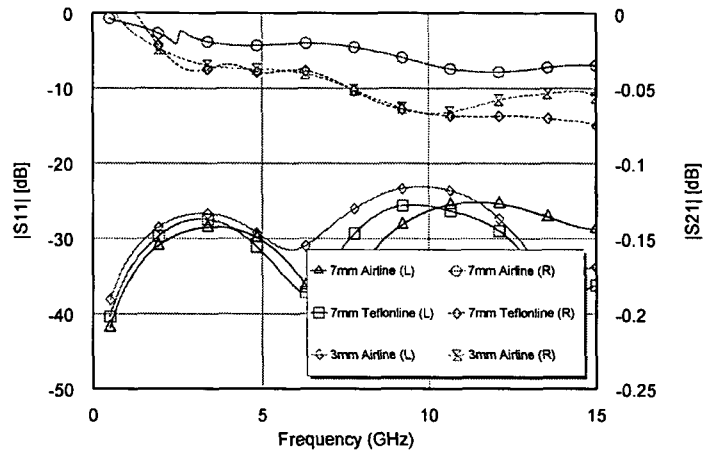


Figure 4.14: Different Coaxial to Slabline Transitions, S-Parameters. (L) means left hand scale, (R) means right hand scale

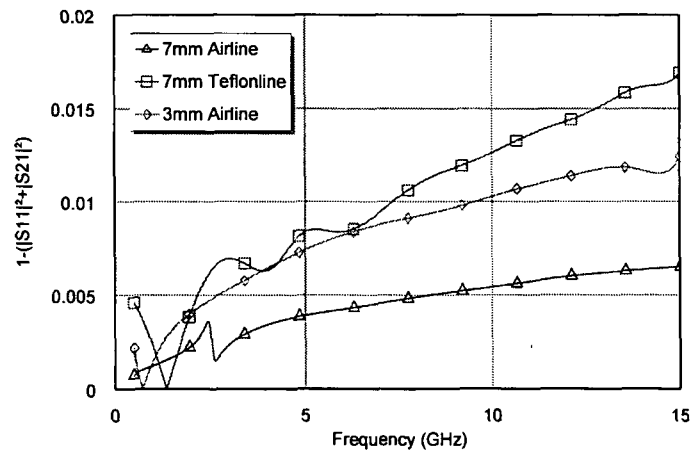


Figure 4.15: Different Coaxial to Slabline Transitions, Loss

by an appropriate adjustment of the fundamental tuner which will be connected in series for a harmonic load pull setup.

Again it turns out that the 7 mm airline is the most promising coaxial transmission line to allow loss minimization as well as good matching of the transition. This approves the selection of APC-7 connectors for the harmonic tuner.

4.6.2 Coaxial to Slabline Transition

As already mentioned above, it becomes necessary to find a high quality transition from 7 mm airline to slabline. Hence, an optimized structure is required. In contrary to the prototype design it was the idea to use a more simple structure for making machining easier. Therefore, it was chosen to put the coaxial line and the slabline directly together on their ends. It should be investigated how far the 3.04 mm conductor of the airline has to reach into the slabline for achieving good performance. Additionally, effects of a cone shaped diameter increase should be simulated. These both parameters, the 'transition position' as well as the 'transition length' are given in figure 4.16. A 3D-view of the structure is given in figure 4.13. Now both variables were varied during a parametric

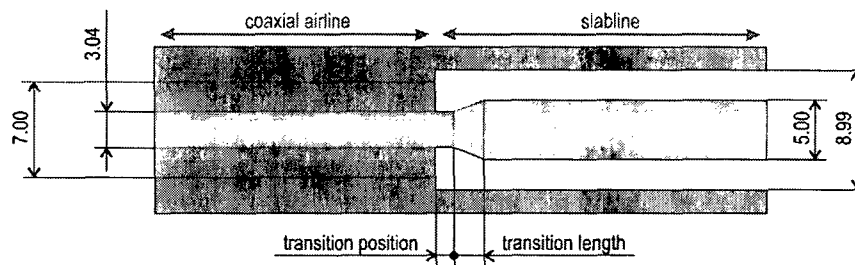


Figure 4.16: Coaxial to Slabline Transmission Dimensions

simulation, showing the worst matching of $|S_{11}|$ over the 0 . . . 15 GHz frequency range. The result of the simulation is depicted in figure 4.17. It can be seen that it should be possible to obtain values of about -24 dB for $|S_{11}|$ for a certain range of parameter combinations. On the one hand good matching can either be achieved by a transition position close to the end of the coaxial line with a non-zero transition length. On the other hand it is also possible to use a stepped transition (transition length = 0 mm) which requires placing the step in the center conductor's diameter in greater distance to the coaxial line.

For the final harmonic tuner realization, of course, the second variant was chosen. The performance is the same and it can be manufactured much easier. So it turned out that the design of the prototype's transition (with reducing the geometry towards the coaxial line) is much too complex for the given requirements.

4.6.3 Slabline – Impedance

As already observed from a theoretical view in section 4.3 a finitely large ground plane leads to a change of the slabline's wave impedance. The analytical estimate used a rectangular trough-line for the estimation of the impedance. Doing a 3D field simulation of a brass-slabline with 60 mm wide ground plates results in a slightly increased wave impedance.

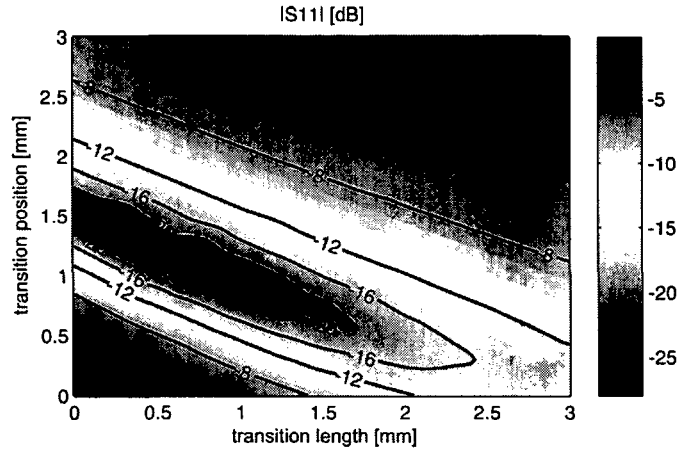


Figure 4.17: Worst case coaxial to slabline transition performance for $f = 0 \dots 15$ GHz

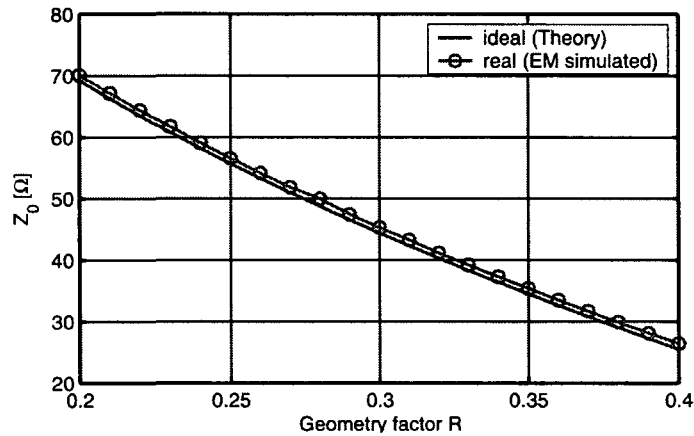


Figure 4.18: Theoretical and real slabline impedance

The result of a simulation for different geometry factors $R = \frac{d}{2D}$ (compare section 4.3) is given in figure 4.18. Hence, the slabline parameter R has to be adjusted from $R = 0.2743$ to $R = 0.2780$ in order to have a 50Ω impedance. Keeping the inner conductor's diameter constant to $d = 5$ mm results in a sidewall spacing of $D = 8.99$ mm. It can be argued that this change is not necessary, because the mismatch is about -20 dB which is in the same range as the mismatch of the coaxial to slabline transition. Because of the fact that the prototype will not be used for the final design a new production of the sidewalls is necessary and therefore the optimum value $D = 8.99$ mm was selected.

4.6.4 Slabline – Measurements

After selecting all necessary parameters for the slabline (used connectors, transition, slabline geometry) a 100 mm long slabline was realized for verification measurements (figure 4.19).

More details of the construction are given in section 4.9, figure 4.48)



Figure 4.19: Realization of slabline with transitions to 7mm airline and APC-7 connectors

This structure was measured in order to verify the expected performance of the slabline and the transition to the 7 mm airline. To simplify the measurements (exact measurements need calibration standards for the airline as well as for the slabline), only the APC-7 interface was used for measurements. This means that a performance degradation has to be expected due to the APC-7 connectors as well as to the length of the slabline. This is an acceptable method since matching has not to be perfect. A mismatch at the fundamental frequency can be compensated by the cascaded fundamental tuner in a harmonic load-pull setup.

The measurement results – compared to the the simulation of two slabline/airline transmissions in back-to-back configuration – is given in figure 4.20

The input matching is > 19 dB in the frequency range $0 \dots 15$ GHz. This is sufficient enough for the application in the harmonic tuner.

4.6.5 Slider with Resonating Stub

For the design of the slider the initial approach which was used in the prototype (a brass sleeve with spring contacts on both ends) is further investigated. The slider's dimensions are given in figure 4.21a. It is important to mention that the outer diameter of 5.8 mm is valid for the unassembled slider. When putting the slider onto the center conductor of the slabline the spring contacts will bend 0.1 mm away from the center, hence resulting in a diameter of 6.0 mm at both ends of the slider which reduces to 5.8 mm in the non-springy area in the middle of the slider. This deformation was taken into account for the field simulations.

It was the goal of the simulations to determine the **influence of mounting a slider on a slabline**. Further it should be analyzed if the slotted slider can be modeled by a solid one, corresponding to a stepped diameter of the conductor (figure 4.21b). If this is possible with negligible error the simulation times can be reduced dramatically. Alternatively it would be possible to increase accuracy while maintaining the simulation time. For the simulations the slider was placed into the middle of a 60 mm long slabline segment (according to figure 4.22a) for the slotted slider and 4.22b) for the solid slider). The results of the 3D-simulator (given in figure 4.23) show expected results: The slider can be seen as a step in the slabline's impedance. Therefore, the behavior should be comparable

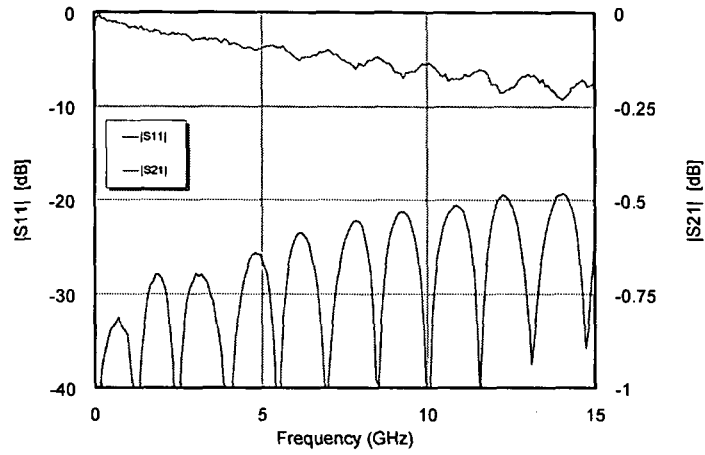


Figure 4.20: Measured S-parameters of empty slabline with transitions to airline/APC-7

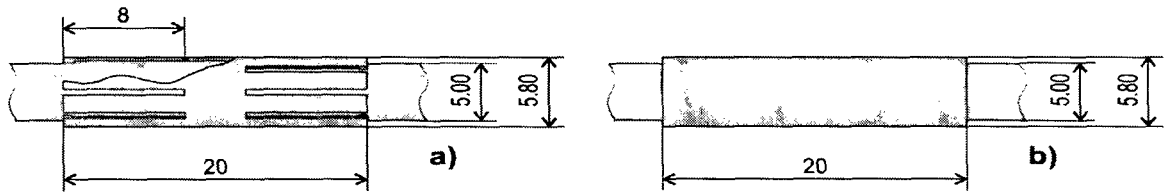


Figure 4.21: Slabline Slider Dimensions

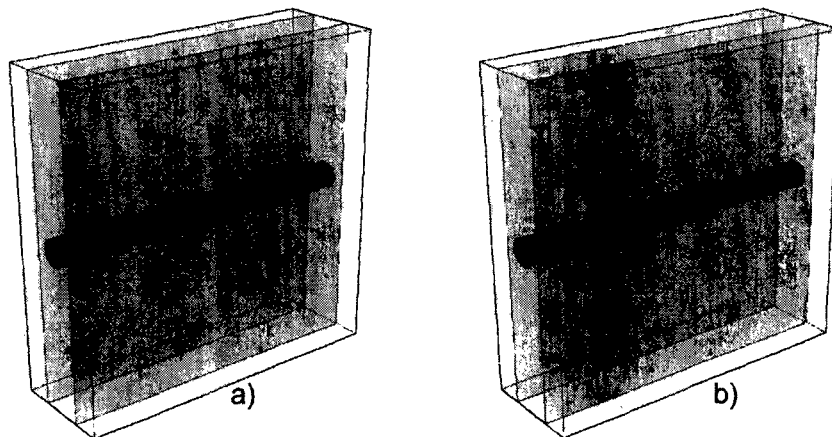


Figure 4.22: Simulation geometry for slider analysis

with a $\frac{\lambda}{2}$ -resonator. Due to the fact that both reflected waves have opposite sign (due to an impedance step up and down) they perfectly cancel out if the guided wavelength is twice as long as the slider. Calculating the corresponding frequency to $\lambda = 2 \cdot 20 \text{ mm} = 40 \text{ mm}$ gives $f = \frac{c_0}{\lambda} = 7.5 \text{ GHz}$ which perfectly corresponds to the simulation of the solid slider. Now the question arises why this is not the same for the slotted slider. Because of its lower

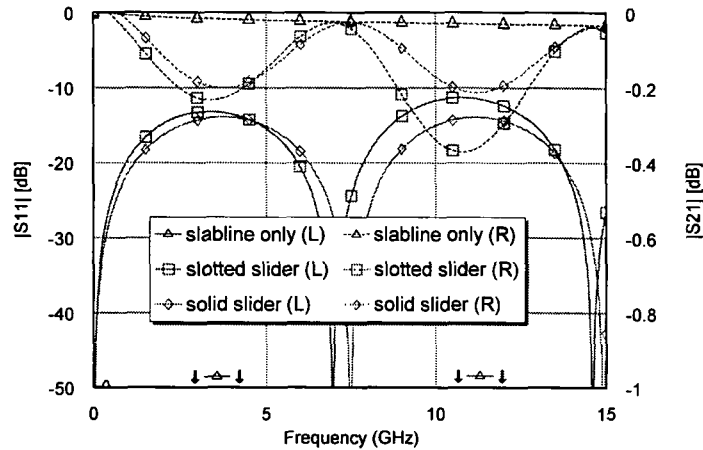


Figure 4.23: Simulation results of slider analysis

resonance frequency it looks like the slotted slider is electrically longer than a solid one of the same mechanical length. Before using a solid slider with increased length instead of a slotted slider for simulations, this effect was analyzed in detail. Therefore, the **field distribution** will be analyzed. To investigate the effect the green area in figure 4.24 (top view onto the slabline setup of figure 4.22a) is analyzed for different phases at $f = 15 \text{ GHz}$. The analysis area is bounded by the sidewall of the slabline on one side and by the inner conductor of the slabline with the slider mounted on it on the other side. The slider's position was chosen in such a way that the slots are in the plane of the E-field simulation.

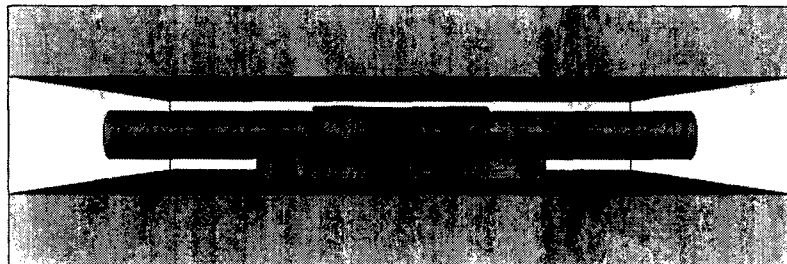


Figure 4.24: Area for E-field simulation of slotted slider

For producing a meaningful plot the signal excitation was set to the left port with $P = 1 \text{ W}$ and $f = 15 \text{ GHz}$. The resulting field magnitudes are depicted in figure 4.25 for a signal phase of $\varphi = \{0^\circ, 30^\circ, 60^\circ, 90^\circ, 120^\circ, 150^\circ\}$. The contour of the spring contacts is marked by black line (please note that the field plot does not cut such a contact), the cut

through the middle ring of the brass slider is marked gray. The resulting field plot (figure

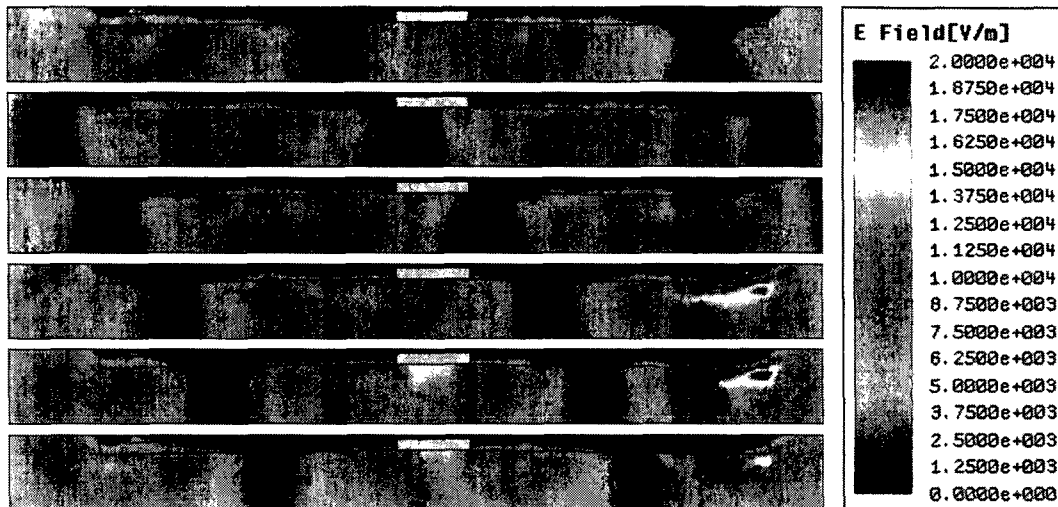


Figure 4.25: E-field animation of slotted slider for $f = 15$ GHz

4.25) shows the following effects:

- It was already assumed that the incoming wave (from the left side) is reflected at both ends of the slider: This is very well illustrated by the increased field strength at the right hand end of the slider (lower three plots). Due to an impedance step from low to high impedance, the expected reflection coefficient becomes positive and, therefore, the field strength increases (compare with reflection of an unterminated open end of a transmission line). This can be seen in the red colored areas on the right. Of course this should be also observed on the left hand side but due to the step from a high to a low impedance the field strength will be reduced which can be hardly seen due to the color grading. Further it turns out that in the middle of the slider – where the resonator is going to be mounted – also a field distortion occurs.
- Having a look at the E-field minima (colored blue) shows that the wave is propagating slightly slower in the range of the slotting (the minima are smaller than in the middle of the slider). So modeling the frequency displacement of the slider by a lengthened solid slider seems acceptable.
- Observing the area close to the center conductors unveils that the field displacement is not perfect in the slotted area, but looks very good in the center of the slider. This is important for ensuring good coupling of the resonator (which is placed in the middle) to the inner conductor.

Summarizing this it can be said, that the field distribution looks quite realistic (hence, an erroneous simulation can be excluded). The only non expected result is the small field distortion in the middle. For giving a statement on the validity of doing the simulations with a solid instead of a slotted slider it is better to do a further analysis to be sure (it must be noted that the resonator is mounted perpendicular to the simulated plane).

After analyzing the behavior of the slider the **combination of slider and resonator** will be investigated. For the 3D field simulation a perfect connection of the resonator to the slider’s body is assumed. The dimensions for the resonator are given in figure 4.26 (only shown for a solid slider but equivalent to a slotted slider). The field simulation should

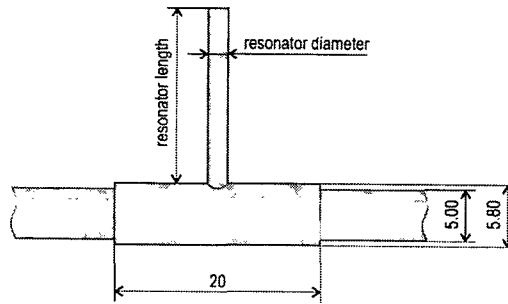


Figure 4.26: Slider with resonator, dimensions

serve to answer the following questions:

- Which reflection coefficient should be possible and how does it depend on the resonator’s length and diameter?
- Does changing the length of the resonator also have an influence other than on the variation of the resonant frequency?
- Does varying the resonator’s diameter change anything else than the bandwidth?
- Again – and finally – it should become clear, if a slotted slider can be simulated by a solid one.

Again, a 60 mm long slabline segment (figure 4.27) was used for the EM field simulator.

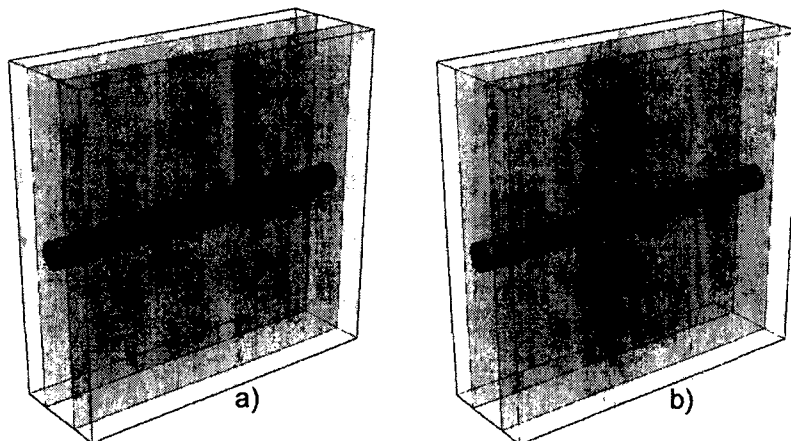


Figure 4.27: Simulation geometry for resonator analysis

Both slider realizations were investigated in order to determine differences. The resonator’s length was chosen to 16.1 mm (measured value of tuned resonator from prototype) in order to achieve a resonance at $2f_0 = 4.289$ GHz. The resonator is modeled by a 1.38 mm \varnothing copper wire (standard wire with 1.5 mm² cross-section). The results of these simulations are given in figure 4.28. This graph now clearly shows that using a solid

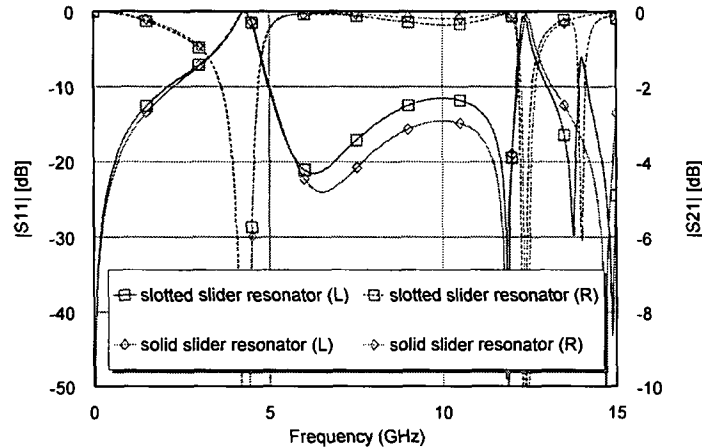


Figure 4.28: Field simulator results for slotted and solid slider with resonator

slider instead of a slotted one gives essentially the same results for the slider combined with the resonator. The solid slider shows exactly the same reflection coefficient (within simulation accuracy) and also the behavior in the frequency region below the resonance is nearly the same. This is very important for calculating the influence onto the fundamental frequency. A deviation of about 3 dB can be observed in the frequency range from $f = 6$ GHz . . . 12 GHz which can be further minimized by adjusting the solid sliders to give a better fit (compare figure 4.23). Therefore, further simulations will always use the solid slider model to save computation time. For the sake of simplicity the solid slider’s length will not be adapted. This decision was made because of both traces being below -12 dB at $f = 6$ GHz . . . 12 GHz and, hence, having negligible influence on the $3f_0$ -resonator’s performance (at $3f_0 = 6.4335$ GHz the return loss of the $2f_0$ -resonator is even better than 20 dB for both simulations).

It can be also seen in figure 4.23 that the resonance is not symmetric in frequency. This is due to the superposition of two effects, the impedance mismatch due to the thickness of the slider (see figure 4.23) and the resonating stub itself. Analyzing the resonator alone gives nearly perfect symmetry. Due to the resonator’s change from capacitive ($f < f_{res}$) to inductive behavior ($f > f_{res}$) the slider’s and the resonator’s reflected waves will constructively interfere for $f < f_{res}$. More energy is reflected in this frequency band, leading to a worse matching. For frequencies above the resonance ($f > f_{res}$) destructive interference will occur, resulting in a steeper decay of S_{11} -values for frequencies closely above f_{res} and, therefore, giving better matching.

It is also important to know the **influence of the resonator thickness on the bandwidth**. To analyze this, a simulation of different resonator diameters was done. The thickness is varied from 0.5 mm to 5.0 mm, the resonator’s length is still set to 16.1 mm.

The results of these 3D field simulations are shown in figure 4.29 and 4.30. As already

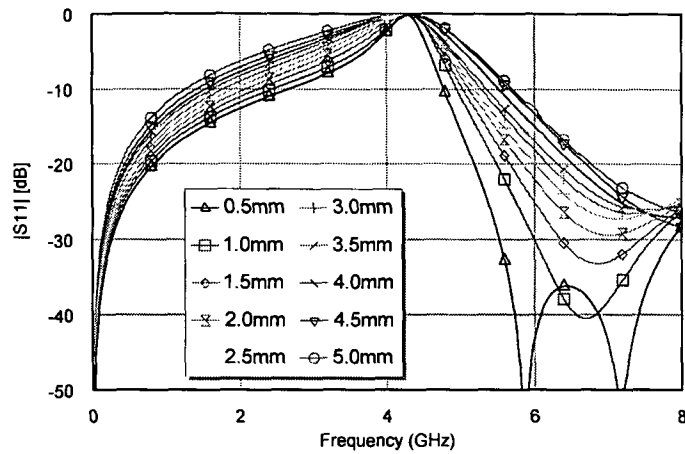


Figure 4.29: Thickness variation of the resonator

expected from antenna design, a thick resonator results in a higher bandwidth than a smaller one. Of course, this eases the tuning of the resonator as well as it allows the application of the harmonic tuner over a wide bandwidth. But there is also a drawback: the increased bandwidth also leads to a higher mismatch at the fundamental frequency f_0 which is not desired.

The influence of the resonator thickness on the resonant frequency and reflection coefficient is shown in figure 4.30 in more detail. It turns out that a too small

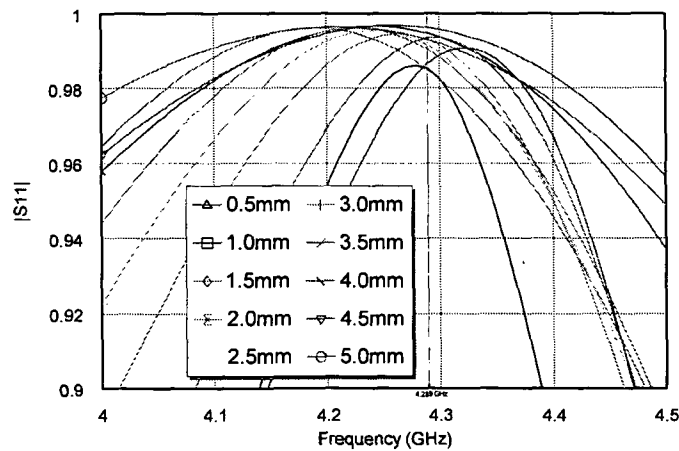


Figure 4.30: Thickness variation of the resonator (detail)

diameter leads to a lower reflection coefficient. This is due to the resonator’s extremely high wave impedance in this case (see tuner modeling in section 4.8 for details). Hence, a minimum diameter of 1.0 mm is recommended for not losing reflection performance. Further it can be observed that the resonance frequency varies when changing the thickness.

It is important to note that this is a non-monotonic relationship due to several factors: parasitic elements of the junction resonator/slider change, ending capacitance of the resonator changes, . . . This effect will not be investigated in detail because the realization of the harmonic tuner requires manual tuning of the resonators anyway.

Summarizing the effects of the resonator’s thickness turns out that the initial choice of 1.38 mm is quite good: It is thick enough to overcome a problems with a lower reflection coefficient, and, it is not chosen too thick in order to minimize the influence on the fundamental wave.

To gain knowledge on the **dependence of the resonance frequency and the reflection coefficient on the resonator length**, another 3D field simulation is done. The thickness of the resonator is set to 1.38 mm, the length varies from 9 mm to 25 mm. The result is shown in figure 4.31. The simulation shows that the achievable return loss re-

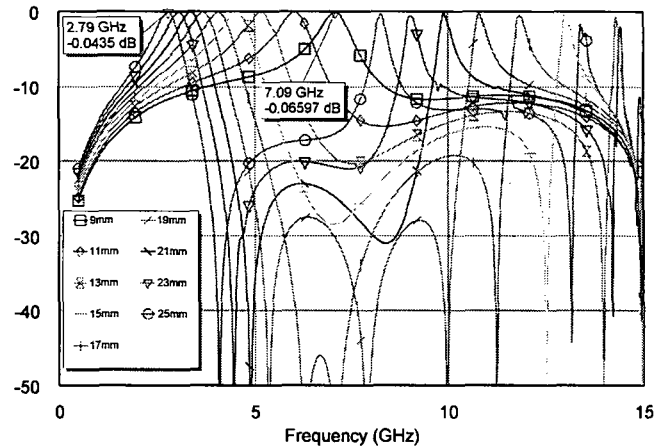


Figure 4.31: Length variation of the resonator

mains lower than 0.08 dB (resp. $|\Gamma| > 0.99$) for the simulated lengths. Due to the fact that high resonant frequencies require short resonator lengths, tuning becomes more and more difficult (a small change in the resonator length results in a huge change of the frequency). Using an overtone for the resonator (to ease up tuning) is possible but gives a significant reduction in the reflection coefficient (see figure 4.31) and is, therefore, not recommended.

Finally the **effects of a small gap between the slider and the inner conductor of the slabline** will be investigated. Because of brass being not a noble material a small oxide layer on the surface can be expected. Thus, a simulation which shows the effect of capacitive coupling of the entity slider and resonator to the inner conductor of the slabline will be done. The simulation uses a resonator with 1.38 mm thickness. The definition of the gap is depicted in figure 4.32. The gap is varied from $0 \mu\text{m}$ (which corresponds to a galvanic connection) up to $250 \mu\text{m}$. The results of this simulation are shown in figures 4.33 and 4.34): The achievable reflection coefficient remains quasi constant – independent of the gap width. Only a small variation in the resonance frequency can be observed as well as a performance degradation besides the center frequency can be observed. This leads to two important interpretations: Firstly, a small oxide layer or dirt between the slabline

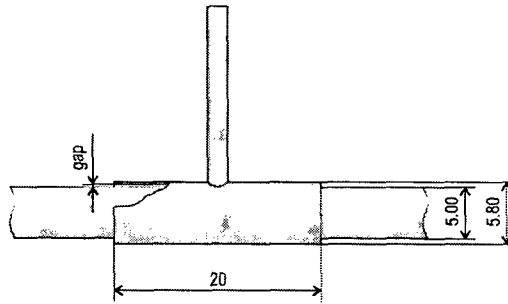


Figure 4.32: Slider with resonator including small gap, dimensions

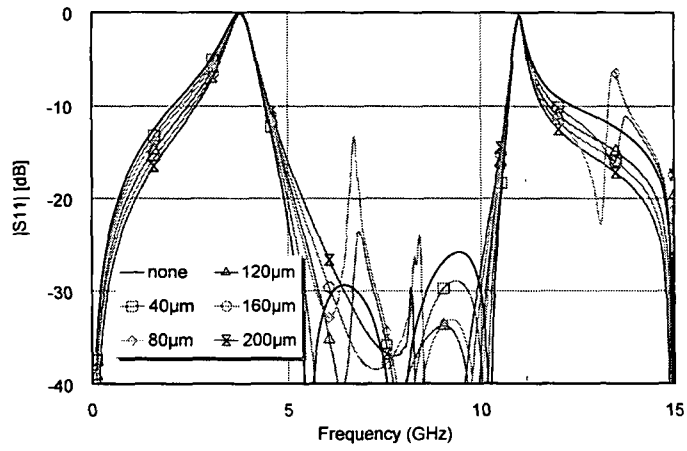


Figure 4.33: Slider with resonator and small gap, simulation results

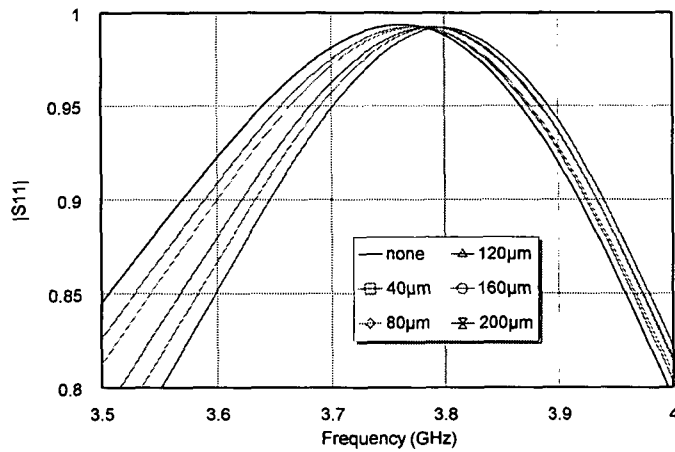


Figure 4.34: Slider with resonator and small gap, simulation results (detail)

conductor and the slider does not influence the performance of the resonator very much. Secondly, the design of the slotted slider can be revised to a simple sleeve. This would make the design of the slider – which is quite complex now – much easier. Attention must be paid on the gap size because of its required high capacitive coupling. Also the resonant frequency varies if a sleeve with a large gap is not perfectly kept in concentric position (which is the case for a simple mechanical realization). Figure 4.33 and 4.34 further show that a sleeve with a small gap can still be modeled as a solid slider with negligible error).

Further simulations, therefore, do not need to take effects into account of a small gap.

4.6.6 Handle

After gaining knowledge about the combination of slider and resonator a manual tuner (e.g. with position marks on the inner conductor) could be realized. Of course this would not be very useful because the resonator is located inside the slabline and is difficult to access. Moreover, the resonator’s reflection changes when touched with the fingers or a tool. Furthermore, an automated system is desired. This rises the need for a mechanical construction which allows movement of the tuner from outside of the slabline without influencing the resonator’s performance too much.

To realize such a handle the following points were considered:

- the material must be non conductive for reducing the influence on the resonator’s S-parameters
- mechanical strength of the handle material is required for moving the resonator without tilting the resonator (to prevent the slider becoming stuck on the conductor of the slabline)
- the handle shall be placed on the opposite side of the resonator to minimize mutual interaction
- a material with a low relative dielectric constant ϵ_r should be used to minimize field distortion; furthermore, a handle with $\epsilon_r > 1$ is preferably placed in the middle of the slabline’s cross-section (because theoretically no E-field exists due to symmetry reasons)
- the materials dielectric loss has to be as low as possible to prevent energy loss due to the handle
- special material’s or mounting techniques should be avoided.

Considering all this, it turned out that materials with $\epsilon_r \gtrsim 1$ are hard to get and do not fulfill the requirements for mechanical strength (some materials are foamed in order to achieve a low ϵ_r). Therefore, it was decided to use a standard substrate material, The idea is to produce a 1 mm wide copper strip on the top edge of the substrate (on both sides) to allow soldering to the slider (see figure 4.35). To determine the influence of the handle two different substrate materials (FR4 and a high frequency laminate, see table 4.4) were tested by a 3D field simulation. All simulations used a 5.8 mm \varnothing \times 20 mm solid slider with a 1.38 mm \varnothing \times 15.5 mm resonator (see figure 4.35 for the simulation setup). The handle material is trapezoidally shaped with an angle of 37° between the left and

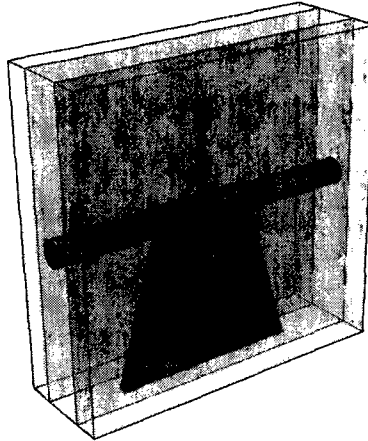


Figure 4.35: Simulation geometry for handle analysis

handle material	ϵ_r	$\tan \delta$	thickness	copper	mech. stability
air (no handle, for reference)	1	0	—	—	—
FR4 substrate	4.1	0.02	1.575 mm	35 μm	high
Rogers RT/duroid 5880 [38]	2.2	0.0009	1.575 mm	35 μm	moderate–good

$\tan \delta$ specified for $f = 10$ GHz

Table 4.4: Simulated materials for mechanical handle

right edge. The top edge length equals the slider length of 20 mm. The results of the simulation are shown in figures 4.36 and 4.37. It can be seen in figure 4.36 that a handle’s main influence is an increase in the reflection coefficient at the fundamental frequency. This could possibly lead into problems fulfilling the design goals of the entire harmonic tuner for the permissible fundamental frequency mismatch (section 4.7 covers this topic in detail). Figure 4.36 further unveils ‘strange’ resonances above 12 GHz, which is far outside the application frequency range. Hence, it was not investigated further if this behavior is caused by resonances inside the handle or by the excitation of higher order modes in the slabline

Similar to other simulation the loss was calculated and is shown in figure 4.37 (both figures show the same with a different scaling of the y-axis). It can be seen that the Rogers RT/duroid 5880 material does not increase the losses of the resonator. On the contrary, using a standard FR4 substrate nearly doubles the losses at the resonant frequency and, therefore, reduces the achievable reflection coefficient. For frequencies $f > 5$ GHz the losses rapidly increase due to the high $\tan \delta$ of FR4. This made the decision quite simple to prefer the Rogers RF substrate material.

4.7 Performance of the Initial Design

After making all the necessary decisions for the realization of a slider with a resonator and a handle, the resonators for $2f_0$ and $3f_0$ were manufactured (see figure 4.38) and put

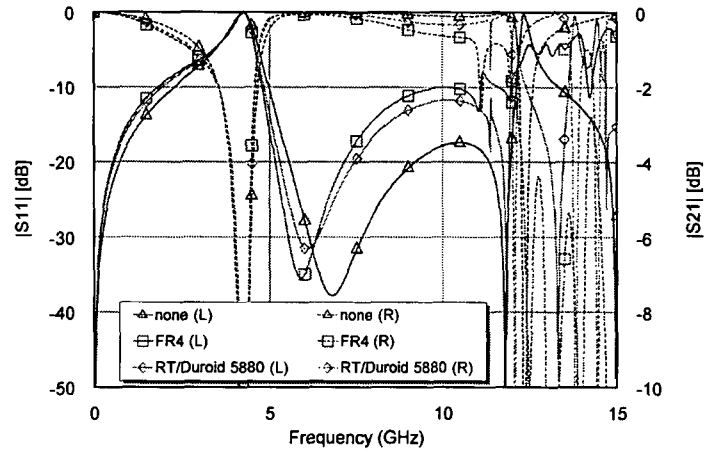


Figure 4.36: Resonator with handle, simulation of different handle materials

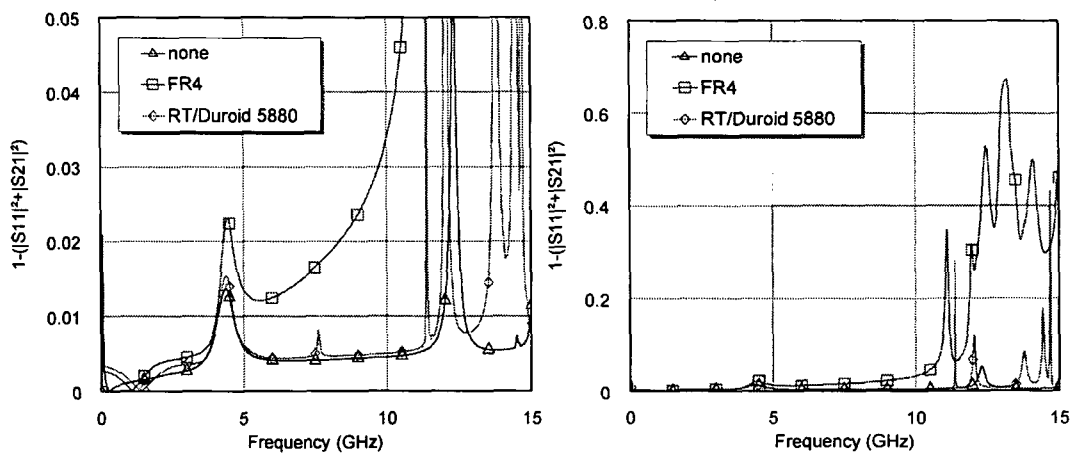


Figure 4.37: Resonator with handle, simulation of losses of different materials

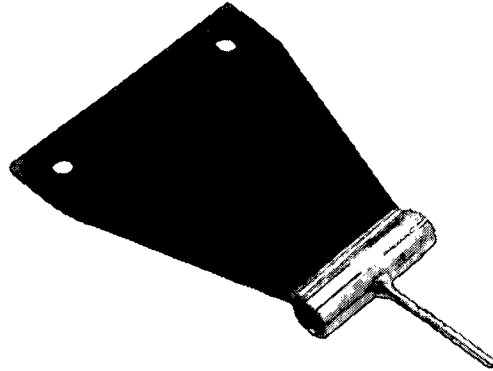


Figure 4.38: Resonator with slotted slider and Teflon handle

into the already produced 100 mm long slabline with an APC-7 interface (figure 4.19) for measurement.

Due to the good performance of the slabline with APC-7 connectors ($S_{11} < -22$ dB for $f = 0 \dots 10$ GHz, see figure 4.20, negligible loss) no further effort was spent on de-embedding the transitions (this would require a slabline TRL-calibration kit). Furthermore it is not necessary, because the simulation of the resonator with handle shows a return loss in the range of $0 \dots 10$ dB in the area of interest – and will, therefore, not be influenced by the 22 dB matching of the slabline transitions. Figure 4.39 shows the comparison between the simulation and the measurements of the $2f_0$ - and $3f_0$ -resonators including the handle. The measurement gives a very good fit onto the 3D field simulation results. The effects

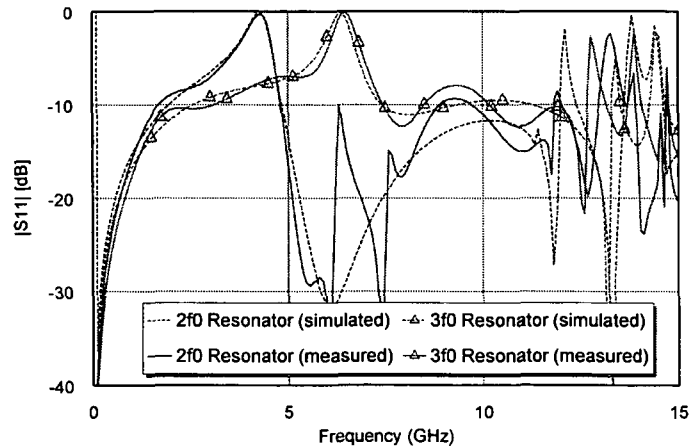


Figure 4.39: Slotted resonator with handle, comparison of measurement and simulation

of the unsymmetrical bandwidth are reproduced very exactly. The only discrepancy can be observed for the $2f_0$ -resonator at $f = 6 \dots 8$ GHz. This unexpected behavior was not further investigated, since it turned out that a redesign is required anyway (see end of this section).

Having now the measurement data available it can be checked if the required performance (-4.815 dB matching for f_0 and $|\Gamma| > 0.95$ for $2f_0$ and $3f_0$) is achieved. Because of the mutual influence of both resonators (e.g. the $3f_0$ -resonator should be perfectly matched at $2f_0$, but shows about 8 dB return loss only) it is necessary to set up a special simulation environment (figure 4.40). This schematic combines the measurement results of

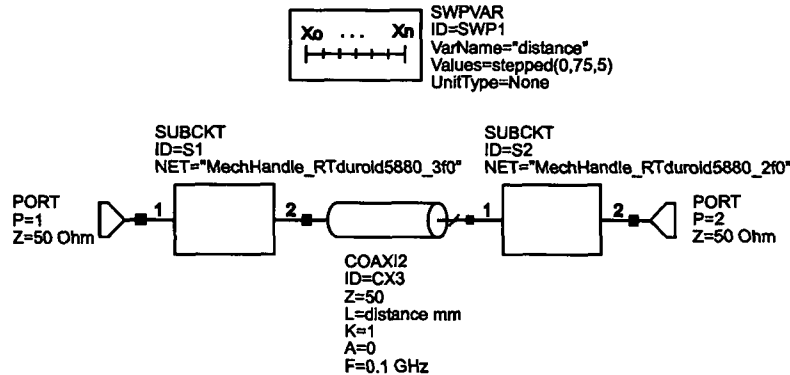


Figure 4.40: Simulation environment for overall performance estimation

both resonators (including handle) and adds a 50Ω -line with variable length in between. If this line is varied in length, the reflected waves from the two resonators are added up with different phase shifts. This means that the fundamental matching of the harmonic tuner varies depending on the resonator’s distance. The simulation result is depicted in figure 4.41. It can be seen that the fundamental return loss varies from 4.415 dB up to > 20 dB.

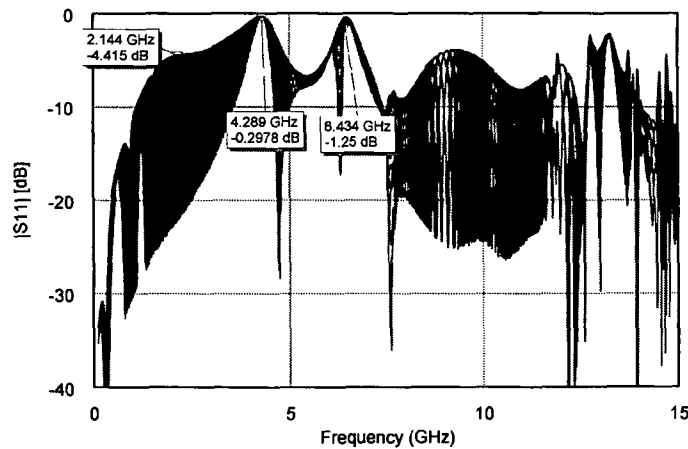


Figure 4.41: Simulation results for overall performance estimation (based on measurements)

At the harmonic frequencies the achievable reflection coefficients are $|\Gamma_{2f_0}| > 0.966$ and $|\Gamma_{3f_0}| > 0.866$. Hence, the design goal for the fundamental matching is missed by 0.4 dB. The reflection at $2f_0$ shows the expected performance whereas the reflection at $3f_0$ is not

acceptable (this could be expected already from the measurements results in figure 4.39). Since a design iteration became necessary mainly due to the poor performance at the fundamental frequency, the behavior at $3f_0$ was not further investigated.

4.8 Design Iteration / Tuner Modeling

As explained in the preceding section a redesign of the resonator is required. Because the fact that the requirements are tightly failed, a modeling approach was chosen to decide for the necessary redesign. Therefore, a simple electrical model for the slider and for the combination slider and resonator was developed. Figure 4.42 shows how the slider was modeled. Since it already turned out that a solid slider can be used for field simulations

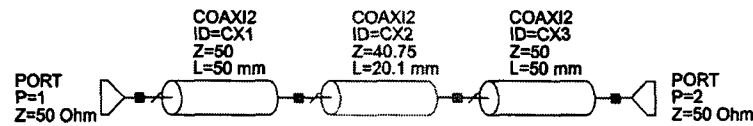


Figure 4.42: Electrical model of the slider

instead of a slotted one, it should be possible to model the slider by a line segment with a non 50Ω impedance. Since the slider has a larger diameter than the conductor of the slabline, the geometry factor R (compare section 4.3) increases which results in a lower line impedance (see figure 4.7). This effect can be also explained by the increased capacity to the slabline ground-plates. The model parameters found to give the best match are shown in figure 4.42, a comparison of the model to the field simulation is depicted in figure 4.44.

To complete the model the resonating line has to be added (figure 4.43). This is done by

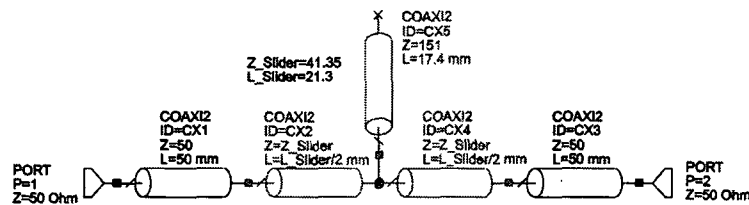


Figure 4.43: Electrical model of the slider with resonator

splitting the slider model into two sections and connecting an additional line at this point. This line represents the resonating stub and can be modeled by a high impedance, because it is also in slabline configuration but has a very small geometry factor R . Optimizing the model for the $2f_0$ -resonator gives the values shown in figure 4.43, a comparison to the 3D field simulation results is shown in figure 4.44.

Both models, the slider with and without resonator, show a very good match to the field simulation and can, therefore, be used for the design iteration.

As already explained in section 4.6.5, the bandwidth of the resonator becomes unsymmetrical (matching decreased/increased for frequencies lower/higher than the resonance frequency). This is the case due to the superposition of the reflected wave from the resonating stub and from the slider itself. Improved performance should be expected if the

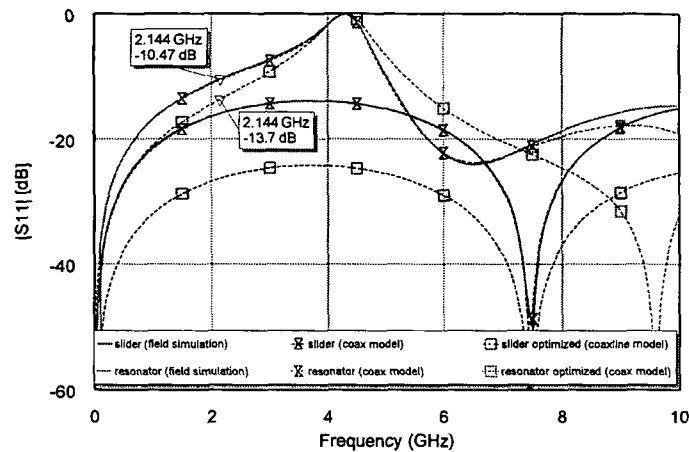


Figure 4.44: Model performance and optimized design

slider’s diameter will be reduced in order to have a lower deviation from the $50\ \Omega$ slabline impedance. What happens if a slider with an outer diameter of $5.35\ \text{mm}$ ⁶ is used instead of the existing $5.8\ \text{mm}$ one is also depicted in figure 4.44: The slider’s matching becomes significantly better and, therefore, the influence on the bandwidth of the resonating stub is minimized (the frequency response shows much higher symmetry around the resonance frequency). This further leads to an improvement of the fundamental frequency return loss from about $10.5\ \text{dB}$ to $13.7\ \text{dB}$. Hence, the conclusion can be drawn that a smaller diameter of the slider can solve the performance problems.

The diameter of $5.35\ \text{mm}$, which was used in the model simulation also corresponds to what can be realized with a standard turning machine (due to a residual metal thickness of about $150\ \mu\text{m}$). As already seen from the results of the gap-simulations (section 4.6.5) it is possible to use a simple sleeve instead of the more complicated slotted design with spring contacts. To ease the production of the slider its length had to be reduced. The final slider, therefore, had a length of $10\ \text{mm}$ with an outer diameter of $5.35\ \text{mm}$ and a wall thickness of $150\ \mu\text{m}$ (an exact drawing is given in figure 4.49). This results in a gap of $25\ \mu\text{m}$ which allows smooth gliding of the slider on the inner conductor of the slabline and should not degrade the coupling performance. A photograph of the reworked slider is given in figure 4.45. At a first glance it becomes obvious that the new design (b) should result in a much lower mismatch than the old one (a). Again, the slider was mounted on a handle and measured in comparison to field simulations. The measurement results (figure 4.46) show a good match to the simulation – the improved matching at the fundamental frequency $f_0 = 2.1445\ \text{GHz}$ becomes obvious when comparing this graph to figure 4.39.

To get an idea on the overall performance, both measurements were combined according to the schematic in figure 4.40. The result of this simulation is given in figure 4.47. The fundamental matching now fulfills the requirements ($-9.8\ \text{dB}$), the reflection coefficients are $|\Gamma_{2f_0}| > 0.987$ and $|\Gamma_{3f_0}| > 0.957$ and hence fulfill the design goals.

Now the slabline and the resonator dimensions are fixed which leads to the final real-

⁶Please note that the diameter of the slotted slider is higher (about $6.0\ \text{mm}$) at its ends, because the springy contacts bend outwards.

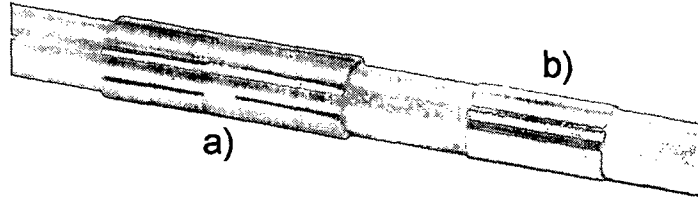


Figure 4.45: Photograph of the old (a) and redesigned (b) slider

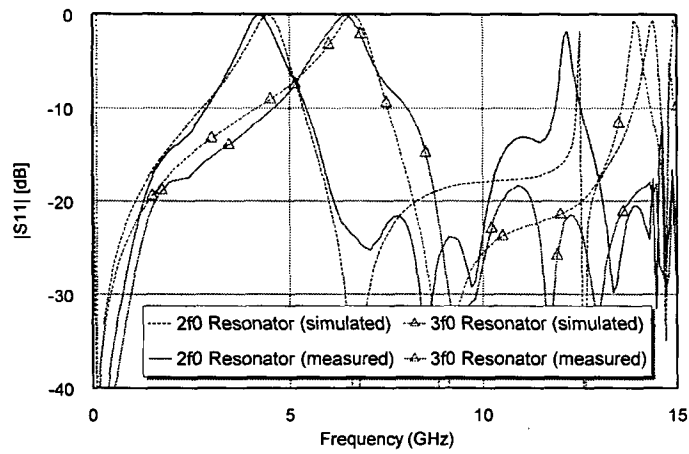


Figure 4.46: Redesigned slider with handle, comparison of measurement and simulation

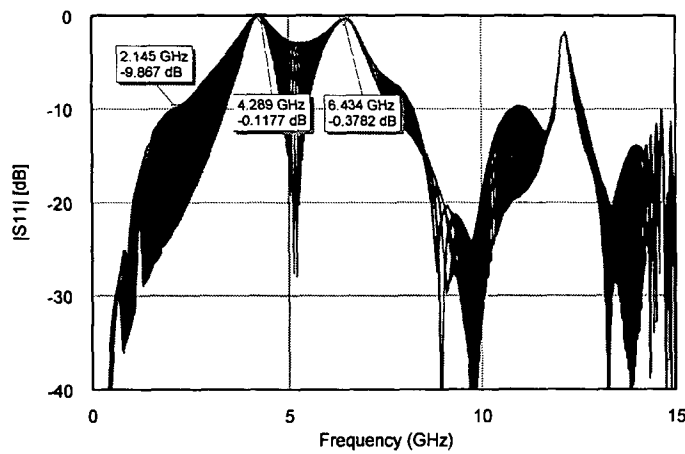


Figure 4.47: Simulation results for overall performance estimation (redesigned slider)

ization of the harmonic tuner.

4.9 Final Realization

For the final setup the length of the slabline has to allow a sufficient movement of each resonator in order to accomplish any phase angle of the reflection coefficient ranging from $0^\circ \dots 360^\circ$. A movement of the resonator by a distance x results in lengthening the way of the reflected wave by $2x$ (wave travels forward and backward). Therefore a movement range of $\frac{\lambda}{2}$ is necessary for each resonator (see table 4.5).

frequency	wavelength λ	required movement range $\frac{\lambda}{2}$
$2f_0 = 4.2890$ GHz	69.9 mm	35.0 mm
$3f_0 = 6.4335$ GHz	46.6 mm	23.3 mm

Table 4.5: Required movement range for resonators

In order to allow an automated positioning of the resonators the handle of the tuner will be clamped by a movable platform outside the tuner. If this platform has a length of 50 mm, the required slabline segment length for each resonator becomes $50 \text{ mm} + \frac{\lambda}{2}$. This gives 85 mm for the $2f_0$ -resonator and 73.3 mm for the $3f_0$ -resonator which sums up to 158.3 mm in total. In order to have some safety margins for the mechanical construction the slabline was chosen to be 200 mm long. For keeping the walls of the slabline correctly spaced apart, two spacers are attached to the slabline on both ends. The required 7 mm-airline interface is accomplished by screwing a turned brass part (with an inner diameter of 7.00 mm) into the slabline's ending parts. This turned part provides the standardized airline interface (compare figure 4.12). The inner conductor of the airline and the slabline is made from 5 mm \varnothing brass bar stock material. Due to the fact that the slabline's inner conductor has a smaller diameter than the airline, the entire conductor can be removed from the structure without the need for unscrewing the airline interface parts. The entire construction is depicted in figure 4.48.

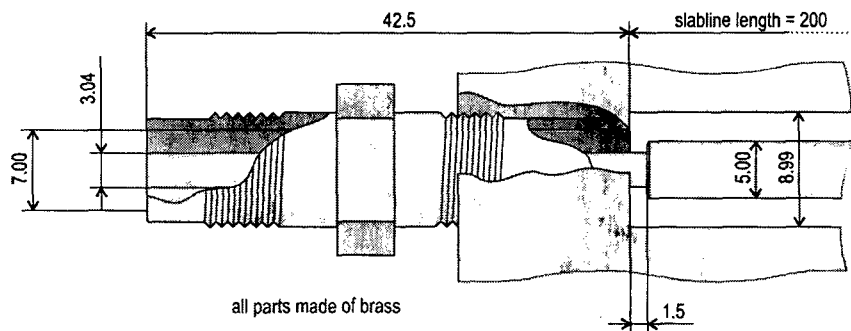


Figure 4.48: Final realization of slabline to 7mm airline transition

For the sake of completeness the final resonator design is shown in figure 4.49. Due to the change in the design of the slider, the resonator lengths had to be adapted also. The final lengths are 15.5 mm for the $2f_0$ -resonator and 9.8 mm for the $3f_0$ -resonator.

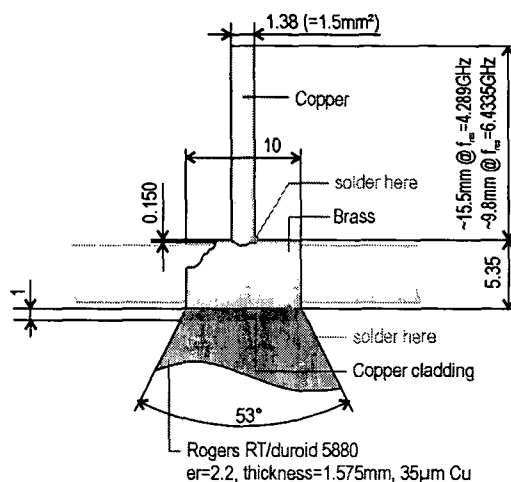


Figure 4.49: Final realization of the slider with resonator and handle

4.10 Electromechanical System for Automation

Because of the fact that the automated system for moving the $2f_0$ - and $3f_0$ -resonators does not influence the RF-performance of the tuners, only a brief description will be given in here: The system uses off the shelf lead screws which are driven by standardized stepping motors for positioning the two resonators. The lead screws have a pitch of 2 mm/turn. Combined with an 1.8° -stepping motor (200 steps per turn) this gives a positioning resolution of $\pm 10 \mu\text{m}$ (corresponds to $\pm 0.1^\circ$ @ $2f_0 = 4.289 \text{ GHz}$ and $\pm 0.15^\circ$ @ $3f_0 = 6.4335 \text{ GHz}$). This is more than sufficient for the desired application – anyway tolerances of the entire system will decrease the accuracy (see performance data in section 4.11).

Each platform (where the resonator’s handle is clamped with grub screws) is centrally mounted with friction bearings onto a shaft made of stainless steel. For a positioning each platform connects to the lead screw by a spindle nut. Additionally, photoelectric barriers limit the movement range and provide an absolute position reference. The stepping motors are controlled by the Maury Microwave motor-controller which is used for positioning the fundamental tuner. This motor-controller allows to approach the programmed positions from the same direction to minimize the effect of tolerances of the spindle nut. Furthermore, the motor-controller can be programmed by commands over the GPIB-bus (general purpose instrument bus), which simplifies system integration. Photos of the final system is shown in figures 4.50 (front side) and 4.51 (back side).

4.11 Performance of the Harmonic Tuner

To characterize the harmonic tuner as well as to see its performance data, a sweep over both slider positions was performed. For each position the S-parameters were measured. Both resonators were moved by a distance $> \frac{\lambda}{2}$ to cover all possible phases of the reflection. Due to the reflection of the wave inside the tuner this distance will be doubled and covers,

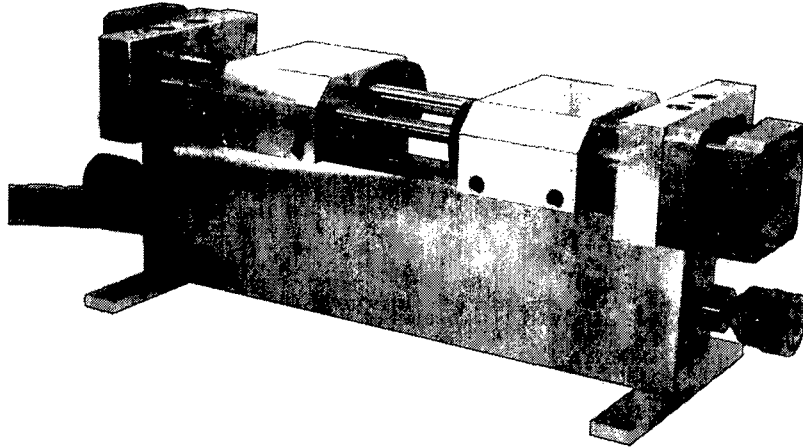


Figure 4.50: Photograph of the realized harmonic tuner (front)

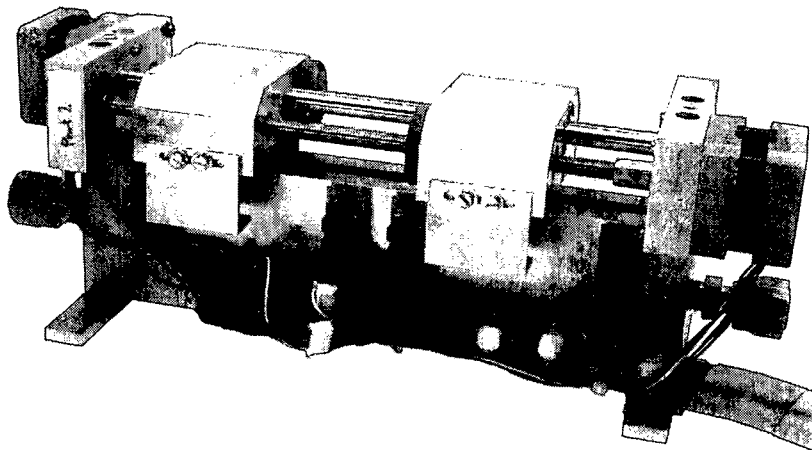


Figure 4.51: Photograph of the realized harmonic tuner (back)

therefore, more than 360° . The following figures (4.52 – 4.54) show the results of these measurements.

Figure 4.52 depicts the performance of the configuration as it was described by the simulation. Coming from the input port of the harmonic tuner (port number 2, explained later on) the first resonator placed on the slabline is resonant at $2f_0$, the second one at $3f_0$ (compare figure 4.40). This ensures good de-coupling of the Γ_{2f_0} and Γ_{3f_0} phases. On

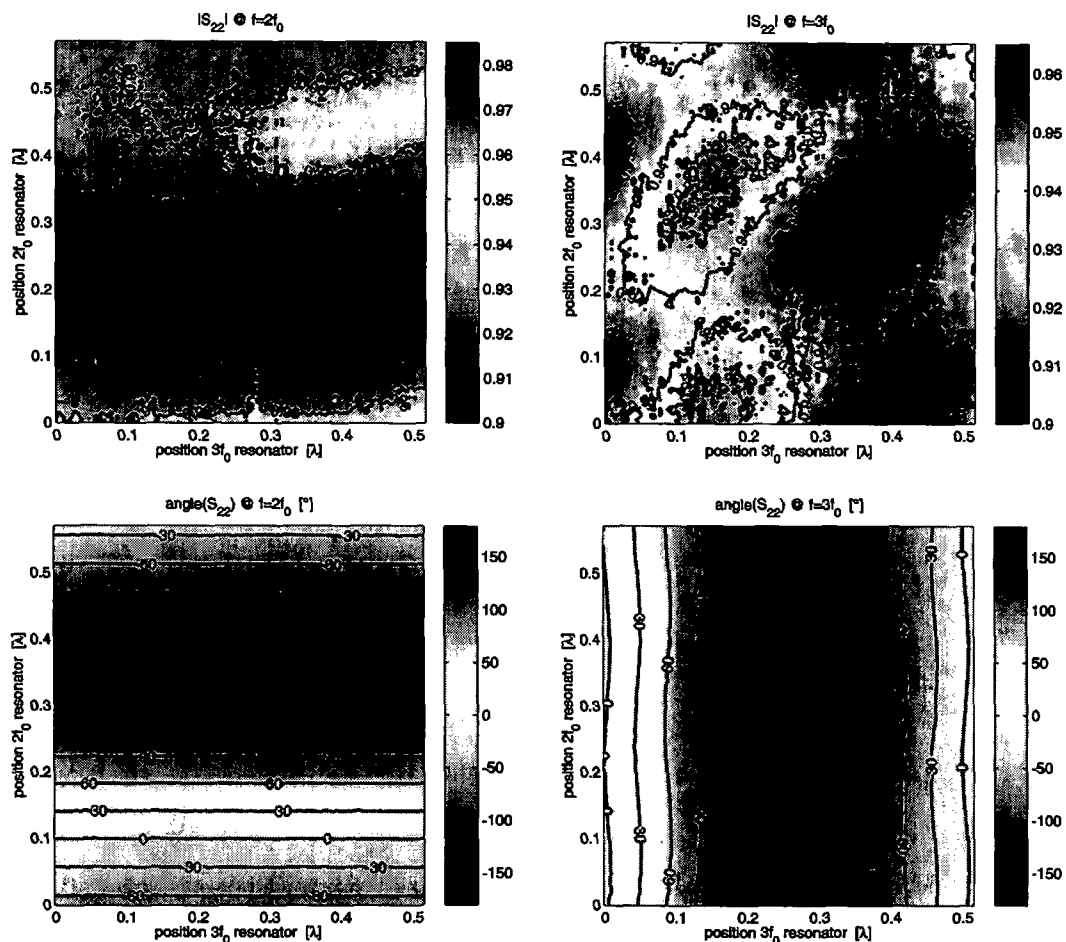


Figure 4.52: Reflection coefficient Γ_{Port2} dependency on slider position

top of figure 4.52 the magnitude of the realized reflection coefficients for the second and third harmonic frequency is shown in linear scale. The resonator positions are measured in wavelengths. Increasing values define a shift of the resonator from port 1 to port 2 (hence, 0 is on the port 1 side of the harmonic tuner). It can be seen that the design goal of $|\Gamma| > 0.95$ is fulfilled for the second harmonic but not for the third one ($\min(\Gamma_{3f_0}) = 0.92$). The second row of figure 4.52 shows the corresponding phase angles. As expected, both harmonic phases can be controlled almost separately. Whereas the second harmonic is entirely independent of the $3f_0$ -slider position, the third harmonic will be influenced by a maximum of $\pm 3.5^\circ$ by a position change of the $2f_0$ -slider. This is a negligible effect for

the most applications. Figure 4.52 also indicates losses along the slabline. This can be seen when looking at the upper left graph for the second harmonic’s magnitude. It should be expected that this graph can be repeated with $\frac{\lambda}{2}$ which is not given for this figure (please note that the range of both axes is a little bit more than $\frac{\lambda}{2}$). It turns out that the magnitudes at $\lambda = 0.5$ are typically 0.1...0.15 higher than at $\lambda = 0$. Because the better values occur when the resonator is closer to the measurement port, this is an indicator for (very small) losses of the slabline.

As the reflection coefficient of the second harmonic shows a higher magnitude than the one for the third harmonic, it was chosen to use the harmonic tuner in the other way round. This is the reason for the swapped port numbers mentioned above. By having now the $3f_0$ -resonator as the first in line, its position is closer to the measurement port (now port 1) than before and thus the insertion loss is lower. The resulting higher reflection coefficient for $3f_0$ comes in quite handy for doing load-pull measurements. Because the third harmonic experiences much higher transformation due to the transistors extrinsic elements (see section 5.5.3), a better reflection at $3f_0$ is needed than for the second harmonic frequency.

The results for the reversed setup are depicted in figure 4.53. Please note that increasing the position value now indicates a movement away from the measurement port. This configuration provides reflection coefficients $|\Gamma_{2f_0,3f_0}| > 0.94$. This still misses the self defined design goal marginally but is still an impressive value. Due to reversing the order of the resonators the de-coupling of the phases is lost for the second harmonic frequency. Now, the position of the $3f_0$ -resonator influences the phase of the Γ_{2f_0} by more than $\pm 20^\circ$. Because the tuner will not be operated by hand even this is not a problem. Hence, changing the third harmonic’s phase requires always a small corrective movement of the $2f_0$ -resonator.

Another important parameter which has to be checked is the mismatch for the fundamental frequency f_0 . Section 4.1 showed that $|\Gamma_{f_0}|$ is required to be less than 0.574. The measurement of S_{11} in figure 4.54 shows a significantly better value, allowing to realize higher reflection coefficients at f_0 .

As a last check, the combination of the harmonic tuner and of a prematching tuner was undergone a reproducibility test. For doing that, the data gained from the performance measurements (figure 4.52 – 4.54) was used to calculate for the required motor positions. Then, 1000 random settings for Γ_{f_0} and for the phases of Γ_{2f_0} and Γ_{3f_0} were chosen. For each set of Γ -values the tuners were set to the calculated position and the reflection coefficients at the input of the harmonic tuner were measured by a vector network analyzer (figure 4.55). The results of this test is shown in figure 4.56 and 4.57. All plots show the error in dependency of the desired fundamental reflection coefficient. The deviation from the set values is shown on the y-axis. All graphs also include a moving average over Γ_{f_0} as well as the corresponding standard deviation by showing the $-\sigma \dots + \sigma$ -region. The phase error of the second and third harmonic reflection coefficients is shown in figure 4.56. Two facts are important to mention when analyzing this graph: Firstly, the phase error has a bias: The reason for this is that the initial position calibration – which was provided by the tuner controller – is not suited for a mechanical construction with tolerances than those of the tuners built by the same manufacturer. This could be improved either by a

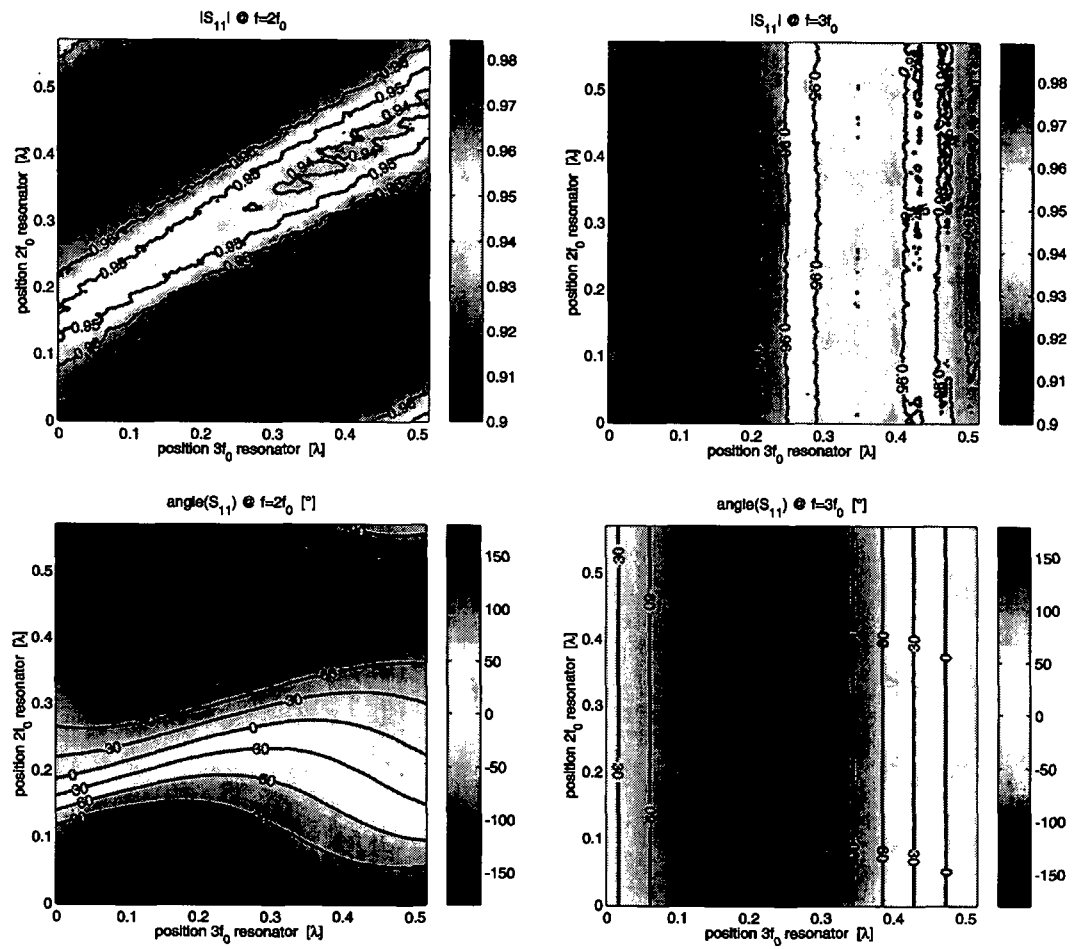


Figure 4.53: Reflection coefficient Γ_{Port2} dependency on slider position

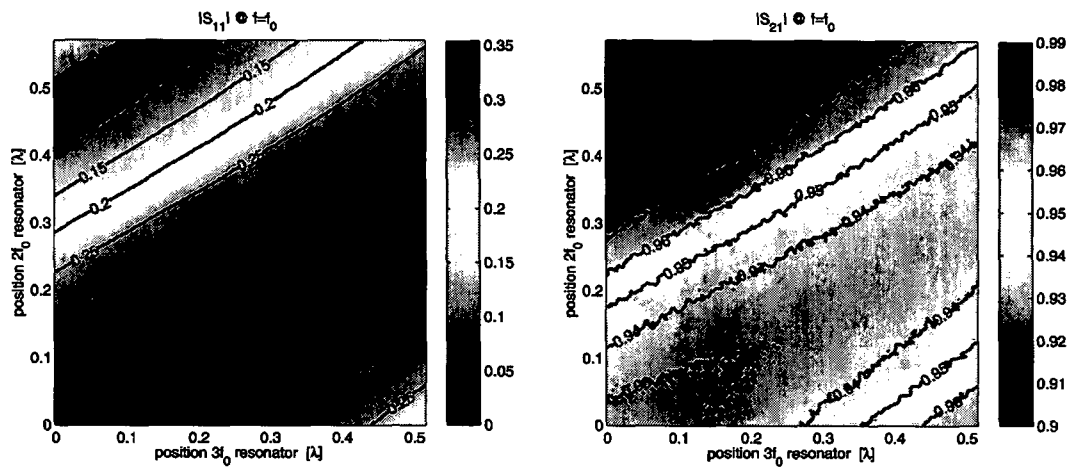


Figure 4.54: Transmission coefficient S_{21,f_0} dependency on slider position

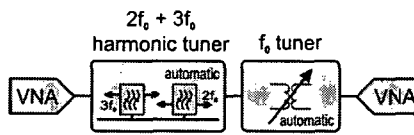


Figure 4.55: Measurement setup for checking reproducibility

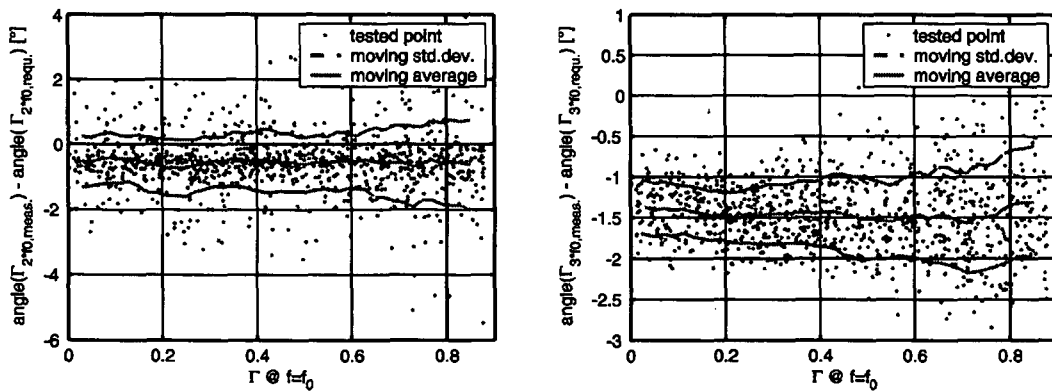


Figure 4.56: Reproducibility test of harmonic tuner, phase error of $2f_0$ and $3f_0$

more exact construction of the harmonic tuner or by a motor controller which allows to use a position calibration routine which can handle play better.

Secondly, it turns out that the standard deviation of the phase error increases with higher Γ_{f_0} . This is an effect due to the fundamental tuner used: Setting a high reflection coefficient means that the tuner (an automatic slide-screw type) moves a stub quite close to the transmission line in order to produce high reflection. Because this mismatch is not resonant at the fundamental frequency, also the harmonics are almost entirely reflected. Hence, the residual parts of the harmonic frequencies – which are not reflected by the harmonic tuner – are reflected by the fundamental tuner. As a result, the reflected wave of the harmonic tuner is superposed by a very small signal of the same frequency but of undefined phase.

There are two ways which would allow for a compensation of this effect. On the one hand, the fundamental’s tuner reflection at harmonic frequencies could be measured during the calibration and also be taken into account when setting the motor positions. On the other hand, a frequency splitter could be inserted between the harmonic and the fundamental tuner in order to prevent harmonic frequencies to be passed on to the fundamental tuner. It is important to mention that the harmonic frequencies have to be terminated by this splitter. Using a standard low-pass would not lead to an improvement, because it typically reflects all frequencies outside its passband. This would give the same result as a highly reflective fundamental tuner.

Finally, the repeatability of Γ_{f_0} was checked. Figure 4.57 shows the error as given by the distance between ideal and measured point in the Smith Chart. Again, it turns out

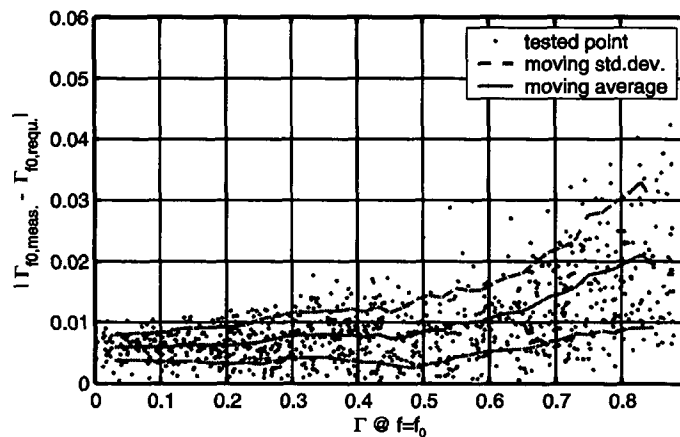


Figure 4.57: Reproducibility test of harmonic tuner, $\Delta\Gamma_{f_0}$

that a high reflection coefficient at the fundamental wave increases the reproducibility. The reason is that the fundamental tuner was not modeled (in contrary to the harmonic tuner) – only about 300 of uniformly spaced Γ -values were used for calibration. Due to the transformation which is applied by the harmonic tuner onto f_0 the distribution of Γ -values becomes non-uniform. This is more and more critical for high reflection coefficients. A possible workaround would be using more points for the fundamental tuner measurement or trying to set up a model for the fundamental tuner which allows interpolation.

Because a phase error of $\pm 2^\circ$ is accurate enough for almost all harmonic load-pull applications (as long they are not used for precise transistor model verification) no further steps were done to reduce this inaccuracy. The same is true for the Γ_{f_0} -error: Because the transistor used for the tuner measurements in chapter 5 requires $|\Gamma_{f_0}| < 0.5$, the expected error is less than 0.02. Again this fits for nearly all applications.

4.12 Summary

This chapter clearly shows that a harmonic tuner can be realized by very simple means without the need for special tools. The realized reflection coefficients are comparable with commercially available tuners. The typical time to set all tuner motors to a new position was about 3...5 s – this allows the application for harmonic load-pull measurements with a high number of Γ -values.

The realized tuner shows good reproducibility which still can be further improved by the methods shown above.

Chapter 5

Realization of Harmonic Load-Pull Setups

To further investigate the harmonic load-pull methods which were outlined in chapter 3, different setups are realized within this chapter. The problems and limitations as well as practical considerations for each setup will be shown. Starting from a passive setup with a triplexer the following systems will improve the tuning range as well as the usable bandwidth by different methods.

5.1 Transistor used for Measurements

To test the different methods for harmonic load pull, a device must be selected for testing. Because there was no ongoing specific project, the center frequency was set to an UMTS carrier at $f_0 = 2.1445$ GHz. The output power was chosen to be about 500 mW for CW signals. Higher power levels would not have been possible because of the output power limitation of the measurement amplifiers available at the institute. For controlling the second and third harmonic frequency, a transistor with a suitable transition frequency had to be chosen in order to provide gain at $2f_0$ and $3f_0$.

Thus, the choice fell onto a GaAs pHEMT (pseudomorphic high electron mobility transistor) with 2.1 mm gate length. This transistor is available as a die only, it uses gold filled vias to reduce source resistance and inductance. The wafer is also thinned in order to allow better heat dissipation. The device was produced by the Fraunhofer Institute for Applied Solid-State Physics (IAF) in Freiburg, Germany. The transistor, a non-commercially available device, was already used in other projects at the institute. In this preceding work it turned out that the device is quite robust in terms of different output loads, it seemed that it was not possible to destroy the device by doing load-pull when operating the transistor below maximum output power. At this point it should be stated again that it was not goal of this work to establish new efficiency records – the intention was to show different methods for doing load-pull.

This transistor also had another benefit: it was already characterized and modeled. So the extrinsic elements as well as a large-signal intrinsic model were already available for comparison.

To get an idea on the device performance the available power gain over frequency is depicted in figure 5.1. The DC-IV curves (figure 5.2) show an instable region (under 50Ω

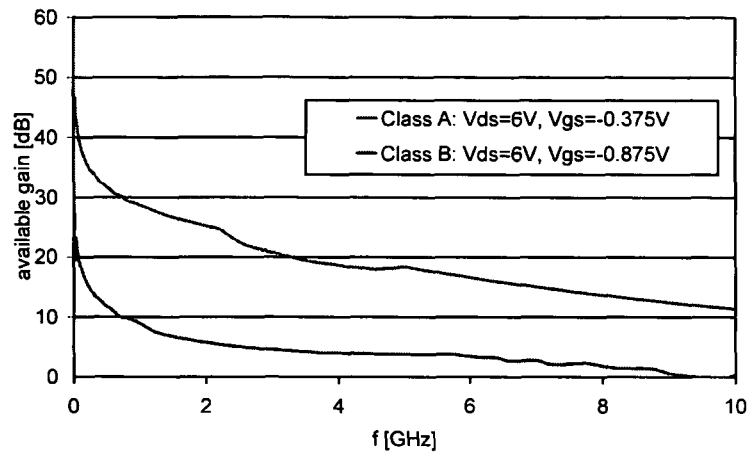


Figure 5.1: Available power gain of IAF 2.1 mm transistor

termination) for higher drain currents. Therefore, the device was not operated at the maximum allowed current in order to reduce the tendency for oscillation.

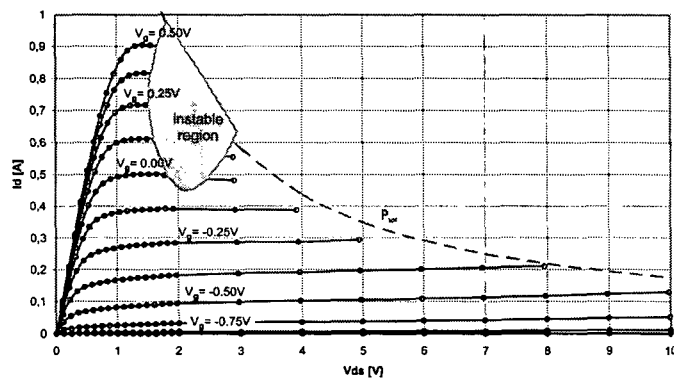


Figure 5.2: DC-IV plot of IAF 2.1 mm transistor

5.2 Test Fixture Considerations

For the calibrated measurement of any microwave device it is necessary to have a reproducible setup. There are two types of calibration worth of mentioning which can be used for such a task:

- SOLT (short open load thru) calibration: This type of calibration requires a standardized connector interface (one, for which an SOLT-calibration kit is available). The reference plane is located inside the connectors. This has the benefit of commercially available calibration standards but the big disadvantage that the measurement

of the transistor always includes the connection lines and the connector itself. This makes it impossible to reuse the measurements if the device is used without the same configuration (line lengths and connectors) in a circuit.

- TRL (thru reflect line) calibration [39], [40]: If the application requires reference planes within a circuit, typically no ready made calibration kit exists. There are too much parameters which have to be taken into account since a printed circuit board (PCB) is not a standardized product in contrast to a microwave connector system. Varying parameters are substrate and conductor thickness, dielectric constant and loss, transmission line type, impedance, ... It is impossible to have a calibration kit for each combination of these values. The solution is the TRL-calibration: By the use of simple line elements the reference plane can be defined in structures where no calibration exists.

This type of calibration is ideal, if the reference plane should be located as close as possible to the device under test. It also enables reuse of measurements in other circuits as long as circuit between both reference planes and the mounting of the transistor remains the same. Therefore, only a small area (typically some mm^2 for smaller transistors) need to be exactly the same, when using the measurement data for other circuit designs.

It was decided to use a microwave substrate with a high dielectric constant ($\epsilon_r = 9.5$) in order to keep all structures as small as possible. Details of the substrate are given in table 5.1. To provide good thermal conductivity it was chosen to split the PCB into two

manufacturer	Taconic
type	CER10-0250-C1/C1
ϵ_r	9.5
$\tan \delta$	0.0035 @ X-band
substrate thickness	0.635 mm
copper thickness	35 μm

Table 5.1: Taconic CER-10 properties

parts and to mount the active device on a brass base in between. The left part of figure 5.3 shows the carrier made of brass with the base for the transistor. In the middle of figure 5.3

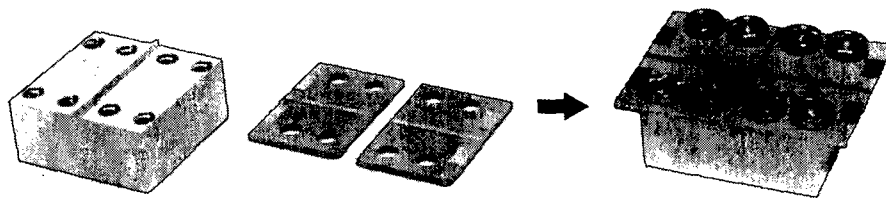


Figure 5.3: Transistor test fixture

both microwave substrates with 50Ω microstrip lines for connecting to the transistor are

shown. The substrates are entirely copper plated on their back side. The final assembly is depicted on the right: both substrates are mounted with screws on the brass carrier. The transistor is bonded with a high thermal and electrical conductive adhesive. Dimension are chosen such that the transistor's surface is on the same height as the microstrip lines. The connection to these lines is achieved by a $25\ \mu\text{m}$ gold-wire wedge-wedge bond. Figure 5.4 shows an enlarged photograph of the transistor mounting.

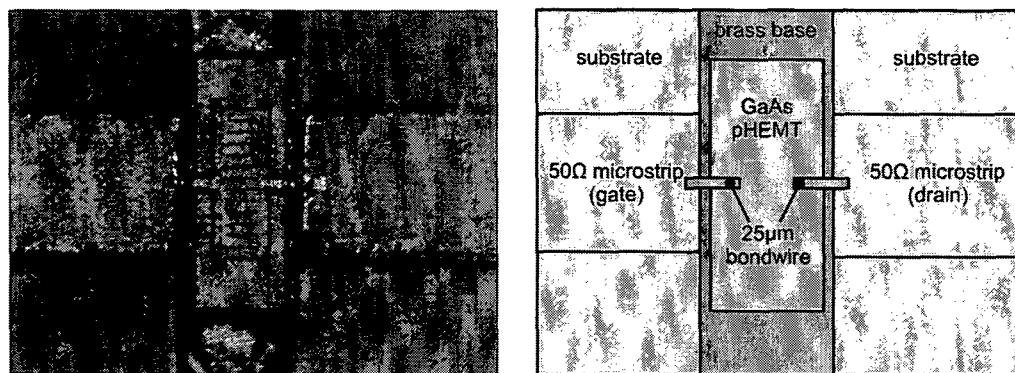


Figure 5.4: Testfixture detail: bonded transistor

The transistor test fixture has to be connected to the outside world – a transition to a microwave connector system becomes necessary. A choice had to be made between the following two alternatives:

- **Mounting of PCB-connectors:** This would require also to use the same connector-system for the TRL-calibration kit in order to have the same errorboxes for each connector. Since this requires identical mounting and soldering of eight connectors (two for the transistor fixture and six for the calibration kit), some uncertainty in calculation the fixture's errorboxes (see next chapter) has to be expected. It would further be necessary to manufacture a metal carrier for the calibration kit to ensure a robust assembly of the SMA-connectors. This also requires pressing down the substrate onto the carrier with screws close to the connectors in order to ensure a good ground contact from the PCB to the connector (with low inductance through possible gaps).
- **Using a test-fixture for PCBs:** In a similar way to the test fixture realized above (to connect to the transistor), test fixtures are available for connecting to printed circuit boards. Such fixtures typically allow contacting to coplanar and microstrip lines. The big advantage of such a fixture is that the assembly of connectors is not required any longer. This reduces the additional precautions listed above; especially the requirement for the identically assembled connectors. The PCB test fixture available at our institute was bought from Connexion Rosenberger and it is depicted in figure 5.5 with a TRL-calibration substrate inserted. The idea behind this fixture is quite simple: At each side an arbitrary number of PCB to SMA transitions can be lined up. These so called launchers can be moved along the PCB edges to be aligned with the microstrip/coplanar lines of the clamped substrate. Also the

distance between the left and right connector block can be varied according to the inserted PCB's dimensions. After setting all these distances the substrate can be clamped by moving the launchers downwards to the substrate on both sides. The mechanical construction of the launchers and the PCB test fixture ensures low reflection at the transitions and high reproducibility. For precise displacement of the connector blocks (needed for TRL calibration), the right block can be adjusted by a micrometer.

Measurements turned out that the repeatability of this PCB test fixture for frequencies $f < 10$ GHz is a little bit better than what can be achieved with multiple soldered connectors. So this fixture was used for all load pull setups within this thesis.

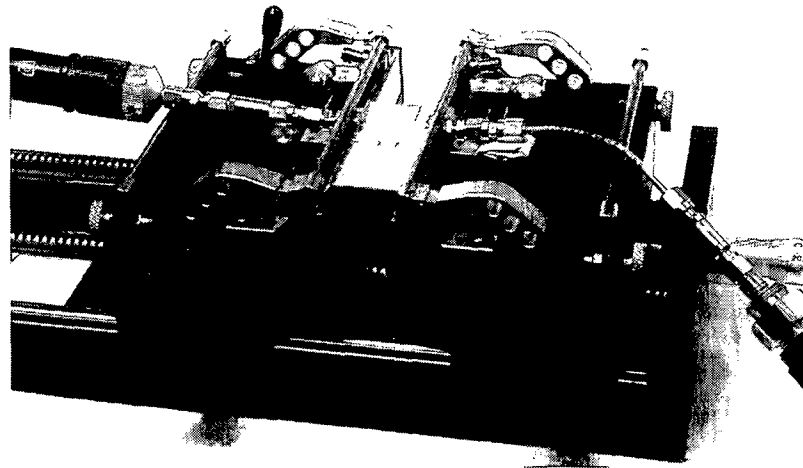


Figure 5.5: Connexion Rosenberger PCB testfixture

5.3 TRL Calibration / Errorbox Extraction

As explained in the preceding section a thru-reflect-line (TRL) calibration [39] will be used for the measurements. The TRL calibration allows to define a reference plane without the need for calibrated reference elements. It uses three elements which are very simple to produce independent of the type of the used transmission mode. The application simplicity does not change if applied to waveguides, coaxial lines or planar transmission lines.

The three elements needed are:

- **Thru:** This element is required for the definition the reference plane; it has zero length and no loss: $S_{21} = S_{12} = 1 \angle 0^\circ$, $S_{11} = S_{22} = 0$.
- **Reflect:** This element must provide a high reflection coefficient. $|\Gamma|$ needs not to be known, $\arg(\Gamma)$ must be known within $\pm \frac{\lambda}{4}$. This means either a non-perfect short or non-perfect open can be used. The reflection coefficient Γ must be the same for both ports.

- **Line:** The impedance of this element defines the reference impedance. The loss of the line needs not to be known. The electrical length must be specified within $\pm \frac{\lambda}{4}$, the optimum length is $\frac{\lambda}{4}$. Therefore, the maximum usable frequency range of a line is 1:8 (start frequency/frequency span) in order to have some degrees of safety margin for the phase. Extending the frequency range requires multiple line elements with different electrical lengths. If there is demand to measure at frequencies down to DC a match with the reference impedance becomes necessary. Because this is often hard to realize (due to parasitic inductance and capacitance), DC measurements are not favorable with a TRL calibration.

To cover the required frequency range from $f_0 = 2.145$ GHz up to $3f_0 = 6.4335$ GHz only one line element is needed, also the S-parameters for DC are not of interest which eases up the design of the calibration. The calibration elements are listed in table 5.2 and they are shown in figure 5.6. One of the reflect elements is obsolete. Also the resonator was used for test purposes only.

element position	calibration element	parameters
1 (top)	thru	—
2	reflect (open)	—
3	reflect (short)	—
4	line	$l = 7.6$ mm, $t_D \approx 78$ ps (1.15 . . . 9.05 GHz)
5 (bottom)	resonator	$l = 7.2$ mm, each gap $d = 0.2$ mm

Table 5.2: Parameters of TRL-calibration kit for $f = 900$ MHz . . . 7 GHz parameters

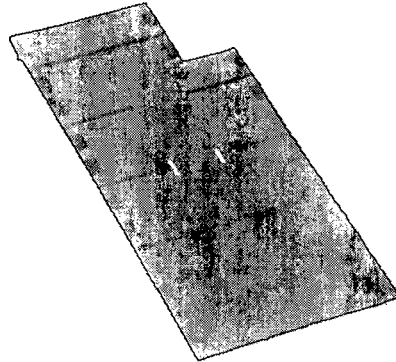


Figure 5.6: TRL calibration kit

With the parameters of table 5.2 a simple calibration with standard network analyzers is possible[40], because the TRL algorithm is implemented as a standard. This allows S-parameter measurements for a device between the reference planes. Due to the occurrence of many phase ambiguities¹, which have to be solved during the calculation of the TRL

¹Phase ambiguities occur, because the TRL-calibration requires to extract roots which have two solutions. To overcome this problem neighboring frequencies have to be observed in order to get a continuous phase of the calculated errorboxes.

errorboxes, it might happen that the calibration is wrong. It turned out that this can happen with the classic Agilent 8510 VNA when using too few frequency points. The newer Agilent PNA series does not suffer from this problem, because additional frequency points are measured by the instrument automatically if problems are expected.

The calibration which we have up to now is still not useful for load pull measurements. This is the case because the VNA calculates TRL errorboxes which cover everything between the TRL reference plane and its internal receivers (including cables, test set, ...). On contrary, for the load pull measurements the errorbox from the reference plane to the PCB test fixture's SMA-connectors is of interest – because from the SMA-connector on the entire load pull system will be characterized. Therefore, it was necessary to calculate the errorboxes manually. This was done in the following way:

1. The VNA will be calibrated to an SMA-connector reference plane by an SOLT-calibration.
2. With this calibration active the VNA is attached to the PCB test fixture and all TRL calibration elements are measured.
3. Now, the TRL errorboxes can be calculated by a self-written software. The resulting errorboxes now include only the transition from the microstrip reference plane to the SMA connectors.
4. Checking the calibration.

Step 4, the verification of the errorboxes, was done in the following way: Different elements were measured with the VNA on the one hand with an SOLT-calibration and deembedding of the calculated errorboxes afterwards. On the other hand the entire TRL-calibration was performed in the VNA and the same elements were measured again for comparison. Two exemplary results are given in figures 5.7 and 5.8. Figure 5.7 shows the comparison of the S_{21} measurement of a mismatched line element (realized by placing a metal part on the line). It turned out that the the deviation for the frequency band of

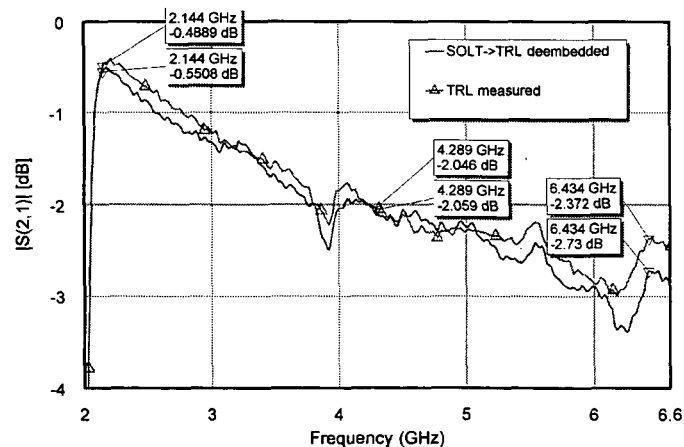


Figure 5.7: Verification of TRL-errorboxes, transmission measurement

interest $f_0 \dots 3f_0$ showed a maximum magnitude error of < 0.4 dB. Of course this is not perfect but would slightly influence the gain-measurements only. Because of the fact that a gain of ≈ 15 dB is expected, the influence on the power added efficiency calculation is negligible. Much more important is that the errorbox at the output of the transistor was calculated exactly. Deviations here would lead to a wrong view of the applied reflection coefficients at the new reference plane.

Having a look on the reflection measurement in figure 5.8 turns out that the errorbox seemed to be very precise in the required frequency range. The test device was a $20\ \Omega$ resistor which was, intentionally, mounted quite lously on the PCB in order to have high parasitic capacitance and inductance. So a larger area of the Smith Chart could be covered with a single measurement.

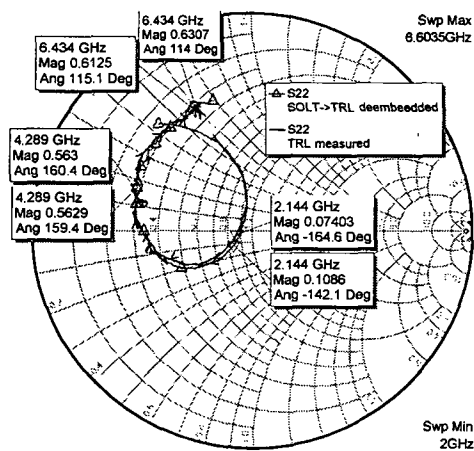


Figure 5.8: Verification of TRL-errorboxes, reflection measurement

With these two errorboxes it is now possible to deembed the test fixture. This is a prerequisite for any load pull measurements of non-connectorized devices. For the circuit designer it is of no interest what happens inside the transistor. For him, the Γ_F of figure 5.9 is of interest.

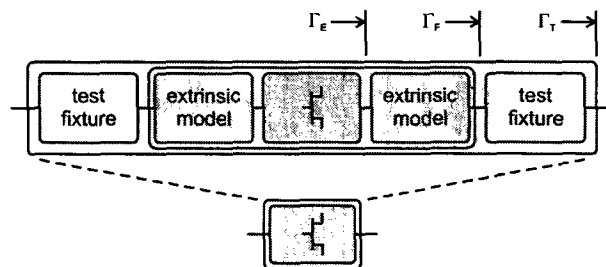


Figure 5.9: Reference planes of the setup

For gaining information on what happens at the intrinsic transistor, a further errorbox has to be determined to enable calculation of the load Γ_E seen at the inner transistor's

reference plane.

5.4 Deembedding of the Transistor's Extrinsic Elements

The extrinsic parasitics describe everything between the test fixture's reference and the so called intrinsic device. The idea behind is to put all linear and passive elements into the extrinsic model (this covers bonding inductances, package capacitances, ...). The remaining nonlinear and active elements make up the 'real' transistor, modeled by the intrinsic device. This is shown by the shaded areas in figure 5.10. This makes transistor modeling much easier due to the reduced number of elements. It is important to be aware of

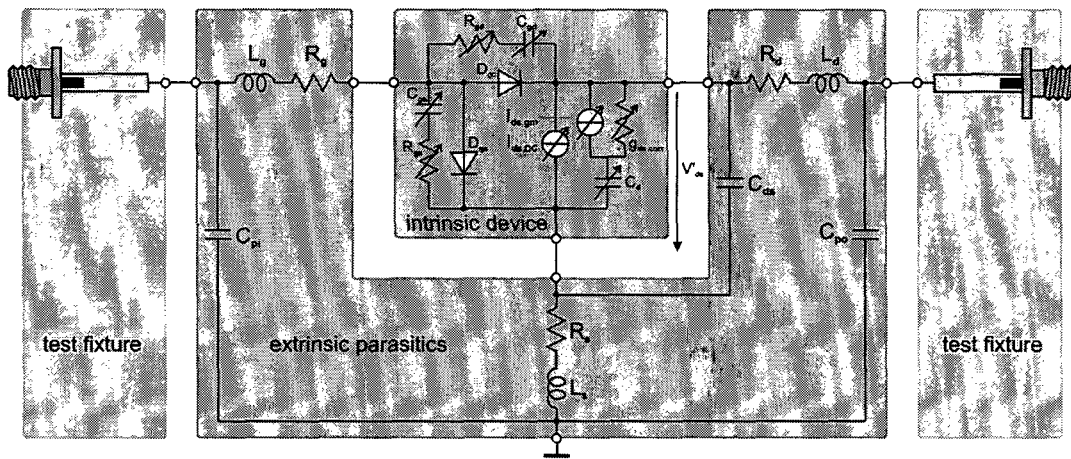


Figure 5.10: Model of the IAF 2.1 mm pHEMT

the fact that the intrinsic transistor is a virtual element which cannot be measured directly. The only way to characterize it is by means of deembedding the extrinsic parasitics.

But what can this information be used for, when not going to set up a nonlinear transistor model? When talking about transistor matching for harmonic operation the theory always assumes a perfect transistor. That means that the short or open required for this kind of operation must be seen at the intrinsic transistor, at Γ_E (compare figure 5.9). Even the circuit designer, who is typically just interested in the optimum Γ_F (compare figure 5.9), should try to further deembed to the inner transistor – especially when it is possible to calculate the intrinsic voltage and current waveforms. With this additional information the reliability of an amplifier design can be improved. It could happen, for example, that the efficiency and other parameters look very good, but the transistor's dynamic load line reaches into the forward breakdown. This can do quite well for a certain time but does not ensure a long lifetime.

To determine the S-parameters of the extrinsic model several ways exist and they are well described in literature. For example, a simple way for MESFETs and HEMTs is shown in [41]. A method suited for LDMOS transistors is described in [42].

For this thesis the determination of the extrinsic element values was not necessary, because as a result of a former project an entire large signal model was developed. The model used (shown in figure 5.10) is based on the COBRA model [43]. Further enhancements

were implemented in order to give a better fit to measured values [44]. The values for the extrinsic elements are listed in table 5.3.

element	value	element	value	element	value
L_g	0.2 nH	L_d	0.24 nH	L_s	0.14 nH
R_g	1.0 Ω	R_d	0.30 Ω	R_s	0.11 Ω
C_p	0.35 pF	C_{po}	0.35 pF	C_{ds}	8.50 pF

Table 5.3: Parameters of IAF-2.1mm transistor model

To calculate the S-parameters of the extrinsic parameters on the drain side, the transistor was replaced by an ideal transformer to have a grounded port at the intrinsic side (figure 5.11). This was done only for the drain side because this work focuses on load-pulling.

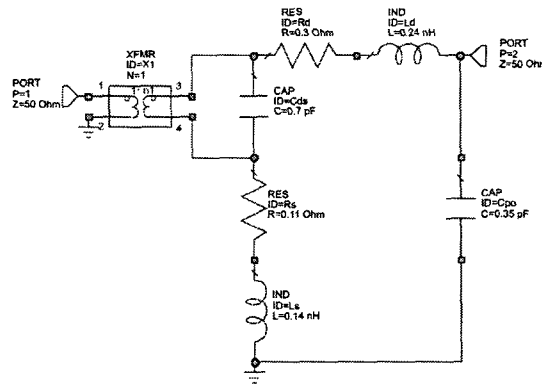


Figure 5.11: Schematic used for calculating S-parameters of drain extrinsic model

Please note that the intrinsic transistor consists of two current sources, which are connected in parallel by a nonlinear capacitance and a nonlinear resistor. Therefore, it is not a must that the optimum load for the transistor (seen at Γ_E) is real valued. Due to the second current source a small imaginary part can be expected.

5.4.1 Triplexer

For the realization of a passive load pull system it is desirable to have independent control of all harmonic frequencies. If standard tuners are available the easiest way to accomplish this is the use of a triplexer filter. This is a filter which separates the first, the second and the third harmonic frequencies from each other. Such filters are not off the shelf products – tuner system manufacturers as well as filter companies offer customer specific designs. This, of course, limits the flexibility in varying the center frequency.

It is also not possible to use commercially available low-, band- and highpass-filters for this task, because the input signal from the device under test must be split into three signals for the different filters (figure 5.12a). Since two filters are always out of band (which corresponds to a reflection of the input signal), mismatching will occur at the triplexer's

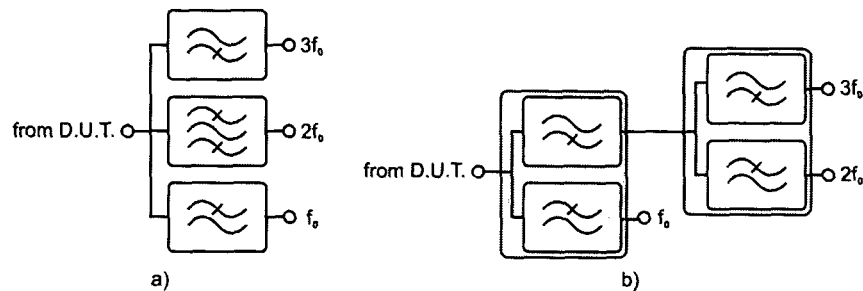


Figure 5.12: Triplexer realizations: a) unpractical, b) recommended

input making the overall circuit unusable. There exists no literature which provides design guidelines in order to achieve matching at the triplexer input by cancellation of the respective two blocking filters. Hence, triplexers are typically realized by the series connection of frequency splitters (figure 5.12b) – it would also be possible to combine bandpass and bandstop filters.

Diplexers (often off the shelf for certain frequencies) ensure matching at the filter's input by the appropriate connection of a low- and a highpass filter. Of course, this only works if both filters are tuned for combined application. Connection of any standard lowpass with a highpass would not give this behavior. When using such a design, attention has to be paid that each stage introduces additional insertion losses and, therefore, reduces the tuning range. It is desirable to combine all three filters into a single package to get rid of unnecessary connector losses.

Because of the lack of components and the requirement of low losses a triplexer, which was developed at the institute, was chosen for the application.

For the design of this triplexer filter the following guidelines were considered:

- The design should have all three filters on a single printed circuit board in order to ease up fabrication. This has several reasons: First of all a huge variety of PCB connectors are available for all standard connector systems (SMA, N, ...). Secondly, the need for precise mechanical construction (like for cavity filters, coaxial filters, ...) is not required – the only part which has to be realized with tight tolerances, the PCB, is produced by a commercial manufacturer which is typically used to work precisely.
- The triplexer must provide a DC feed through in order to apply a bias to the device under test. Of course it would also be possible to use a bias-tee in-between the DUT and the triplexer; this would have the disadvantage of additional losses and thus would lead to a reduced tuning range (i.e. a smaller realizable reflection coefficient) seen at the DUT
- The insertion loss of the triplexer should be as low as possible. Again, paying not attention on this would reduce the tuning range.
- All ports should be matched to $50\ \Omega$ impedance. If a design with a slight mismatch would lead to a lower insertion loss, this would be more desirable.

- The bandwidth should cover at least 15 MHz so as to allow the application for load-pulling with WCDMA-signals since its 5 MHz baseband results in the threefold bandwidth at the third harmonic frequency range.

The triplexer used is based on [45] and [46] with center frequencies set to $n \cdot 2.1445$ MHz, with $n = 1, 2, 3$. It uses three directional filters using stripline technology. Each of these filters consists of two broadside couplers connected together so as to form a resonant ring at the desired frequency. The principle is documented in figure 5.13. Each stage separates one frequency and passes the residual signal on to the next stage (compare figure 5.12b). Coming from the left (the DUT side) the third harmonic frequency range is separated from

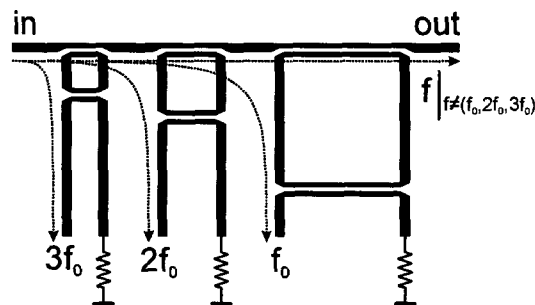


Figure 5.13: Triplexer based on directional filters, schematic

the main signal trace (the one which connects in and out). Following this comes the second harmonic and then the fundamental frequency. On the one hand this order is necessary, on the other hand it has an advantage for the application in load pull systems. First to the necessary part: Because the ring length of the fundamental frequency's directional filter is also resonant for integer multiples of its own frequency, the signal must be applied from the side of the third harmonic resonator. Doing it the other way round would result in coupling out all three frequencies at the f_0 -port.

Additionally, placing the $3f_0$ -resonator as the first in line also minimizes the insertion loss from the input port to the coupled output. Especially for load-pull application the third harmonic tuner has to provide the highest tuning range, because the transformation due to the transistor's extrinsic elements becomes more and more crucial for higher frequencies (compare section 5.5.3). Hence, providing low insertion loss for the third harmonic frequency enables a wider tuning range for load-pull measurements.

A photograph of the final design is shown in figure 5.14. In contrary to [45] a very thin microwave substrate with double side copper cladding was used for the circuit structure ([45] uses two 3.175 mm thick single side copper cladded substrate with a thin substrate layer in between). This removed the need for aligning of the upper and lower PCB. But still, the thin microwave substrate is covered on top and bottom by a thick substrate before mounting two brass ground plates which also serve for mechanical stability.

Having a look at the three-resonator design might raise the question why the last stage of the fundamental frequency coupler is necessary. When using a mechanical tuner (which provide \sum a DC feed-through typically) a separation of the fundamental frequency f_0 would not be required at all. Doing the realization this way would provoke another problem: Assume a slidescrew tuner (compare section 3.1.2) attached at the f_0 /DC output. If this

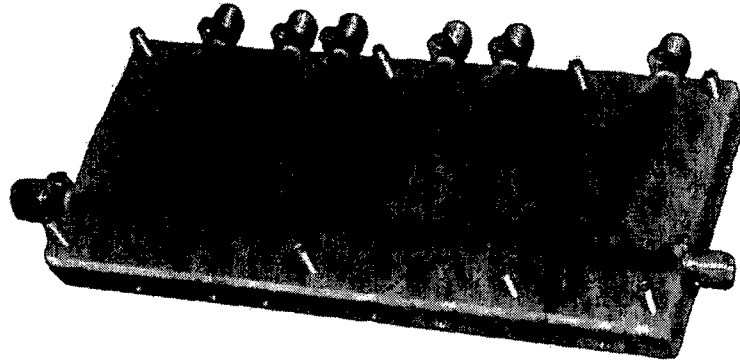


Figure 5.14: Photograph of the triplexer

tuner is set to a certain position for matching the fundamental frequency also reflection at the harmonic frequencies occurs (in consequence of the operational principle of a slidescrew tuner). This could result in providing high reflection coefficients for the harmonics. Hence, harmonic frequencies are reflected from two tuners; the fundamental one as well as from the corresponding harmonic's one. This would impair the the harmonic tuner's overall performance and make the triplexer unusable, because the tuning range of the load pull-setup would be reduced extremely, in particular for a high $|\Gamma_{f_0}|$. An f_0 -branch is therefore required for proper decoupling of the three frequencies.

The output of the triplexer (figure 5.13) provides a DC feed-through as well as all other frequencies except integer multiples of the fundamental frequency f_0 .

Due to the design with a DC (low frequency) feed-trough the triplexer has an additional benefit. It is possible to apply a termination for frequency bands beside multiples of the fundamental frequency also at the DC port. Exactly speaking the name 'DC port' is therefore incorrect but defines its primary function. By applying a termination at this port the risk of unwanted oscillations can be dramatically reduced. This is especially a problem at low frequencies where the transistor has a high gain. Commercially available triplexers often suffer from this problem because they do not provide an output for frequencies outside the ones of interest. Therefore, the energy in these bands is reflected instead of terminated which aids to fulfill the oscillation condition.

The measured data of the triplexer is given in figures 5.15 and 5.16. In these measurements port 1 corresponds to the input of the triplexer whereas port 2 was connected to the different filtered outputs. The measurement shows that the three filtered outputs are decoupled better than 20 dB, but it also indicates a high S_{21} of about -1 dB. This can be explained by the non-perfectly matched ports of the triplexer. Having a look on the transmission losses (5.16) shows that the power loss is not as high as expected. Assuming e.g. a perfect S_{11} at f_0 and calculating the S_{21} from the loss measurement would give -0.53 dB (instead of -0.93 dB shown in figure 5.15). This indicates that there could be a performance increase by adding matching networks to the filtered outputs. These networks can be very simple because they must serve for one frequency only and can therefore be realized in stripline technology also. For the application in the harmonic load pull measurements the triplexer was left unmodified: Having also the matching network included would not give a sufficiently high tuning range at the intrinsic transistor for the passive

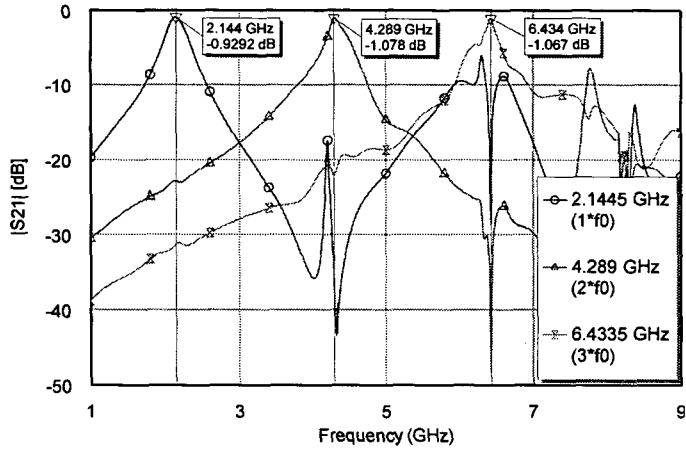


Figure 5.15: Triplexer transmission measurement

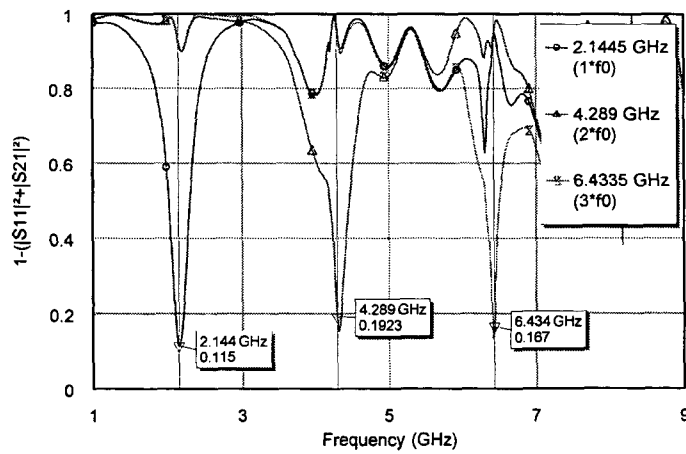


Figure 5.16: Triplexer losses

load pull realization — for active load pull the losses do not carry so much weight, because they can be entirely compensated.

5.5 Passive Harmonic Load Pull with Triplexer

To have a reference for the other load pull systems discussed in this thesis, a harmonic load pull setup was realized with commercially available tuners and software from Maury Microwave [17]. This system allows the realization of different setups, including noise measurements, fundamental load pull, harmonic load/source pull. Measurements can be done with single carrier, dual tone as well as modulated signals. Harmonic tuning is only supported with triplexers – resonant harmonic tuners are neither supplied by Maury Microwave nor can they be used by the software. For automation of the entire setup the software provides drivers for a wide range of instruments needed for load/source pull (power supply, noise figure meters, vector network analyzers, signal sources, ...). So the user's task is 'just' a proper connecting of all parts of the setup.

5.5.1 System Setup

A typical block diagram for harmonic load pull is given in figure 5.17. The signal source

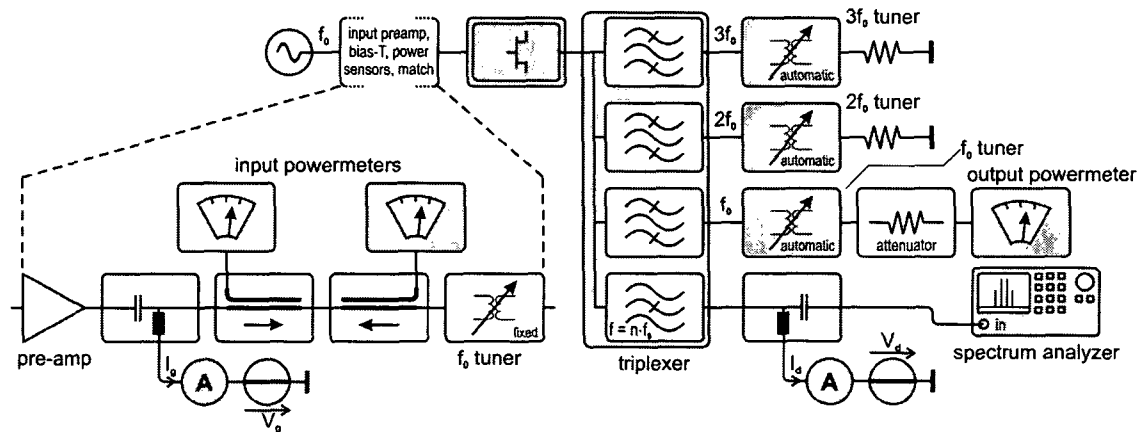


Figure 5.17: Passive harmonic load pull with triplexer, block diagram

(figure 5.17 left) generates a continuous wave (CW) excitation signal for the device under test (DUT). Of course, the source can also be extended by a second one for dual tone tests as well as replaced by a modulated source for e.g. WCDMA signals. To increase the drive power an amplifier was connected in series to the source. Following the DC supply for the gate voltage of the DUT is added; the gate current was measured because an increase turned out to be a good indicator for an oscillating device. For the measurement of the input matching directional couplers with power meters were used. The input matching itself was achieved by setting a manual double slug tuner in such a position that as little power as possible is reflected from the DUT side. The entire gate side setup (ranging from the pre-amplifier to the manual tuner) was kept the same for all other harmonic load pull setups. The setting of the manual tuner was not changed either.

After the gate matching the central part – the device under test – follows. Figure 5.17 indicates that also the effects of the test fixture are included here.

On the output side of the DUT the triplexer follows. Please note, that the triplexer in figure 5.17 only symbolizes the function but not the internal realization (see section 5.4.1 for details on this). At each filtered output an automated tuner (Maury MT982A02, VSWR > 15 : 1) was attached. The harmonic tuners at $2f_0$ and $3f_0$ were terminated with 50Ω . At the fundamental frequency $f_0 = 2.1445$ GHz a 10 dB-attenuator was connected in order to reduce the output power to the measurement instruments allowed input power levels. Finally a power meter detects the output power.

For the drain supply the DC port of the triplexer was used. Because of the fact that all frequencies except of integer multiples of f_0 are also present here, it was necessary to use a bias-tee in order to provide a 50Ω termination for all RF frequencies.

The setup shown in figure 5.17 could also be extended by power meters for the harmonic frequencies instead of the terminations to know about the harmonic power levels. It should also be stated here that the input power meters are not a requirement. If the input matching of the transistor is already known they can be omitted since they are not needed for the entire system's calibration (see below). Also the spectrum analyzer at the output side is not absolutely necessary; It is used to detect possible oscillations of the device under test.

5.5.2 System Calibration

The following calibration procedure is used in order to simply the number of required measurements: First of all the automatic tuners have to be characterized. This can be a time consuming procedure which can be done in two different ways by the supplied software:

- A method very well suited for the tuners at the harmonic frequencies $2f_0$ and $3f_0$ is the specification of the mechanical positions of the tuner's carriage and stubs. Because the main purpose of harmonic load pull – the design of harmonic controlled amplifiers – requires high reflection at the the $2f_0$ and $3f_0$ frequencies the entire tuning range need not to be characterized. Therefore, a recommended calibration would specify a stub position as close as possible to the inner conductor of the tuner (highest reflection) and would step the carriage over the corresponding $\frac{\lambda}{2}$ -distance. Doing it this way allows a characterization of a harmonic tuner within about five minutes.

Applying this method for the fundamental frequency (where different stub positions are needed also), would result in overnight calibration times. Also the distribution of realized reflection coefficients becomes non uniform (assume 30 Γ -values with $|\Gamma| = 0.8$ as well as 30 ones with $|\Gamma| = 0.1$, the latter ones would be – unnecessarily – crowded in the Smith Chart).

- When characterizing the fundamental tuner the method of choice is a calibration which is based on a tuner model. This is performed the following way: The user of the software can specify the number of positions used for modeling as well as the final Γ -density in the Smith Chart. Provided with this information the software uses the initial measurements to set up a model for the tuner. With this model the tuner

motor positions are calculated in such a way, that they result in equally spaced values of the reflection coefficient. Of course, this modeling is not perfect and, therefore, each of these positions is set and measured by a vector network analyzer (VNA).

A calibration for 300 different Γ -values will last about 1.5 hours.

Please note, that the time durations given above apply for one frequency each. Calibration for an additional frequency requires the same procedures again because different motor positions must be used due to the changed wavelengths. For practical measurements it is often sufficient to characterize the system for one frequency only and for its harmonics.

For the harmonic load pull setup (figure 5.17) the tuner calibration could be done in two different ways. One possibility is to measure each tuner as well as the triplexer separately. All S-parameter files can then be used by the tuner system software. Since this requires many different VNA-measurement setups (as well as a 4-port measurement of the triplexer) a different method was chosen: Due to the high decoupling of the triplexer (> 20 dB, compare section 5.4.1) the tuners were characterized with the triplexer already attached (figure 5.18a). The connection to the VNA can be kept the same for characterizing all tuners because S_{21} of the harmonic tuners is not of interest. The value will not be used for calculations in the software because no power meters are attached at these tuners. This speeds up the measurement as well as improves accuracy because the connections between the tuners and the triplexers can remain unchanged when inserting this part (figure 5.18a) into the entire setup (figure 5.17).

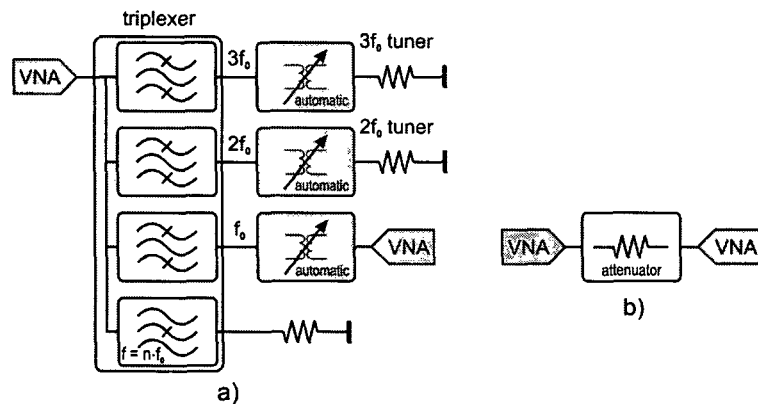


Figure 5.18: Passive harmonic load pull with triplexer, calibration

The S-Parameters of the attenuator and of the 6 dB-splitter are also required for the calibration (figure 5.18b). Specifying the insertion loss only could lead into a deviation from the calibrated Γ -values at f_0 if the attenuator is not perfectly matched at its input. To obtain an exact calibration, of course, it would also be necessary to characterize the input matching of the spectrum analyzer and of the output power meter (both are connected at the 6 dB-splitter). This was not done (both instruments were assumed have a perfect input match), because even a total reflection $|\Gamma| = 1$ on both instruments would lead to a matching of -29 dB at the attenuator's input. This can be simply explained: A wave coming from the input of the 10 dB-attenuator is reduced by 16 dB when impinging at the

instrument inputs. Here, perfect reflection would occur and both signals are again reduced by 16 dB on the way back. In the worst case constructive interference between both signals occurs, giving a 3 dB higher signal. This results in $(-16 \text{ dB}) + (-16 \text{ dB}) + (3 \text{ dB}) = -29 \text{ dB}$. Hence, the matching of the instrument's input can be neglected.

After entering the S-parameters of the test fixture's error boxes, setting the manual input to 50Ω , and inserting a thru-element into the test fixture the entire setup is now ready for system calibration. By knowing the S-Parameters from the DUT on down to the output power meter it is possible to calibrate for the available DUT input power. By setting the f_0 output tuner to different Γ -values, the reflection coefficient of the source can also be determined. So, even a mismatch from 50Ω of the input tuner would be corrected as long as the tuner's insertion loss remains constant (measurement turned out that this is approximately true for $|\Gamma| < 0.2$ of the double slug tuner). This can be done for different power levels of the RF source in order to compensate for nonlinearity.

After this the system is entirely calibrated and it can be used for measurements.

5.5.3 Achievable Tuning Range

A key figure of each load pull system is the realizable reflection coefficient at the input of the tuner system. This corresponds to Γ_T in figure 5.9 which is the triplexer input for this system.

The tuning range of the passive harmonic load-pull setup for all three frequencies is shown in figure 5.19. The reduced tuning range due to the triplexers insertion loss is

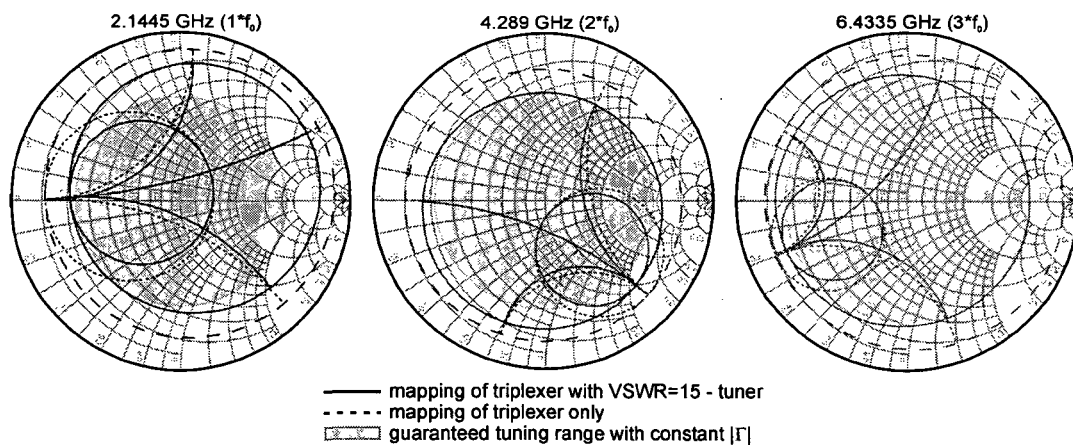


Figure 5.19: Passive harmonic load-pull, tuning range at triplexer input

shown with a dashed line. As already indicated in section 5.4.1, the triplexer was not perfectly matched. This is the reason why the resulting tuning range is not perfectly centered around the origin in the Smith Chart. Furthermore, the dashed lines show how reflection coefficients at one of the triplexer outputs are mapped to the input. Having a look at the fundamental frequency in figure 5.19 shows that the Smith Chart is rotated by about 180° as compared to its default position. This means that an open at the f_0 -output of the triplexer is transformed into a low resistance (but not into a short due to insertion

losses) by the triplexer. Whereas applying a short at the f_0 -output will be transformed into a reflection coefficient which is away from the real axis. This means that equally spaced Γ -values at the f_0 -tuner's input result in an unequal density at the triplexer input. Hence, it was a good choice to connect the triplexer for the tuner calibration, because the software tries to realize an equal density of Γ -values at the measurement port (which was the triplexer input).

The Smith Charts drawn with solid lines in figure 5.19 indicate what happens when a VSWR 15:1 tuner is attached at the triplexer's outputs: A further reduction of the tuning range occurs. For having a fair comparison it is important to use the $|\Gamma|$ -value for comparison which can be guaranteed independent of the phase. The resulting tuning range at the input of the triplexer is shown by the shaded area in figure 5.19. Of course, higher Γ -values can be obtained but only for a limited phase range. This might improve the tuning range for some applications but cannot be seen as a general measure for the performance of a tuner setup.

The achievable reflection coefficients at the triplexer input are listed in table 5.4. The

frequency [GHz]	$ \Gamma $	(max. $ \Gamma $)
$f_0 = 2.1445$	0 ... 0.62	(0.85)
$2f_0 = 4.289$	0 ... 0.65	(0.76)
$3f_0 = 6.4335$	0 ... 0.72	(0.72)

Table 5.4: Achievable Γ of passive load-pull system (at triplexer input)

reflection coefficients which can be achieved for each phase are listed in the $|\Gamma|$ -column. The maximum value (achievable for a certain phase only) is shown in the max. $|\Gamma|$ -column. It would be unfair for comparison to use this value as a performance measure.

It can be seen that the largest tuning range of $|\Gamma|$ is available for the third harmonic frequency $3f_0$. This can be simply explained by the realization of the triplexer: $3f_0$ is the first frequency component which is separated from the rest of the spectrum and experiences, therefore, a lower insertion loss due to short transmission line lengths. The last stage of the triplexer separates f_0 – hence, two resonant coupler stages have already been passed which leads to a higher insertion loss and, consequently to lower achievable values of $|\Gamma|$.

When using the tuner system for the measurement of the selected pHEMT-transistor a further reduction of the tuning range due to the test fixture has to be accepted. Further deembedding to the inner transistor's view (Γ_E) shrinks the tuning range again. Figure 5.20 shows the range of realizable reflection coefficients at the reference plane of the fixture and the intrinsic transistor. The tuning range is based on the transformation of the shaded (the guaranteed) tuning areas of figure 5.19.

The values shown in figure 5.19 mainly depend on the extrinsic elements of the device under test. They can only be used as a performance measure when using the same transistor with the same test fixture with different tuner systems (as done within this thesis). A tabular listing of the realizable Γ -values does not make sense at this reference plane. Assume having a power transistor which requires an output match of 5Ω . A ten times larger tuning range for the harmonics ($0.5\Omega \dots 50\Omega$) would be definitely enough. The required tuning range would be located to the left of the matching point in the Smith Chart. It would be necessary to re-normalize the Smith Chart to the device's fundamental

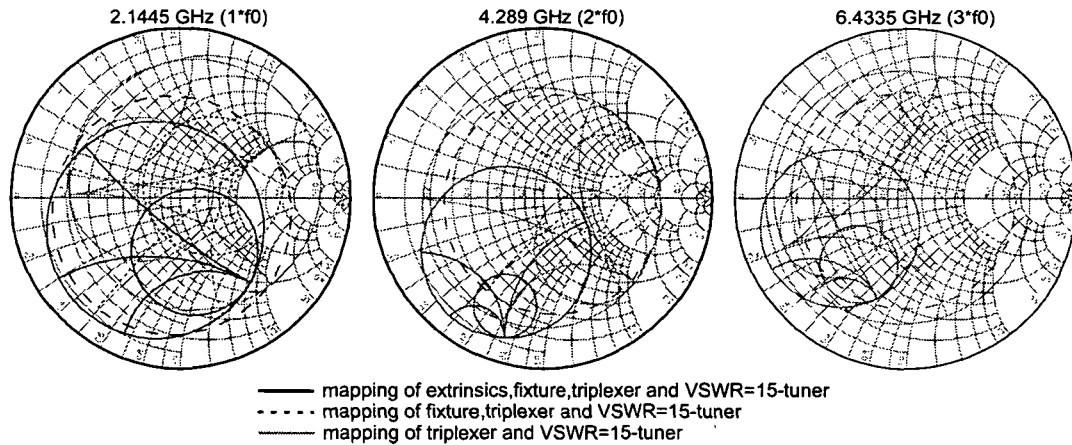


Figure 5.20: Passive harmonic load pull, tuning range at fixture and intrinsic transistor

output impedance in order to have a tuning range which is centered around the origin. — To avoid confusion by the use of different reference impedances, the tuning range for the inner device will only be shown in the way like figure 5.20 does. It can easily be seen from this graph also, if harmonic tuning still makes sense or if the tuning range is too small.

Due to the lowpass characteristic of the extrinsic elements the tuning range gets smaller and smaller with higher frequencies. So it comes in quite handy that the triplexer provides the highest tuning range for $3f_0$ – a fact which should be mentioned when buying or designing a triplexer.

5.5.4 Setting of Fundamental Match and Bias Point

Because this was the first measurement of the selected transistor within this thesis, an appropriate bias point as well as a fundamental load had to be determined. This is an iterative process which will be only sketched here. Explaining the search for perfect bias conditions and terminations goes beyond the scope of this thesis – this is often a quite intuitive process. Also, an optimum point was not required because the transistor served for the comparison of load-pull measurement setups only. It was chosen to find a gate match which allows the operation of the device in class F. The importance of an appropriate gate termination was mentioned already in chapter 2.

The selection of the bias point and of the fundamental load was done in the following way:

1. The transistor was set to an initial class-B bias condition. The harmonic terminations were set to 50Ω (this value is arbitrary, as long it is kept constant for the next steps).
2. Gate matching is set to maximize output power.
3. Different fundamental loads are tested for achieving high output power and efficiency.
4. The optimum point (a trade-off between efficiency and output power) will be chosen and a power-sweep will be done.

5. An input power level close to the 1 dB-compression point was chosen.
6. Bias conditions are modified a little bit with respect to a higher efficiency..
7. From step 2 on, the measurements are repeated until a satisfying bias point and fundamental load is found

With this method the gate bias was set to $V_G = -0.85$ V, the drain bias was set to $V_D = 6$ V. The input power was set to +15 dBm. The result of a fundamental load pull with this settings is shown in figure 5.21. Please note that a only a subset of Γ -values, distributed within the tuning range of the fundamental tuner, was used for the measurement. The mechanical tuner's resolution is extremely finer but it is not required for this measurement. Also some gamma points are a little bit outside of the calculated tuning range of figure 5.19. This is the case because the used automatic tuner's VSWR was somewhat higher than guaranteed by the manufacturer.

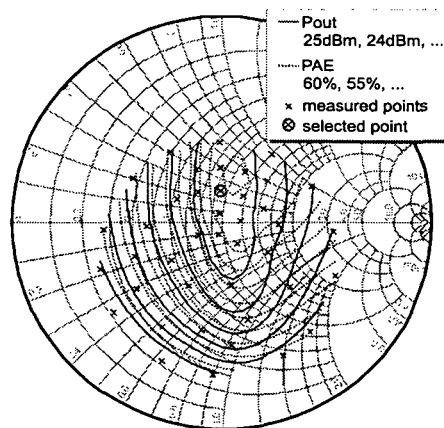


Figure 5.21: Results of fundamental load pull

For having high output power as well as high efficiency it was chosen to use $\Gamma_{E,f_0} = 0 + j0.17$ resp. $Z_{E,f_0} = (42 + j15) \Omega$ (impedance seen by the intrinsic device; the Γ_E -plane in figure 5.9). As expected by the type of the intrinsic model the impedance is not purely real but located closely to the real axis of the Smith Chart.

No attention was paid to the value of the input matching. Since this work focuses on the output side, the input match was kept constant for all load pull measurements.

5.5.5 Measurement Results

Having a look at the chosen Γ_E and the available tuning range in figure 5.19, it becomes quite clear that harmonic tuning does not make much sense with this configuration. The achievable reflection coefficients at the harmonic frequencies are extremely limited in phase. This can be seen in figure 5.22 where the second harmonic tuner setting was swept along the border of the possible tuning range. Figure 5.22 has to be read in the following way: Measured points are marked with crosses. The P_{out} - and PAE-lines between these points are based on data interpolation. Nevertheless, the lines connect two points with the same

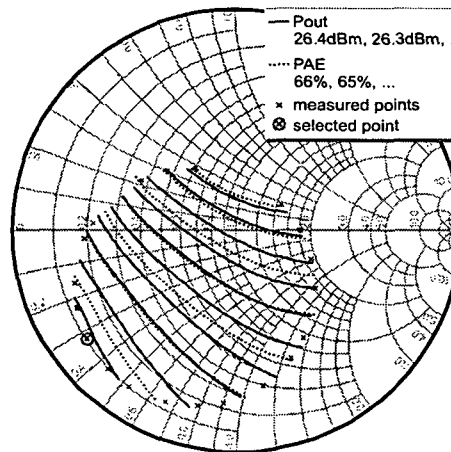


Figure 5.22: Results of second harmonic load pull

output power resp. efficiency value to make reading of the graph easier. It is clearly indicated by this graph that a better performance (both for P_{out} and efficiency) can be achieved with a highly reflective load at the second harmonic. By analyzing the displayed lines it turns out that they do not depend on the magnitude of the reflection factor only. It can be guessed that the optimum match might reside at $|\Gamma| = 1$ (this is what theory tells us) with a phase of about $-120^\circ \dots -180^\circ$. Because this guess is based on extrapolation of measurement data this does not need to be true. It could even happen that loads with an angle of $\approx 70^\circ$ might give comparable or even better results.

Limited by the tuner range, the choice for the second harmonic impedance fell onto $\Gamma_{E,2f_0} = -0.68 - j0.49$ resp. $Z_{E,2f_0} = (5 - j16) \Omega$ (again measured at the intrinsic reference plane). While keeping the loads of the fundamental and second harmonic frequency constant the $3f_0$ -load was moved along its border of the tuning range. Due to the limitations of the realizable reflection coefficients at the third harmonic it turned out that essentially nothing happened, see table 5.5. A correlation to the set reflection coefficient was still

	min. observed value	max. observed value
P_{out}	26.43 dBm	26.47 dBm
PAE	66.10%	66.63%

Table 5.5: Results of third harmonic load-pull

present, so the resulting variation is not a consequence of noisy measurements.

The design of a class F amplifier was not possible under these conditions. Therefore, the harmonic tuner designed in this thesis (compare chapter 4) was used for the measurement. The results of this measurement are presented in section 5.6.4. An other alternative for an improvement of the tuning range would be the insertion of a defined mismatch into the setup. Using non 50Ω -lines as transformers is often a good starting point. Attention has to be paid that the line does not worsen the tuning performance at f_0 and $2f_0$ when designed e.g. for the third harmonic. A design allowing an improvement for all frequencies is often quite complicated to realize. Also the extrinsic parameters of the transistor are needed

in order to know what to compensate for. The S-parameters of such a correction element must be entered into the used tuner software application to keep the setup calibrated.

5.5.6 Summary

Harmonic load-pull with the use of a triplexer suffers from the insertion loss within the setup. The tuning range for the fundamental and the harmonic frequencies is too limited to give meaningful measurements. A suitable fundamental match and bias point was determined and kept constant for all further measurements within this thesis to allow for comparison. Pulling the second harmonic showed only that output power and efficiency increase with a more reflective termination. The tuning range was too small to allow precise statements about the best phase setting. It could only be expected by extrapolation that a phase angle of $-120^\circ \dots -180^\circ$ might give best results.

It is a must to improve the tuning range to allow proper harmonic load-pull measurements.

5.6 Passive Harmonic Load Pull with "Harmonic Tuners"

As shown in section 5.5 the insertion loss of the triplexer limits the tuning range so much that a harmonic load-pull measurement up to the third harmonic did not make any sense for the transistors used. To overcome this problem with a passive system several ways are possible. Firstly, a corrective matching – see last section – can be applied. Since this must be adapted individually for each measurement setup it must be rather seen as a workaround than as an improvement of the system. Secondly, a triplexer with lower insertion losses could be used. This was not possible with the used triplexer design, and so a customized triplexer would have been needed. Because of its high costs and an expected improvement of only $0.2 \dots 0.3$ dB this method was abandoned also. So the third possibility was chosen, i.e. the use of a harmonic tuner. This tuner was realized within this thesis (chapter 4) to show that a satisfactory performance can be achieved even with a simple mechanical construction.

5.6.1 System setup

The block diagram for the application of the harmonic tuner is depicted in figure 5.23. Of course, this looks a little bit simpler now, because no triplexer is used for this con-

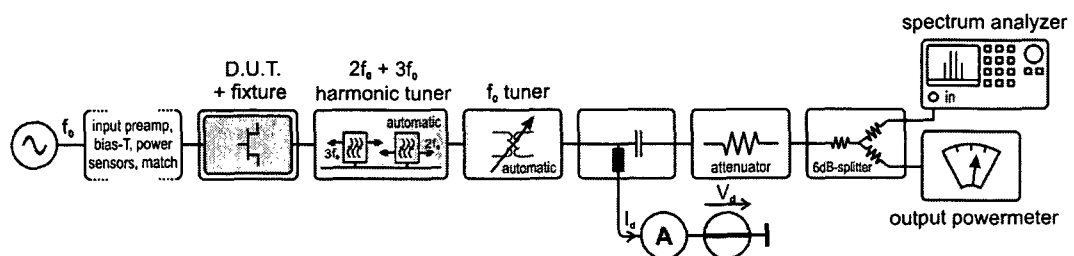


Figure 5.23: Passive harmonic load pull with harmonic tuner, block diagram

figuration. The entire input side was left unchanged, for details see figure 5.17. At the DUT's output the combination of the realized harmonic tuner and the fundamental tuner (Maury MT982A02, VSWR > 15 : 1) is connected. Because both tuners are realized with a TEM-transmission line, a DC path is provided. Again, this allows to place the bias-tee after the tuners and thus its losses do not degrade the tuning range. Finally, the output signal will be attenuated and fed to a spectrum analyzer and a power meter. The spectrum analyzer is now used for oscillation detection as well as for ACPR (adjacent channel power ratio) measurements. For an absolute power reference the output power meter is needed.

5.6.2 System calibration

For setting any desired phase-value for the harmonic frequencies $2f_0$ and $3f_0$ it is necessary to characterize the harmonic and the fundamental tuner first. This was done by for the harmonic tuner in the following way: The tuner was connected to a VNA and the S-parameters (figure 5.24a) for the fundamental and the harmonic frequencies were measured for a set of more than 1000 combinations of resonator positions. With this information and the knowledge of the internal realization it is possible to interpolate between measured points with very high accuracy. The error due to interpolation was smaller than the the tuner's reproducibility error and, therefore, could be neglected.

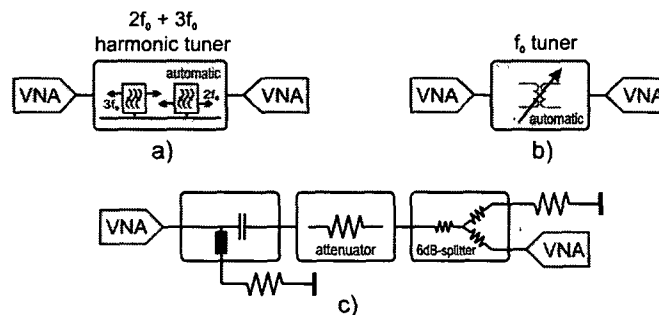


Figure 5.24: Passive harmonic load pull with harmonic tuner, calibration

The fundamental tuner was characterized in a quite similar way (figure 5.24b). By using the software supported by the manufacturer the tuner was calibrated for 300 equally spaced Γ -values. For the harmonic load-pull measurement a Matlab-code will then do the calculation of the required motor/resonator positions of both tuners. Depending on the calculated transformation of f_0 due to the harmonic tuner, the developed code identifies the required setting of the fundamental tuner. Then the closest reflection coefficient from the 300 calibrated values will be chosen. The fundamental tuner was not modeled because on the one hand too little was known about its mechanical dimensions (this would require a disassembly of the tuner) – on the other hand, the additional error was acceptable for the measurement. Using the tuner for model verification would require an interpolation of the fundamental tuner as well, in order to have sufficient accuracy for the fundamental reflection coefficient.

Finally, it is required to measure the insertion loss of the remaining setup, i.e. from the bias tee to the power meter (figure 5.24c). Having all this information, a measurement

can be started.

5.6.3 Achievable Tuning Range

To get an idea on the improvement by using a resonant harmonic tuner the achievable tuning range is depicted in figure 5.25. The solid lines indicate the performance at the harmonic tuner's input reference plane (at the APC-7 connector on port 1). The dashed line is what is seen from the intrinsic device and depends on the extrinsic elements of the transistor as well as on the measurement setup. Because of the omission of the non-

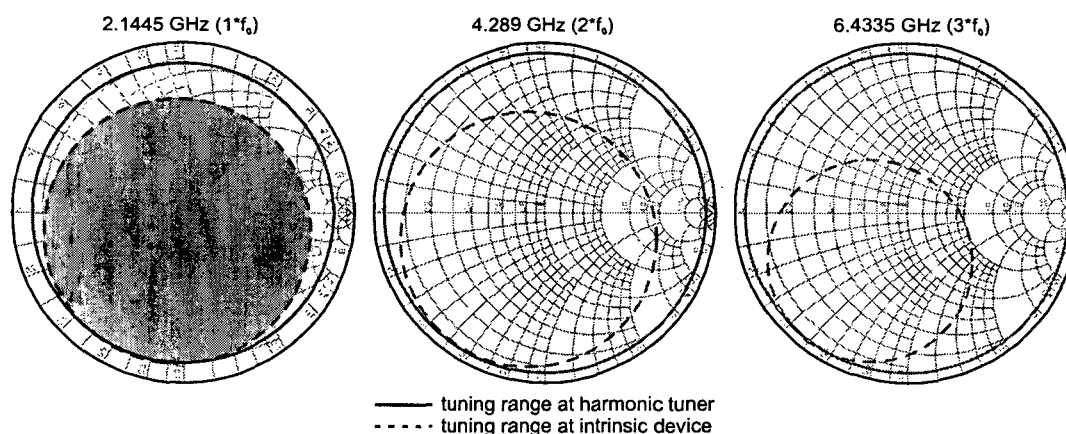


Figure 5.25: Passive harmonic load pull with harmonic tuner, tuning range

perfectly matched triplexer the tuning ranges are now centered around the origin. For the fundamental frequency the entire area inside the tuning range circles (shaded area in figure 5.25) can be used. For the harmonic frequencies $2f_0$ and $3f_0$ it is only possible to realize reflection coefficients which reside on the circle. This is not disadvantageous since a $|\Gamma| = 1$ is desired for the harmonic frequencies. It can also be seen that tuning range of the fundamental frequency seems to be not influenced by the harmonic tuner; the achievable VSWR for f_0 at the harmonic tuner's input is still $\approx 15 : 1$ (the specification of the used fundamental tuner). This can be explained by the much better performance of the f_0 -tuner at this frequency². The realizable reflection coefficients are listed in table 5.6.

frequency [GHz]	$ \Gamma $
$f_0 = 2.1445$	$0 \dots 0.87$
$2f_0 = 4.289$	$\gtrsim 0.94$
$3f_0 = 6.4335$	$\gtrsim 0.94$

Table 5.6: Achievable Γ of passive harmonic load-pull system with harmonic-tuner (at tuner input)

Figure 5.25 also illustrates the need for a high reflection at the harmonic frequencies.

²Manufacturers always specify a minimum VSWR of their tuners. The real VSWR is often much higher for certain frequency bands.

Whereas the tuning range of the f_0 -component at the input of the harmonic tuner is the smallest one (compare table 5.6), it is still the largest seen from the intrinsic transistor.

5.6.4 Measurement Results

To demonstrate the possibilities of the setup the selected transistor was measured with single-tone excitation. The bias conditions $V_G = -0.85$ V and $V_D = 6$ V remained unchanged. The input power level was +15 dBm, the center frequency was $f_0 = 2.1445$ MHz which was already taken into account at the design of the resonant harmonic tuner. To see the effect of the harmonic match, it was chosen to measure output power and power added efficiency over a two dimensional sweep of the harmonic phases. The entire measurement was controlled by a self-written Matlab code. The commercial software from Maury Microwave neither supports a combined sweep like this nor resonant tuners (they always use triplexers for harmonic tuning). The measurement results are shown in figure 5.26.

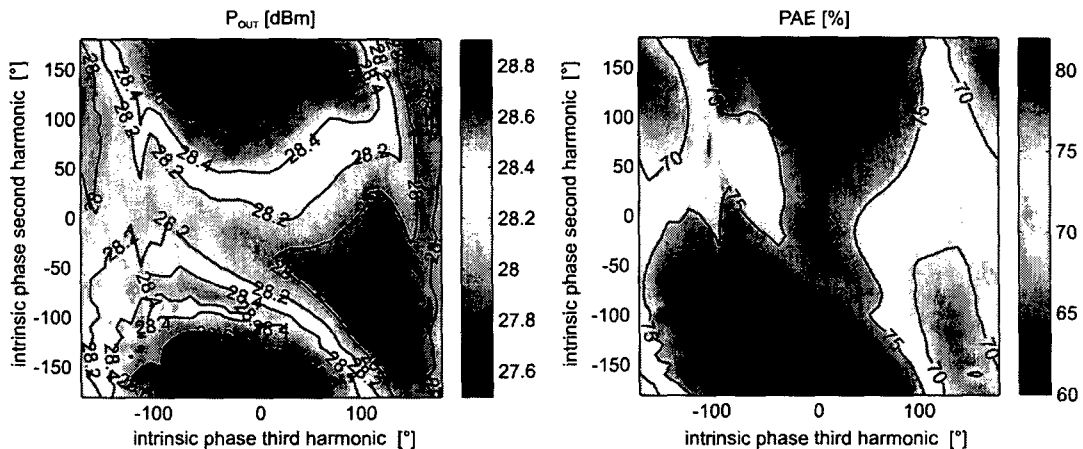


Figure 5.26: Singleton P_{OUT} and PAE dependence on harmonic phases

Analyzing the graphs clearly shows that the transistor shows the best performance in a class F mode. Both, P_{out} and PAE, reach their maxima at a 180° phase of $2f_0$ and 0° phase of $3f_0$. This corresponds to a short circuited second harmonic and an open at the third harmonic. Figure 5.26 also indicates that an inverted class F cannot be realized with the chosen input matching.

The reason for the contour lines not being smooth, especially for negative phases of the third harmonic, is neither a result of measurement noise nor repeatability problems of the harmonic tuner. Because of using no interpolation model for the cascaded fundamental tuner, the realizable Γ -values are limited. Since a movement of the harmonic resonators require an adjustment of the harmonic tuner the discontinuities in the measurement perfectly correlate with the selection of a new reflection coefficient of the fundamental tuner. This could be easily improved by a calibration for more Γ -values or by the development of a tuner model.

Because of the passive nature of the system and the low delay times, it can be used for broadband load-pull as well. The bias condition for this measurement was left unchanged ($V_G = -0.85$ V, $V_D = 6$ V) but input power was reduced to +8 dBm. The signal used for

measurement was an UMTS uplink signal as used for voice and lower-data rate applications at $f_0 = 2.1445$ MHz. The bandwidth of such a signal is approx. 5 MHz. Again, a combined sweep was performed and now the adjacent channel power ratios were measured as well. The results are presented in figure 5.27 and 5.28. The output power contour as well as

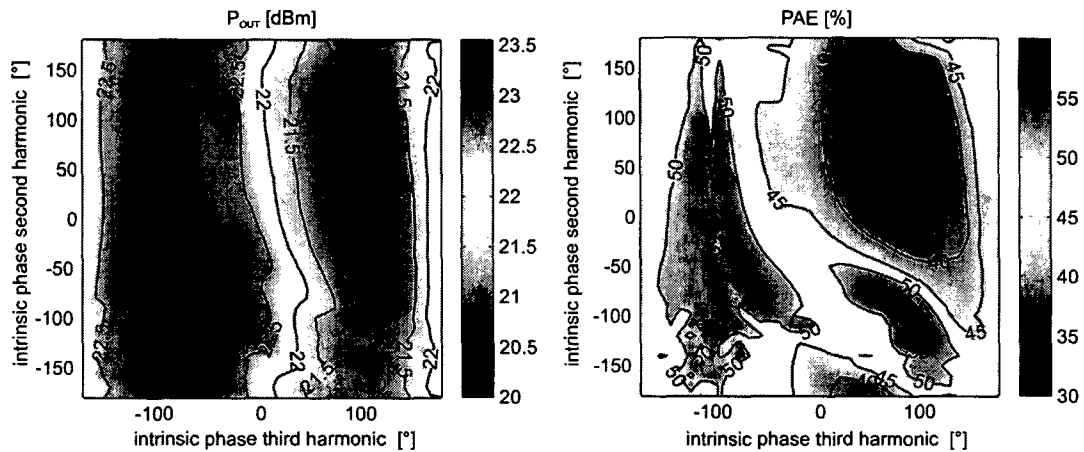


Figure 5.27: WCDMA P_{OUT} and PAE dependence on harmonic phases

the power added efficiency in figure 5.27 show an interesting behavior. Contrary to the single-tone case the optimum values do not reside at $180^\circ/0^\circ$ any longer. It turns out that two efficiency maxima with different power levels exist. An erroneous measurement can be excluded; after setting a set of terminations the signal source is firstly set to single-tone and then to WCDMA. The measurement and processing of the P_{out} and PAE values is then done with *exactly* the same functions. These functions further have no information on the type of signal used. It was not possible to do a reference simulation on this effect because of convergence problems of the used transistor model under multi-tone excitation. Again, discontinuities are a result of the stepped Γ_{f_0} .

Because linearity would also be a main issue for the design of an UMTS amplifier, the ACPR was measured and is shown in figure 5.28.

The worse value of the lower and upper first neighboring channel power ratio is shown in the ACP1-graph. For the second neighboring channel (± 10 MHz carrier distance) the result is given in the ACP2-graph. It turns out that the amplifier is driven with a too high input power level to fulfill the UMTS standard requirement of $ACP1 < -33$ dBc (FDD-mode for user equipment [[47]]). The mostly vertical aligned contour lines in these graphs further indicate that the intermodulation is more dependent on the third than on the second harmonic. This is something expected because in-band intermodulation effects are produced by odd-order nonlinearities only (see figure 5.46). Varying the third harmonic termination has more influence on the third order nonlinearity than a variation of the second harmonic. The dominant dependence of the ACPR on the third harmonic phase is illustrated very well for the ACP2 measurement (right graph in figure 5.46). Applying a phase of $120 \dots 180^\circ$ gives the best suppression of intermodulation because of quasi 'short-circuiting' the third harmonic and, therefore, reducing the interference of the third order nonlinearity as well.

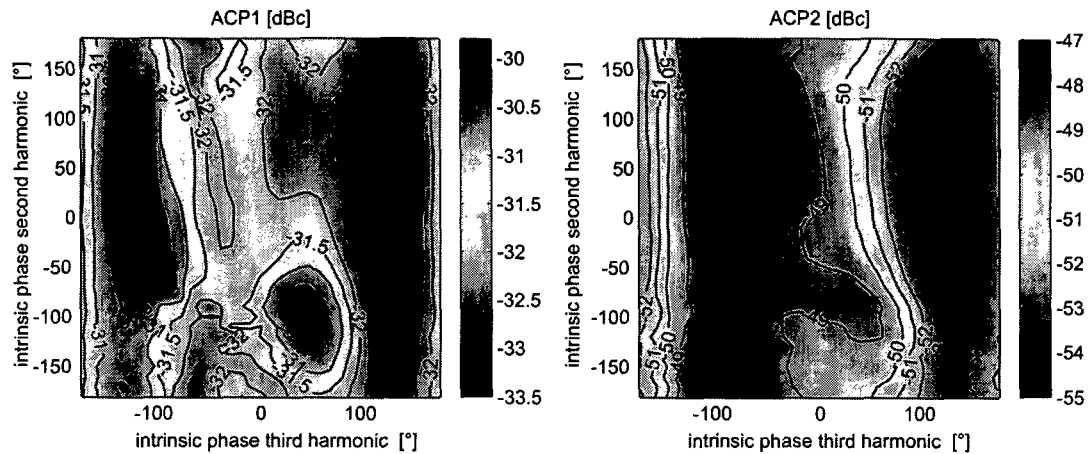


Figure 5.28: WCDMA ACP1 and ACP2 dependence on harmonic phases

5.6.5 Summary

Using a cascaded combination of a harmonic tuner and a fundamental tuner gives much better results than the application of a triplexer. Whereas measurements with the triplexer showed no significant dependence on the third harmonic matching due to the limited tuning range, this setup gives proper results. Comparisons of the results with the triplexer setup are, therefore, not possible.

The tuning of Γ of the harmonic frequencies is only possible with respect to its phase angle which is not a disadvantage. High efficiency amplifiers need a load reflection coefficient as high as possible. The reproducibility of the harmonic tuner was high enough and could be used for model verification as well.

The only possible improvement which turned out would be the modeling of the fundamental tuner as well. This would allow to keep the Γ_{f_0} more constant at the input of the fundamental tuner while changing the harmonic phases.

During the measurement no stability problems were detected. An oscillation of the transistor was only possible for certain sets of reflection coefficients when the input power level was increased to 18 dBm for single-tone measurements.

5.7 Active Harmonic Load Pull (Open Loop, Single Tone)

Although the use of a harmonic tuner (chapter 5.6) improved the realizable reflection coefficient many applications still demand for even higher VSWR of the tuner system. This can be achieved by the use of active loads as described in section 3.4. Because the fundamental tuning range was large enough active loads were used for the harmonic frequencies only. In order to prevent oscillation of the active loads an open loop design was chosen.

Furthermore, the required measurement of the actual reflection coefficients was done with an RF sampling oscilloscope instead of a VNA. This allowed to relate the phase of different frequencies to each other to allow for the reconstruction of voltage and current

waveforms inside the device under test.

It was chosen to do the setup without special components by using locked RF-generators instead of a chain of a frequency multipliers, variable attenuators, variable phase shifters and additionally required gain blocks. By using frequency locked generators the internal attenuators as well as phase shifting capabilities can be used. The disadvantage of such a setup is that even by an external synchronization of the generators the output phases still vary slowly with respect to each other.

5.7.1 Measurement Setup

The block diagram of the realized setup is given in figure 5.29. The input side of the device under test was kept the same as in all other measurements. It consists of a pre-amplifier, a manual tuner and directional couplers to measure input power and input matching (compare figure 5.17). On the output of the DUT two directional couplers are used to monitor the forward and backward travelling waves. Both are measured with an RF-sampling oscilloscope which is triggered on a synchronized trigger source. Also it would have been possible to use a power divider at the output of the signal source to generate this trigger signals. Using a second source guaranteed a constant trigger position while varying the the input power of the DUT. This is not a necessary prerequisite for this setup but simplified the testing of the written code. (The setup was entirely controlled over GPIB by a self-developed Matlab code).

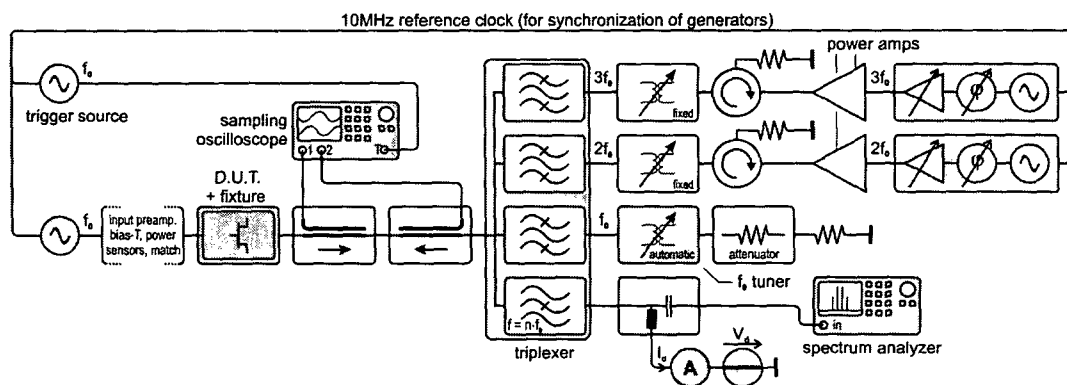


Figure 5.29: Active harmonic load-pull setup (single tone)

A triplexer was connected to the directional coupler in order to split the signal into its harmonic frequencies. Each harmonic output used a manual tuner to compensate for the mismatch at the triplexer ports. It should be noted here that the combination triplexer and manual tuner is not a requirement. It is also possible to use directional couplers or power combiners instead. Using a triplexer has the advantage of reducing the output power of the amplifiers required for the active load. The active load itself is realized by an isolator to terminate the forward travelling wave and to insert the required backward travelling wave. These are generated by a standard RF-generator with an additional power amplifier. The required phase and magnitude adjustment is done within the generator itself. RF generators usually allow for a very fine adjustment of the output power (typically 0.01 dB)

and the phase (typically $\leq 0.1^\circ$). Both harmonic RF generators are synchronized over the 10 MHz reference frequency with the RF source at the input.

It was required to disable the use of mechanical step attenuators inside the generators. These attenuators change the length of the RF path when switching their attenuation, which corresponds to an unknown phase shift. By using the electronic (phase stable) attenuators typical RF signal sources still provide a dynamic range $> 30 \dots 50$ dB which is definitely much more than required by this application.

The fundamental matching is done with the automatic tuner already used in the preceding setups. Because the absolute voltage and currents can be calculated from the time domain measurement it is not required any longer to have a power meter connected in the fundamental frequency path. Since the actually set reflection coefficient can be measured now under operation, it would also be possible to substitute the calibrated automatic tuner by an uncalibrated manual one.

The spectrum analyzer is used for oscillation detection only. Broadband input signals cannot be used in this setup.

5.7.2 Calculating the Intrinsic Waveforms

It was the intention for this measurement setup to give access to the time domain waveforms. Hence, it is required to calculate with absolute values instead of scattering parameters only. S-parameters (equation 5.1) relate two waves (a_i and b_j) to each other, which eliminates their absolute magnitude as well as their absolute phase, and can, therefore, not be used.

$$S_{ij} = \frac{b_i}{a_j}, \quad \begin{bmatrix} b_1 \\ b_2 \end{bmatrix} = \begin{bmatrix} S_{11} & S_{12} \\ S_{21} & S_{22} \end{bmatrix} \cdot \begin{bmatrix} a_1 \\ a_2 \end{bmatrix} \quad (5.1)$$

The forward travelling wave (into a device) a_i and the backward wave (from a device) b_i are related to the port voltages and currents by formula 5.2 and 5.3:

$$a_i = \frac{V_i + Z_0 I_i}{2\sqrt{Z_0}}, \quad b_i = \frac{V_i - Z_0 I_i}{2\sqrt{Z_0}} \quad (5.2)$$

$$V_i = \sqrt{Z_0} \cdot (a_i + b_i), \quad I_i = \sqrt{Z_0} \cdot (a_i - b_i) \quad (5.3)$$

The port voltages V_i are measured to ground, the direction of I_1 points into the device. Z_0 denotes the chosen real reference impedance (50Ω).

To calculate the intrinsic voltages and currents the signal flow-chart according to figure 5.30 was used. All blocks are characterized by their small signal S-parameters. The extrinsic model is described in detail in section 5.4, the determination of the test fixture errorbox is presented in section 5.3. It is important to use the same reference planes for measurements. This means that the test fixture also includes the cable to the directional coupler, whereas the directional coupler includes also the cabling to the sampling oscilloscope. Now an equation relating the oscilloscope measurement of $b_{3,C}$ and $b_{4,C}$ to the intrinsic waves $b_{2,DUT} = a_{1,E}$ and $a_{2,DUT} = b_{1,E}$ need to be derived. In order to simplify the calculation a perfect matching of the oscilloscope was assumed ($a_{3,C} = a_{4,C} = 0$). This was supported by using 10 dB attenuators before each (included in the directional coupler's scattering parameters). With these attenuators the return loss was better than -32 dB for both channels. During calibration of the directional coupler by a VNA, the free coupling ports were always connected to the corresponding oscilloscope input which allowed to include

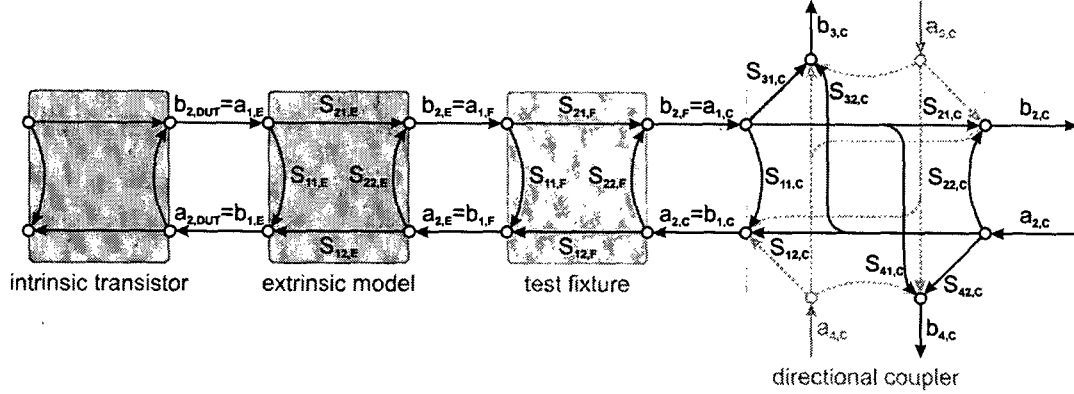


Figure 5.30: Signal flow-chart of active load-pull setup

mismatch effects of the oscilloscope inputs into the coupler's S-parameters. Thus the assumption of perfectly matched ports results in a negligible error due to different reference impedances. This error was further reduced by calibrating the oscilloscope inputs with a $50\ \Omega$ -source.

The waves $b_{3,C}$ and $b_{4,C}$ coming from the directional coupler therefore relate to the measured voltages according to formula 5.4:

$$b_{3,C} = \frac{V_{\text{channel 1}}}{\sqrt{Z_0}}, \quad b_{4,C} = \frac{V_{\text{channel 2}}}{\sqrt{Z_0}}, \quad (5.4)$$

Solving the signal flow-chart of the directional coupler for $a_{1,C}$ and $b_{1,C}$ gives:

$$a_{1,C} = \frac{b_{3,C}}{S_{31,C}} \cdot \frac{1 - \frac{b_{4,C} S_{32,C}}{b_{3,C} S_{42,C}}}{1 - \frac{S_{41,C} S_{32,C}}{S_{31,C} S_{42,C}}} \quad (5.5)$$

$$b_{1,C} = \frac{b_{4,C} S_{21,C}}{S_{42,C}} \cdot \frac{1 - \frac{b_{3,C} S_{41,C}}{b_{4,C} S_{31,C}}}{1 - \frac{S_{32,C} S_{41,C}}{S_{42,C} S_{31,C}}} + a_{1,C} S_{11,C} \quad (5.6)$$

Equations 5.5 and 5.6 show also show that the reflection coefficient seen into the directional coupler $\Gamma_C = \frac{b_{1,C}}{a_{1,C}}$ depends only on the ratio of the measured waveforms $\Gamma_C = f\left(\frac{b_{4,C}}{b_{3,C}}\right)$. This shows that a deembedding could of course be done with the S-parameters also if the loss of the magnitude information can be accepted. An application would be an active harmonic load-pull setup which does not need to reconstruct time waveforms.

Knowing now the forward and backward travelling waves the extrinsic and fixture two-ports need to be embedded in order to get the intrinsic waves. This is now much easier: starting with the S-parameters of a two-port (figure 5.31), the calculation makes use of the **T**(transfer)-Matrix.

The **T**-matrix relates the waves on port 1 to those on port 2. So, the **T**-matrix is ideally suited for the concatenation of two-ports The definition for the **T**-matrix is given

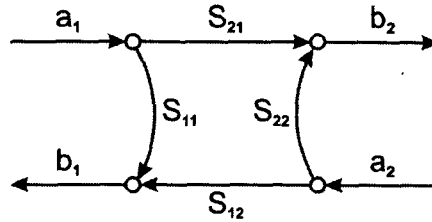


Figure 5.31: Signal flow-chart two-port

in formula 5.7:

$$\begin{bmatrix} a_1 \\ b_1 \end{bmatrix} = \begin{bmatrix} T_{11} & T_{12} \\ T_{21} & T_{22} \end{bmatrix} \cdot \begin{bmatrix} b_2 \\ a_2 \end{bmatrix} \implies \mathbf{T} = \frac{1}{S_{21}} \begin{bmatrix} -(S_{11}S_{22} - S_{21}S_{12}) & S_{11} \\ -S_{22} & 1 \end{bmatrix} \quad (5.7)$$

The resulting equations for embedding a two port are:

$$a_1 = b_2 \cdot \frac{1}{S_{21}} - a_2 \cdot \frac{S_{22}}{S_{21}} \quad (5.8)$$

$$b_1 = b_2 \cdot \frac{S_{11}}{S_{21}} - a_2 \cdot \frac{S_{11}S_{22} - S_{21}S_{12}}{S_{21}} \quad (5.9)$$

Of course, all formulas need to be calculated for each frequency separately because the S-parameters are frequency dependent.

5.7.3 Amplitude and Phase Extraction

For the application in a harmonic load-pull system all waves a_i and b_i need to be represented as the superposition of the fundamental and the harmonic frequencies. This is illustrated in figure 5.32 for the fundamental, the second harmonic and the third harmonic frequency.

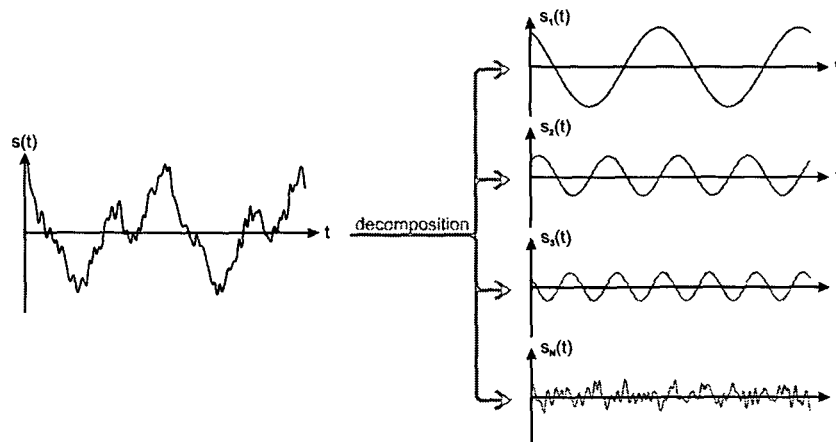


Figure 5.32: Decomposition of measured signal into single frequencies

For setting the amplitude and phase of the active load generators, the knowledge of the fundamental frequency is obsolete. If it is the goal to display the time-domain waveforms of voltage and current, of course, the fundamental as well as higher harmonics need to be taken into account.

To explain this, frequencies up to the third harmonic are used. The composed signal $s(t)$ can be expressed as the sum of the k_n -weighted real functions $b'_n(t)$ and the residual noise $n(t)$ which also includes the non separated higher order harmonic frequencies:

$$s(t) = \sum_{n=1}^6 k'_n b'_n(t) + n(t) \quad (5.10)$$

$$\begin{aligned} b'_1 &= \cos(2\pi f_0 t) & b'_2 &= \sin(2\pi f_0 t) \\ b'_3 &= \cos(2\pi 2f_0 t) & b'_4 &= \sin(2\pi 2f_0 t) \\ b'_5 &= \cos(2\pi 3f_0 t) & b'_6 &= \sin(2\pi 3f_0 t) \end{aligned} \quad (5.11)$$

The correspondence to a Fourier series is quite obvious. To determine the unknown factors k'_n of equation 5.10 the signal $s(t)$ is projected onto the normalized basis functions $b_n(t)$:

$$k'_n = \frac{1}{\|b\|} \int_{t=0}^{2\pi} s(t) b_n^*(t) dt \quad (5.12)$$

By combining the real valued factors k'_n to complex factors \mathbf{k} the signal $s(t)$ can be represented as to sum of three sines for f_0 , $2f_0$ and $3f_0$.

$$s(t) = \operatorname{Re} \left\{ \sum_{n=1}^3 \mathbf{k}_n b_n(t) \right\} + n(t) \quad (5.13)$$

$$b_n(t) = e^{j2\pi n f_0 t} \quad (5.14)$$

The complex magnitudes \mathbf{k}_n are defined by:

$$\begin{aligned} \mathbf{k}_1 &= k'_1 + jk'_2 \\ \mathbf{k}_2 &= k'_3 + jk'_4 \\ \mathbf{k}_3 &= k'_5 + jk'_6 \end{aligned} \quad (5.15)$$

With this complex representation the waveforms a_i and b_i can now be calculated for any reference plane within the setup. To reconstruct the time-domain signals, formula 5.3 needs to be applied.

5.7.4 Phase Stability of Generators

Due to the use of separate RF generators to produce the harmonic frequencies that are needed for the active load, also a small phase instability is introduced. Even when locking the PLLs of the generators by connecting the instruments together via the standardized 10 MHz reference clock this problem cannot be solved. Of course, all generators now have the same average frequency and phase but still small deviations are possible.

To analyze the influence of this residual phase variation a test setup according to figure 5.33 was realized. The RF sources were operated at the same frequencies as within the

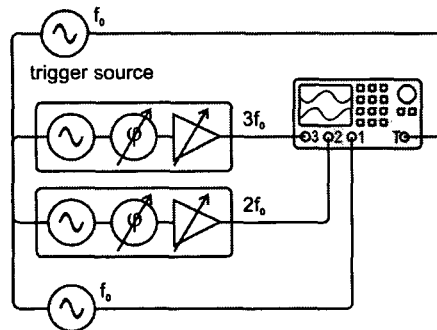


Figure 5.33: Test setup to measure phase drift of locked generators

active load-pull setup ($f_0 = 2.1445$ GHz). The phase shift of each generator was measured against the trigger phase multiple times per second over a period of more than six hours. The result is plotted in figure 5.34, the trigger source generator served as the 10 MHz-clock master³. All instruments were warmed up for at least two hours. To exclude environmental influence the room was kept at constant temperature. The graph clearly shows that the

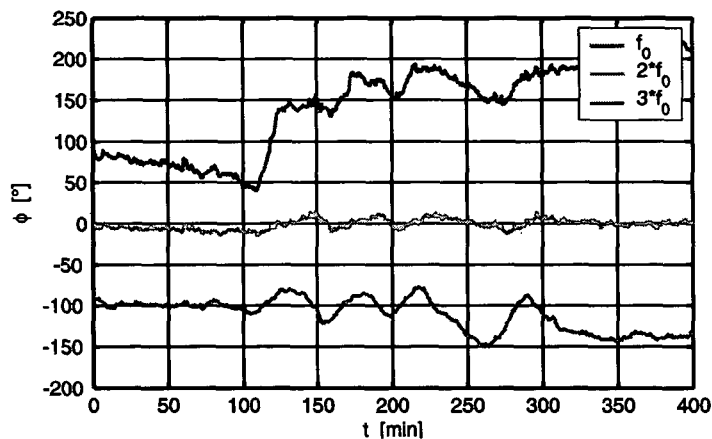


Figure 5.34: Phase deviation of the generators over time

phases show a long term variation. To analyze the influence of the measurement accuracy it is important to have a look on the short time stability. It is of major interest how large this change is within a certain time to know what maximum cycle times of a control system are possible in order to track the phase drift. The resulting probability density function (PDF) is depicted in figure 5.35. The data gained from the long time measurement was also used for this graph. For the application in the harmonic load-pull system the stability of the harmonic phases in relation to the fundamental phase is important. If for example the f_0 -phase changes by 10° , the $2f_0$ -phase by 20° and the $3f_0$ by 30° this corresponds to a timeshifted picture on the oscilloscope screen but does not influence the measurement. The

³After trying different 10 MHz masters this one turned out to be the most stable one.

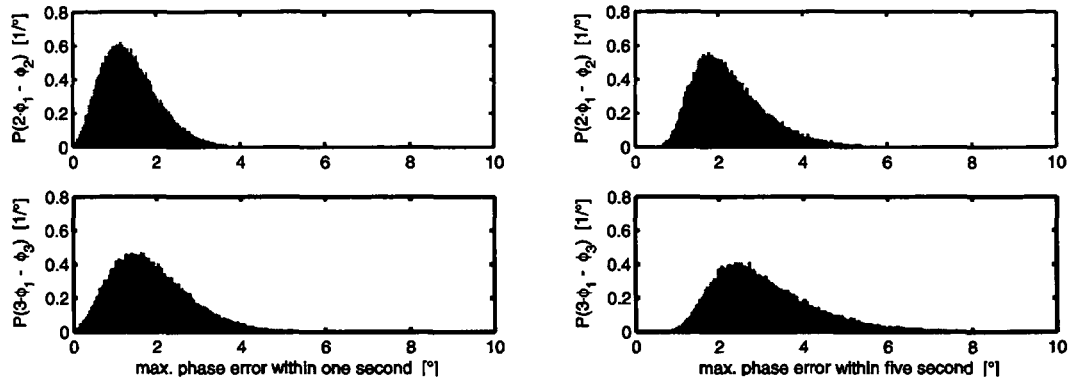


Figure 5.35: Measured phase drift within one and five seconds (PDF)

active loads would still realize the same reflection coefficients. The time-domain waveforms becomes shifted in time which is still not a problem. Therefore the differences $2\phi_{f_0} - \phi_{2f_0}$ as well as $3\phi_{f_0} - \phi_{3f_0}$ are shown. The absolute drift speed of the fundamental frequency f_0 is not of interest since a passive termination needs no tracking.

It turns out that the average phase drift of the third harmonic within one second is less than 2° with a maximum possible drift of $\approx 5^\circ$. Within a five second observation period the average deviations increase to 3° (8° maximum).

Due to this error (which can also be interpreted as measurement noise) the overall phase accuracy will be reduced. It becomes necessary to implement control loops for both harmonic frequencies for permanent tracking of the phase.

5.7.5 System Calibration

To prepare the measurement setup for operation it is necessary to entirely characterize the directional couplers and the RF sampling oscilloscope. By referring to a power meter the inputs of the sampling oscilloscope are calibrated in amplitude (figure 5.36a). Furthermore, the delay difference between between both inputs must be compensated. The absolute delay to the trigger signal is of no importance. As mentioned in section 5.7.2 the

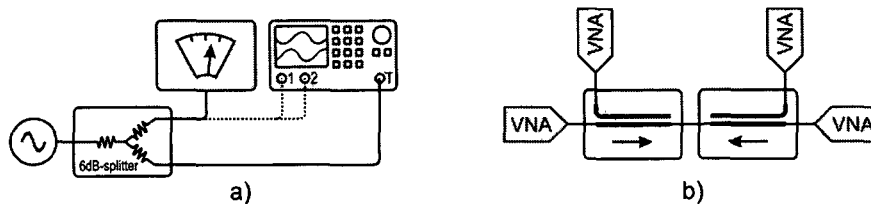


Figure 5.36: Active harmonic load-pull (singletone), calibration

S-parameters of the directional coupler are required (figure 5.36a). This was done by arranging multiple two-port VNA measurements to a four-port file. For reducing errors due to mismatched oscilloscope inputs the coupling ports were connected to the corresponding

input of the sampling oscilloscope when not in use for the VNA measurement.

If the time-domain waveforms are not of interest it would also be possible to connect a non-characterized directional coupler output to the uncalibrated oscilloscope and perform an SOLT calibration at the directional coupler's input port. This, of course, does neither give the phase difference between different harmonic frequencies nor information on the absolute magnitudes.

5.7.6 Achievable Tuning Range

By using active loads for the harmonic frequencies it is possible to achieve any matching as long as the amplifiers used for the setup deliver sufficient output power. The linearity of these amplifiers is uncritical because the setup is used for single-tone signals only. The implemented amplifiers allowed to achieve a reflection coefficient for the harmonic frequencies $|\Gamma_{2f_0,3f_0}| = 1$ (figure 5.37). This, of course, requires reflection coefficients at the input of the directional coupler with $|\Gamma| > 1$ to compensate for the insertion losses. Of course, a reflection coefficient >1 would also be possible at the reference plane of the intrinsic transistor but it cannot be achieved in a final amplifier design. By having control of the

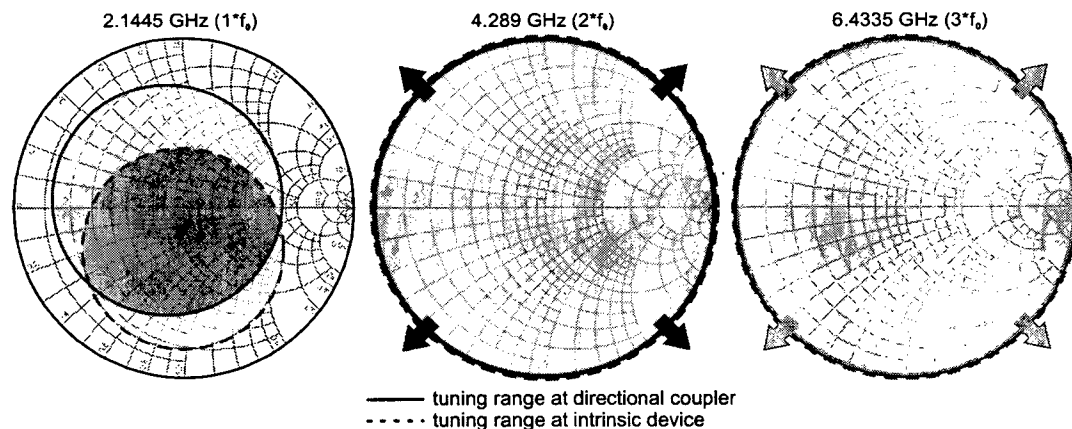


Figure 5.37: Active harmonic load pull (singletone), tuning range

phase and magnitude of the RF sources used for the harmonic frequencies it is also possible to realize impedances with $|\Gamma| < 1$. That means, in contrary to the passive harmonic tuner that the tuning range covers now the entire Smith Chart and not only points which lie on a circle with radius < 1 .

Due to the use of a mismatched triplexer the fundamental tuning range is not centered inside the Smith Chart. The realizable reflection coefficients are summarized in table 5.7. For a fair comparison the $|\Gamma|$ column describes the range of reflection coefficients which can be achieved with any phase. Due to the non centered tuning area at the fundamental frequency, higher reflection occurs for a limited phase range only.

5.7.7 Control Algorithm

To set the desired phases for the $2f_0$ and $3f_0$ reflection coefficients it was necessary to realize a control algorithm which programs the output power and phase of both RF sources.

frequency [GHz]	$ \Gamma $	(max. $ \Gamma $)
$f_0 = 2.1445$	$0 \dots 0.57$	(0.79)
$2f_0 = 4.289$	$0 \dots \geq 1$	—
$3f_0 = 6.4335$	$0 \dots \geq 1$	—

Table 5.7: Achievable Γ of active singletone load-pull system (at coupler input)

Due to the phase variation of the generators over time it was not possible to use gradient algorithms. Hence, a controller was implemented in Matlab which is based on the following considerations:

- Both harmonics are independent of each other. One and the same algorithm can, therefore, be used for the control of the second and of the third harmonic. Different parameters are allowed.
- Phase and magnitude are controlled separately.
- The implementation was done with a two-position controller: if the measured reflection coefficient has a too small magnitude the power of the corresponding amplifier is increased by a certain step and vice-versa. The same principle was used for the control of the phase.
- If the error between the required and the realized Γ -value drops below a certain threshold level, the step sizes for the power- and phase-control starts to decrease slowly over time.
- The correct setting is assumed to be reached if the decreasing phase-step gets lower than the average phase drift (see figure 5.35). Using smaller phase steps would allow the phase to drift faster away than what is possible to compensate for with the phase step size.

The step size parameters were chosen by empirical tests.

During the implementation it turned out that the number of points measured with the RF sampling oscilloscope needed to be reduced to allow faster cycle times. By this the accuracy of the signal decomposition algorithm (compare section 5.7.3) was lowered. This resulted also in noisier measurements of the actual Γ -values. A trade-off between phase drift and measurement accuracy was found in measuring 1024 samples of the forward and backward travelling wave which allowed cycle times of < 1 s.

5.7.8 Measurement Results

To allow comparison with other measurements the transistor bias point was set to $V_G = -0.85$ V and $V_D = 6$ V, the input power level was +15 dBm (same values as in all other single-tone measurements). The center frequency was set to $f_0 = 2.1445$ MHz. Because broadband measurements are not possible with this setup a two-dimensional sweep was done for a single-tone signal only. The result is presented in figure 5.38.

As for the measurement with the harmonic tuner it is evident that the best power added efficiency is achieved in class F operation. In contrast to the passive solution it

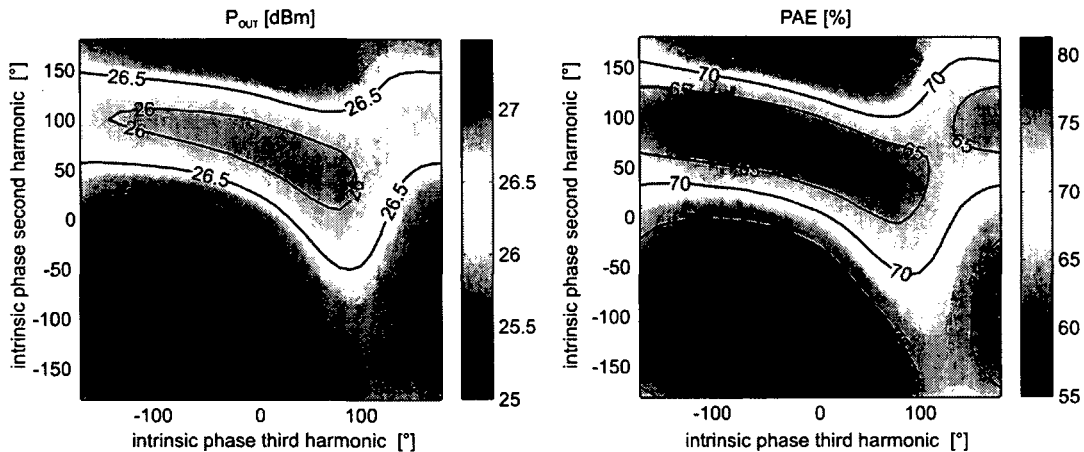


Figure 5.38: Singletone P_{OUT} and PAE dependence on harmonic phases

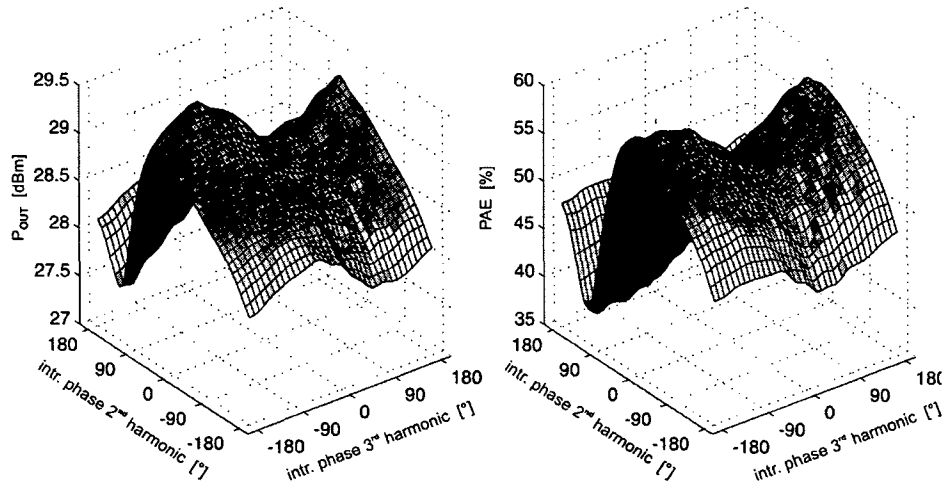
turns out that the maximum power is located at a different phase combination (but close to a Class F matching). This is what is expected from theory (chapter 2): the waveforms which give maximum output power are not the same which give maximum efficiency (an amplifier designer mostly has to deal with finding a trade-off between both).

Comparing this result with the one gained from the passive harmonic load-pull before further reveals some differences. Redoing both measurements (including calibration) led to the same difference again. It seems that the influence of the higher order harmonic frequencies (which are not taken into consideration) do have an effect on the measurement. This problem was already addressed in section 3.1. Since the termination for higher order harmonics is not the same for both setups, this is likely to happen. One setup uses a resonant tuner whereas the setup in this chapter uses a triplexer with an additional directional coupler. So the higher order harmonics are terminated undefined in both cases. It was not possible to explain this difference by any other reasons.

5.7.9 Excursus: Time Domain Measurement Results for Inverted Class F

As active harmonic-load pull setup was designed to allow the calculation of time domain signals, an example should be given now. This example is also used to prove the importance of the gate match. For the measurement the bias conditions were kept unchanged ($V_G = -0.85$ V, $V_D = 6$ V) but the input matching was changed. As a result it was possible to operate the transistor in inverted class F with a higher output power but lowered efficiency [26]. Also a higher input power of +17 dBm was needed. The graphs given within this section are shown as 3D-plots instead of contour plots. This, of course, makes the reading of certain values more difficult but allows much better understanding of some fundamental effects of harmonic controlled amplifiers.

In the first 3D-plot (figure 5.39) the output power and the power added efficiency are shown. With the changed input matching it is now possible to efficiently operate the transistor in inverted class F mode. The efficiency maximum is perfectly located at a phase combination of 0° for the second harmonic's reflection coefficient and 180° for the third one. It can be observed that the maximum power is reached by a phase combination

Figure 5.39: PAE and P_{out} dependence on harmonic phases

which is close to the PAE maxima. Having a look at the plotted surface's borders it can be seen that the achieve P_{out} and PAE depends more or less sinusoidally on the set phases. It turns out further that the influence of the second harmonic on P_{out} and PAE is much larger than the one of the third harmonic frequency (can be seen by the different peak-to-peak values of the sinusoidally shaped border lines). This is what was already explained with table 2.1 in the amplifier theory chapter.

With this setup it is also possible to investigate the dependence of the intrinsic voltage and current magnitudes on the harmonic loads. The corresponding 3D-graphs are shown in figure 5.40 and 5.41. Applying a short circuit at the second harmonic (180°) leads to

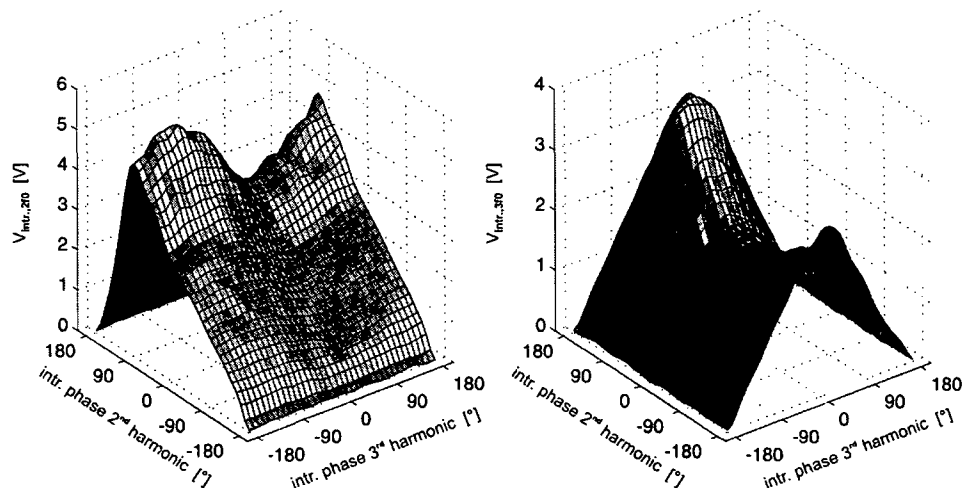


Figure 5.40: Intrinsic voltage magnitude dependence on harmonic phases

zero voltage of the second harmonic at the intrinsic device (figure 5.40, left) . Setting an

open (0°) gives results in maximizing the intrinsic voltage. The same can be seen for the third harmonic in the right plot in figure 5.40. The maximum voltage (which results by using an open) further depends on the other harmonic. Again, the influence of the second harmonic is higher (right graph) than the influence of the third harmonic frequency (left graph).

The same analysis can be done for the intrinsic currents. Applying an open gives a zero current (figure 5.41).

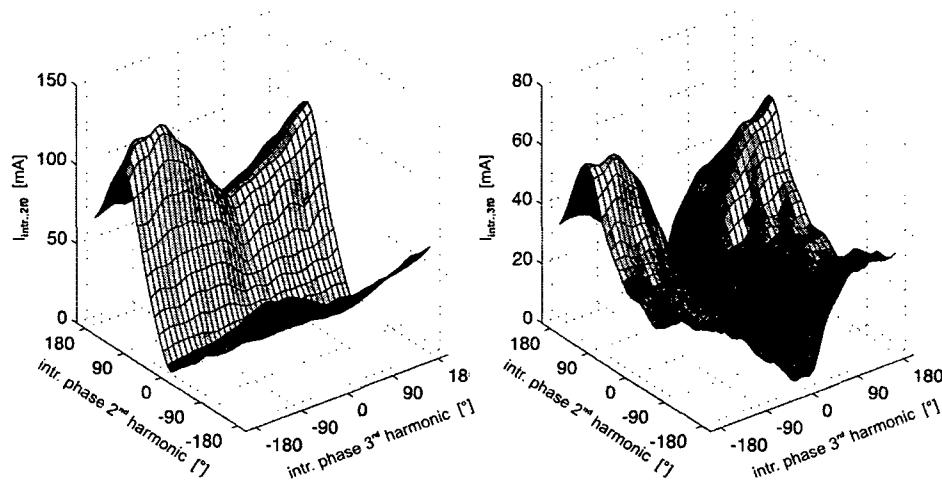


Figure 5.41: Intrinsic current magnitude dependence on harmonic phases

By calculating the time domain waveforms it is further possible to compare the measurement to simulated waveforms. The result of this is shown for the dynamic loadline in figure 5.42. An open was used at the second harmonic frequency and a perfect reflection with an angle of -120° for the third harmonic. This setting had shown maximum output power in the harmonic load-pull measurement. For comparison the transistor model (figure 5.10) was put into the harmonic balance simulator Microwave Office [48] and terminated with exactly the same loads on gate and drain as in the load-pull setup. The measured results correspond very well with the simulation. The maximum deviation between both traces occur at $V_{\text{DS}} = 0 \text{ V} / I_{\text{DS}} = 350 \text{ mA}$. The measurement shows negative voltages which is unphysical. This might be a problem because the measurement only used the fundamental and the first two harmonic frequencies for signal reconstruction. The measurement of higher harmonics was not possible due to limitations of the used instruments. It can be expected that this deviation vanishes when taking the fourth and fifth order harmonics into account as well.

Figure 5.43 shows the same waveforms over time.

5.7.10 Summary

With the use of standard laboratory equipment it was possible to realize a working active harmonic load-pull setup. Using synchronized generators for the harmonic active loads turned out to be a limiting factor for the achievable accuracy due to the phase drift

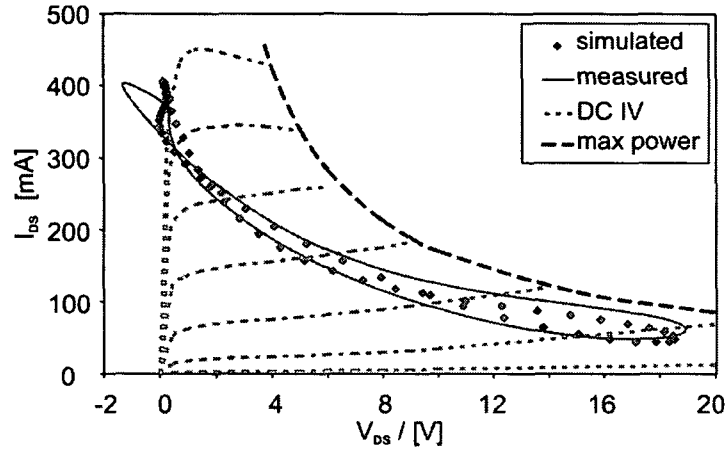


Figure 5.42: Comparison of measured and simulated intrinsic dynamic load line

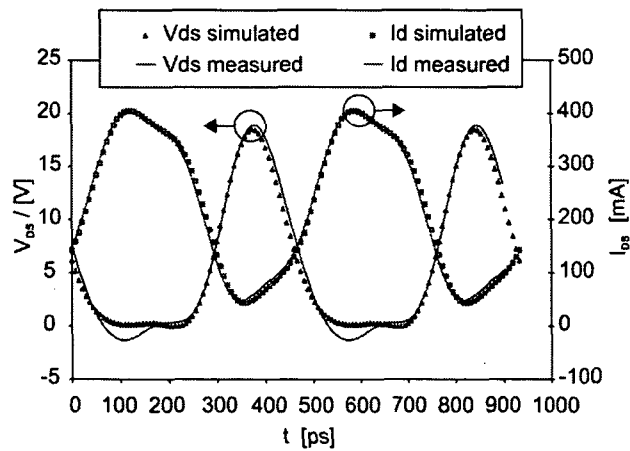


Figure 5.43: Comparison of measured and simulated intrinsic voltage and current over time

between different generators. A simple control algorithm was implemented to allow setting of the desired reflection coefficients. Attention was paid that this algorithm can cope with the phase drifts. In order to know the statistical behavior of the phase variation a long time measurement was done.

To achieve best possible accuracy much waveform data needed to be transferred over the GPIB-bus. This slowed down the measurement and increased the control algorithms cycle time, resulting in too high phase drifts. A trade-off between accuracy and phase drift had to be found.

The results of a sweep over both harmonic phases turned out not to be perfectly comparable to the passive load-pull setup with the harmonic tuner. The reason for this is expected to be a result of the undefined termination of the higher order harmonic frequencies which is entirely different for both setups.

Also the capability of time domain measurements was shown including a good match to simulated voltages and currents.

Furthermore, the influence of the input matching was proven. One and the same device at the same bias conditions showed maximum efficiency for class F operation in both setups. After changing the input matching maximum efficiency was found for inverted class F operation.

5.8 Active Harmonic Load Pull (Open Loop, Broadband)

The driving factor for this concept was the requirement to do active load pull with broadband signals. It was the idea to realize a setup based on open loops with modulated sources. Because of having the possibility to have entire control of the equivalent baseband waveforms it is possible to compensate for delays which are the limiting factor for bandwidth. The system should serve as a test-platform for this new concept. It was the idea to show that it is possible to use such a setup for harmonic-load pull measurements in principle and to find out what improvements are necessary. Of course, some simplifications had to be made to realize this rather expensive test platform.

5.8.1 System setup

This harmonic load-pull system can be seen as an extension of the active single-tone setup of the preceding chapter. Instead of the CW generators this system requires modulatable sources. All RF sources are now modulated by a separate arbitrary baseband generator (figure 5.44). The input matching was set to the reflection coefficient which allows class F operation. At the output side of the device under test the same directional coupler was used. Then the signal passes the triplexer and is separated into its spectral components. At both harmonic frequencies active loads are used, the fundamental frequency is matched by a passive tuner. Each active load uses an RF source which is modulated by a dedicated arbitrary signal generator. Phase shifting and amplitude variation is done by the RF generators. Again, the RF signal sources are locked by a 10 MHz clock. The arbitrary baseband signal generators use another 10 MHz signal as well as a trigger signal for synchronization. It is not necessary to use a single 10 MHz phase reference for the RF generators and the baseband generators.

Different to the single-tone measurement the forward and backward travelling waves

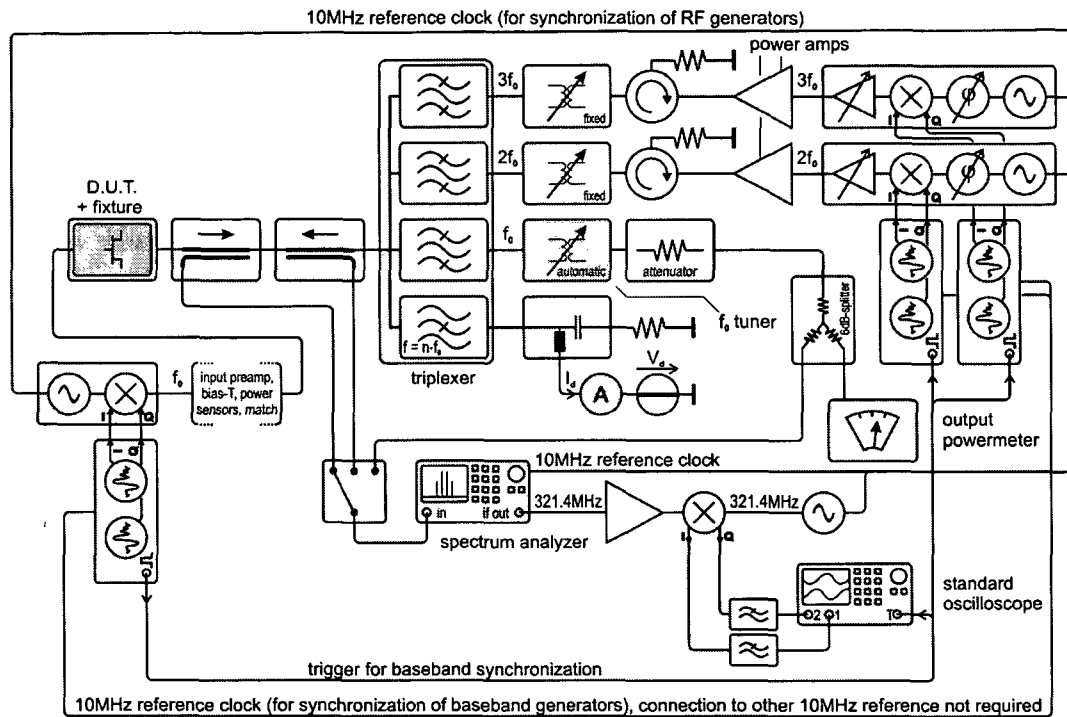


Figure 5.44: Active harmonic load pull for broadband signals, block diagram

are not measured at RF any longer (this is not possible for modulated signals, because a sampling oscilloscope needs repetitive signals). A synchronized spectrum analyzer was set to zero span to act as a mixer (The spectrum analyzer can also be switched to the f_0 output in order to measure parameters like ACP.) The IF output of the spectrum analyzer is externally I/Q-demodulated. Depending on the switch setting and the set frequency on the spectrum analyzer it is now possible to measure the equivalent baseband signal for the fundamental and every harmonic frequency for both directions (forward/backward). The signal acquisition can now be done with a standard oscilloscope.

To have an absolute power reference a power meter is connected at the f_0 output.

Different to the preceding setups, the fundamental frequency had to be reduced to $f_0 = 2.133$ GHz because the available modulatable signal generators had an upper frequency limit of 6.4 GHz. So the third harmonic frequency was located at $3f_0 = 6.399$ GHz. This problem did not arise for single-tone active load-pull because the available CW sources allowed much higher frequencies.

5.8.2 Equivalent baseband signals for harmonic frequencies

Before using the proposed setup for measurements it is necessary to calculate the equivalent baseband signals for the harmonic frequencies. The problem which has to be solved is depicted in figure 5.45. The input source of the device under test is modulated with a complex baseband signal. Now this signal is passed on to the device under test. Due to the nonlinearity of the device harmonic frequencies will be generated. To act as an active

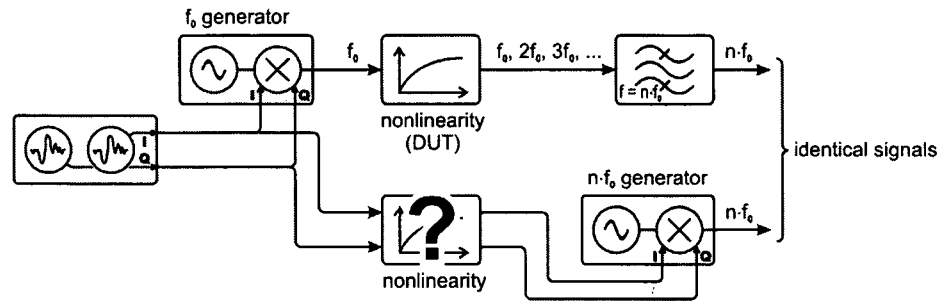


Figure 5.45: Required nonlinearity for baseband processing

load, it is required to generate exactly the same signal as the one which is terminated in the corresponding isolator. Therefore, it is necessary to know how a passband nonlinearity can be represented by a baseband nonlinearity in order to realize the same output signal within the second or third a harmonic zone.

To simplify the calculation the passband nonlinearity is modeled by a memory-less (instantaneous) Taylor series:

$$s'(t) = \sum_{n=1}^{\infty} a_n s^n(t) \quad (5.16)$$

The output signal $s'(t)$ is the infinite sum of different powers of the input signal $s(t)$ weighted by the Taylor coefficients a_n . The signal $s(t)$ is represented by a magnitude and a phase term:

$$s(t) = A(t) \cos[\omega_0 t + \Phi(t)] \quad (5.17)$$

$A(t)$ denotes the actual magnitude, $\Phi(t)$ the actual phase and ω_0 the angular carrier frequency.

Assuming a fifth order nonlinearity the Taylor series can be expanded to:

$$s'(t) = \sum_{n=1}^5 a_n s^n(t) \quad (5.18)$$

$$\begin{aligned} n = 1 : &= a_1 \{A(t) \cos[\omega_0 t + \Phi(t)]\} \\ n = 2 : &+ a_2 \left\{ \frac{1}{2} A^2(t) + \frac{1}{2} A^2(t) \cos[2(\omega_0 t + \Phi(t))] \right\} \\ n = 3 : &+ a_3 \left\{ \frac{3}{4} A^3(t) \cos[\omega_0 t + \Phi(t)] + \frac{1}{4} A^3(t) \cos[3(\omega_0 t + \Phi(t))] \right\} \\ n = 4 : &+ a_4 \left\{ \frac{3}{8} A^4(t) + \frac{1}{2} A^4(t) \cos[2(\omega_0 t + \Phi(t))] \right\} \\ &+ a_4 \left\{ \frac{1}{4} A^4(t) \cos[4(\omega_0 t + \Phi(t))] \right\} \\ n = 5 : &+ a_5 \left\{ \frac{5}{8} A^5(t) \cos[\omega_0 t + \Phi(t)] + \frac{5}{16} A^5(t) \cos[3(\omega_0 t + \Phi(t))] \right\} + \dots \\ &+ a_5 \left\{ \frac{1}{16} A^5(t) \cos[5(\omega_0 t + \Phi(t))] \right\} \end{aligned} \quad (5.19)$$

Using the identity

$$A^x(t) \cos[y(\omega_0 t + \Phi(t))] = s^y(t) |s^{x-y}(t)| \quad \forall x \geq y; x, y \in \mathbb{N} \quad (5.20)$$

and the representation of the signal $s(t)$ by a complex baseband modulation with $\underline{b}(t)$

$$s(t) = \text{Re} \{ \underline{b}(t) e^{j\omega_0 t} \} \quad (5.21)$$

gives the signals for each harmonic zone:

$$\begin{aligned} s'(t) &= \frac{1}{2} a_2 |\underline{b}^2(t)| + \frac{3}{8} a_4 |\underline{b}^4(t)| \\ \omega_0 &: + \text{Re} \left\{ e^{j\omega_0 t} \left[a_1 \underline{b}(t) + \frac{3}{4} a_3 \underline{b}(t) |\underline{b}^2(t)| + \frac{5}{8} a_5 \underline{b}(t) |\underline{b}^4(t)| \right] \right\} \\ 2\omega_0 &: + \text{Re} \left\{ e^{j2\omega_0 t} \left[\frac{1}{2} a_2 \underline{b}^2(t) + \frac{1}{2} a_4 \underline{b}^2(t) |\underline{b}^2(t)| \right] \right\} \\ 3\omega_0 &: + \text{Re} \left\{ e^{j3\omega_0 t} \left[\frac{1}{4} a_3 \underline{b}^3(t) + \frac{5}{16} a_5 \underline{b}^3(t) |\underline{b}^2(t)| \right] \right\} \\ &+ \dots \end{aligned} \quad (5.22)$$

The equivalent baseband signals can now be found in the $[\]$ -brackets. Due to the nonlinearity the output signal $s'(t)$ now consists of parts at DC, the fundamental zone at f_0 and the harmonic zones at nf_0 . Hence using a carrier with a rectangularly shaped spectrum as input signal $s(t)$ will result in an output spectrum according to figure 5.46. The figure shows those parts which are explicitly shown in formula 5.22. Due to a fifth order nonlinearity signals will be found up to the fifth harmonic zone. Figure 5.46 shows also the order of the intermodulation terms by the corresponding numbers. What is true for dual-tone applies for broadband signals as well: At the fundamental frequency only

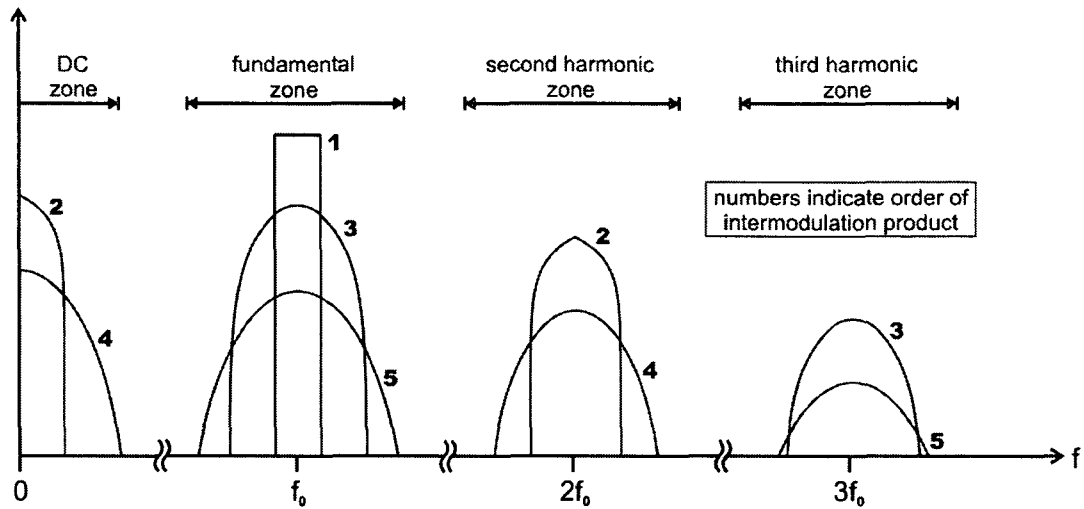


Figure 5.46: Spectrum of a nonlinear distorted broadband-signal

odd order terms exist. In the DC zone (order 0) as well as for all other even order harmonic zones only intermodulation products of even order can be found. Because the corresponding equivalent baseband signals are given by powers of the original baseband signal $\underline{b}(t)$ the spectrum corresponds to a multiple convolution of the original baseband spectrum. Therefore, the bandwidth increases by the order of the intermodulation product.

With the assumed reduction to a fifth order nonlinearity equivalent baseband signals needed for the generation of the harmonic frequencies are:

$$\underline{b}_{2f_0}(t) = \frac{1}{2}a_2\underline{b}^2(t) + \frac{1}{2}a_4\underline{b}^2(t)|\underline{b}^2(t)| \quad (5.23)$$

$$\underline{b}_{3f_0}(t) = \frac{1}{4}a_3\underline{b}^3(t) + \frac{5}{16}a_5\underline{b}^3(t)|\underline{b}^2(t)| \quad (5.24)$$

As the weighting factors a_n are not known for a transistor, a further simplification will be made. It is assumed that the dominant part of the sums in equations 5.23 and 5.24 is the lower order nonlinear term. The validity of this assumption will be shown by measurements of the equivalent baseband signals at the end of this chapter. By this simplification only one weighting factor has to be determined. Because the harmonic load-pull system control loop is in charge of setting the correct gain and phase shift of the generators at the harmonic frequencies, an amplitude weighting or a phase shift does not have any influence here.

The finally used equations for the analytical generation of the equivalent baseband signals are:

$$\underline{b}'_{2f_0}(t) = \underline{b}^2(t) \quad (5.25)$$

$$\underline{b}'_{3f_0}(t) = \underline{b}^3(t) \quad (5.26)$$

For the verification of formulas 5.25 and 5.26 a test setup according to figure 5.47 was realized. This setup allowed to measure the equivalent baseband signals after a pass-band nonlinearity. The test devices were a frequency doubler and a frequency tripler. A

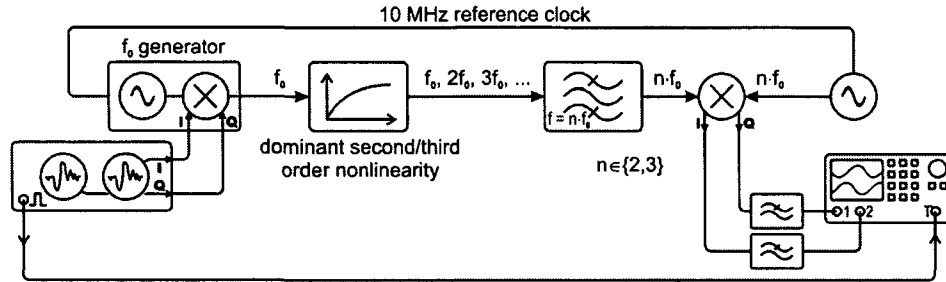


Figure 5.47: Test setup for verification of equivalent baseband signals

WCDMA signal was used for verification. The residual error between both signals was determined by subtracting the measured I/Q-waveforms from the amplitude and phase adjusted analytical ones. The error signal turned out to be less than < -10 dBc for both harmonic frequencies.

Using these baseband signals for the active loads results in their nonlinear behavior. Baseband signals with higher accuracy would require knowledge of the Taylor series coefficients. But can such signals be used for active terminations? As long as the device under test is operated far enough in the back-off (typical conditions for a broadband amplifier because linearity is needed), the higher order intermodulation products are small compared to the effect of the low order term. Hence, the generated signal should be quite a good copy of the DUT's output signal at each harmonic zone. Still, returning a signal which is different to the output signal introduces additional intermodulation. Because the error signal is about 10 dB down, it can also be expected that the intermodulation introduced by this error signal is also 10 dB below the 'real' intermodulation products and does not influence the performance of the DUT too much. This effect cannot be analyzed analytically here because an exact mathematical model of the DUT would be required.

If the device under test is operated in a very nonlinear region, the error of the generated signals will increase dramatically. Because the higher order coefficients of the Taylor series become larger in this case the splitting of equation 5.23 into a dominant part is not possible any more. So the application of this simplified system is limited to weakly nonlinear devices.

5.8.3 Calculation of Reflection Coefficient

For the control of the phase shifter and of the attenuators inside the RF sources it is again necessary to measure the actually realized reflection coefficient. Since this is done in baseband now, two complex signals (the forward and the backward travelling wave) need to be compared. Each sample of the waveform which is recorded by the oscilloscope shall be used for calculation in order to increase the accuracy. Therefore, a least square fitting can be calculated:

$$err = \min_{\Gamma} \|s_{fw}\Gamma - s_{bw}\| \quad (5.27)$$

Because the forward travelling wave s_{fw} relates to the backward travelling wave s_{bw}

by the reflection coefficient Γ , the best match for Γ is found by minimizing the quadratic norm in formula 5.27.

For reference purposes a much simpler estimation of the reflection coefficient was also tried according to formula 5.28.

$$\Gamma = \overline{\left(\frac{s_{bw}}{s_{fw}} \right)} \quad (5.28)$$

Each set of complex samples is divided and the resulting values are averaged. To limit the noise enhancement introduced by the division only sample values of a minimum magnitude were used for the calculation.

To test both algorithms the entire setup was set into operation and the harmonic generators were set to a random amplitude and phase each. To test the algorithms for their noise sensitivity vertical resolution of the oscilloscope was intentionally set to be very coarse in order to have a low signal to noise ratio. Then time-segments of the forward/backward equivalent baseband signals at $2f_0/3f_0$ were recorded. The signals (each 5000 samples long) were used to test both algorithms (equations 5.27 and 5.28). The results for both estimators are shown in figure 5.48. Because the setup did not track the phase, the

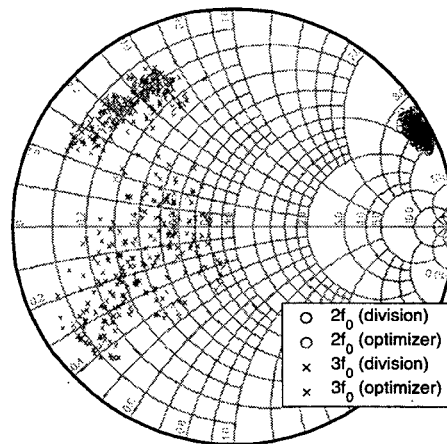


Figure 5.48: Comparison of different Γ -estimators

measured points for $3f_0$ show a large deviation over the measurement time. The phase for $2f_0$ was relatively stable. It turned out that both algorithms gave different estimates for the reflection coefficient. The reason was found in a DC offset of the measurement and could be easily calibrated. Still, the division-algorithm showed a much higher sensitivity on noise (points are more scattered in Smith Chart). This corresponds to what was expected from a division: noise enhancement. Therefore, this method was cancelled and the least square estimator was used.

Compared with the estimation of the reflection coefficient for single-tone signals the results were noisier for broadband signals.

5.8.4 System calibration

In contrary to the active single-tone harmonic load-pull system delays are also of interest now. Whereas a delay of a CW signal can be entirely compensated by a phase shift, this is not possible for broadband signals. Therefore, the calibration requires an additional delay compensation. To measure the delays between the three sources (input, 2nd and 3rd harmonic at output) a 6 dB-splitter/combiner is connected to the reference planes of the fixture and the directional coupler (figure 5.49). Additionally, a thru element is inserted into the test fixture. The rest of the setup is left unchanged.

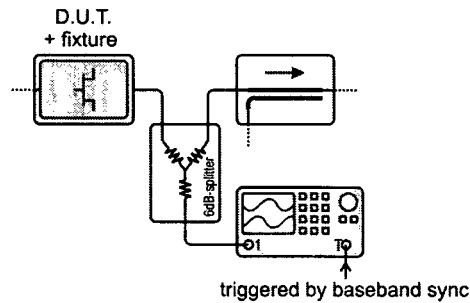


Figure 5.49: Calibration of time delays

For calibration it is also necessary to know the delay of the output fixture that can be gained by a broadband VNA measurement and to know the delay difference between the 6 dB-combiner branches that is typically zero. Then the modulation sources of all baseband generators were programmed to output a single pulse which was as short as possible (10 ns). By using an RF sampling oscilloscope it is possible to measure the time from the baseband trigger to the peak of the measured RF pulse. This has to be done for each source separately, the other sources are switched off in the meanwhile. Considering the effects of the fixture and the 6 dB-combiner, the time-shift of the signals at the fixture reference plane can be calculated.

It turned out that the dominant delay differences were introduced by the baseband generators. These arbitrary generator's trigger delay uncertainty is specified to be one sample interval⁴. Thus, the maximum clock rate of 100 MHz was used to reduce this error to 10 ns. This corresponds to a phase error of $\pm 9^\circ$ for a $BW = 5$ MHz WCDMA carrier at $f = 2.1445$ GHz (compare section 3.1.2). The phase deviation of the fundamental frequency is already close or outside the acceptance limit depending on the application. Calculating the error for the third harmonic frequency triples the error at least. Because the bandwidth at the harmonic zones is also higher, the phase error for the third order intermodulation product at $3f_0$ ($BW = 15$ MHz) finally has a nine-time higher error. This cannot be accepted for any measurement.

It is therefore necessary to shift the analytically generated baseband signals of the harmonics b_{2f_0} and b_{3f_0} in time. Because the required time accuracy is below the generator's clock period some mathematics have to be applied. The simplest way to solve this problem

⁴It turned out that this error remains constant as long as the instruments are switched on. Thus, a compensation is only valid until the baseband generators are power-cycled.

is the convolution of the time signal with a time shifted si-function $v(x)$:

$$\underline{b}''(t) = (\underline{b}' \otimes v)(t) = \int_{-\infty}^{\infty} \underline{b}'(\tau)v(t - \tau)d\tau \quad (5.29)$$

$$v(x) = \text{si}(x - t_o f_{\text{DAC}}) = \frac{\sin(t - t_o f_{\text{DAC}})}{t - t_o f_{\text{DAC}}} \quad (5.30)$$

where \underline{b}' is the unshifted and \underline{b}'' the time shifted baseband signal, f_{DAC} denotes the clock rate of the baseband arbitrary generators and t_o is the required time shift. So it is possible to perfectly compensate the delays at any desired reference plane which enables the use of broadband signals.

The remaining system calibration is quite similar to the one for single-tone harmonic active load-pull. The combination of the directional couplers and the switch have to be characterized by a VNA measurement (figure 5.50a). Additionally, a broadband measure-

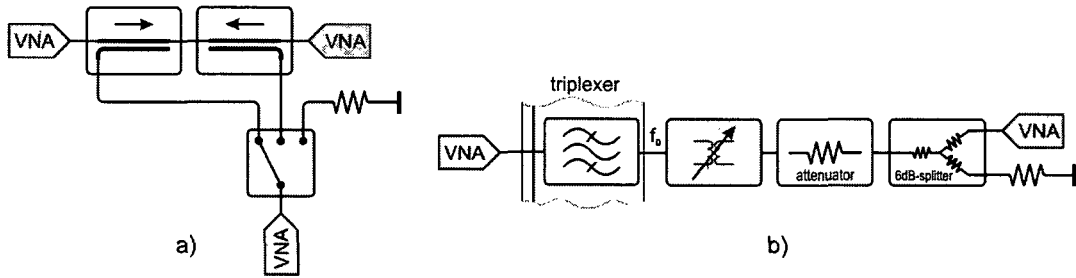


Figure 5.50: Active harmonic load pull for broadband signals, calibration

ment is required to determine the time delays. This information is needed to shift the demodulated and sampled I/Q-waveforms in time before they are passed to the calculation of the reflection coefficient (explained in section 5.8.3). The delay introduced by the down-conversion path (cables, VNA, mixer, filter, ...) is not of interest, because it is constant which does not influence the measurement.

Two ways are possible to get an absolute power reference for the fundamental frequency. This reference is not needed for the harmonic frequencies because this harmonic load-pull-system will not be used to calculate time-domain waveforms. One possibility for the power calibration is to characterize the entire down-conversion path, another idea is to use a power meter cascaded to the f_0 -tuner. The first method was not used because only small time segments of the signals are sampled by the oscilloscope. Due to the varying envelope the calculated power from this segment would be only a rough approximation for the average power. Using a power meter (figure 5.50b), on contrary, would give an exact readout due to the much longer integration time. The disadvantage is the requirement of a calibration which includes the tuner. The S-parameters of the arrangement shown need to be known for all tuner-positions. Because a constant termination was used for the fundamental frequency within this thesis, the separate characterization of the tuner, the triplexer, and the attenuator/divider could be omitted.

5.8.5 Achievable Tuning Range

Having the same combination of elements between DUT and fundamental tuner, the fundamental tuning range would be exactly the same as for the active single-tone setup (section 5.7). Because the center frequency had to be changed to $f_0 = 2.133$ GHz (due to a limitation of 3rd harmonic RF source) the insertion loss of the triplexer also changed. Because the triplexer's resonant frequency was closer to 2.133 GHz than to 2.1445 GHz, the insertion loss decreased. Similar to the preceding system, the active harmonic loads allow the realization of reflection coefficients over the entire Smith Chart (figure 5.51).

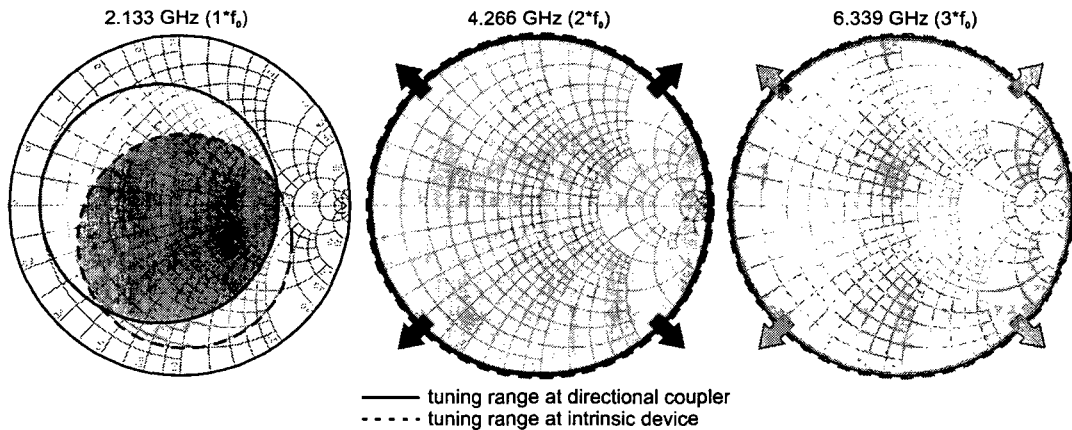


Figure 5.51: Active harmonic load pull (broadband), tuning range

The achievable values for the reflection coefficients are listed in table 5.8. Again, the

frequency	$ \Gamma $	(max. $ \Gamma $)
$f_0 = 2.133$ GHz	$0 \dots 0.58$	(0.82)
$2f_0 = 4.266$ GHz	$0 \dots \geq 1$	—
$3f_0 = 6.399$ GHz	$0 \dots \geq 1$	—

Table 5.8: Achievable Γ of active broadband load-pull system (at coupler input)

$|\Gamma|$ -column denotes a reflection coefficient which can be realized for any phase angle.

5.8.6 Control Algorithm

For setting the attenuators and phase-shifters of the harmonic generators the same control algorithm as for single-tone active harmonic load-pull was used (see section 5.7.7). Only the step-size parameters and the limits were adjusted. It turned out that the cycle time increased dramatically because of the more complicated measurement: the VNA had to switch between different harmonic frequencies, the forward and backward wave needed to be selected by an RF switch. Thus, six oscilloscope measurements were necessary to calculate the actual reflection coefficients for f_0 , $2f_0$, and $3f_0$. Also more samples compared to single-tone were required for broadband signals. This was necessary to reduce the error of the Γ -calculation algorithm which is produced by the fact that the generated

wave (backward travelling) is not a perfect copy of the forward travelling wave from the transistor. It turned out that the cycle time was too high to allow proper operation of the control algorithm.

To decrease the cycle time, measurements of the fundamental wave were omitted while setting the harmonic reflection coefficients to their desired values. Because the fundamental matching was realized passively this was not a problem. As a further acceleration for single-tone measurements, the number of sample points for the calculation of the reflection coefficient was dramatically reduced. This could be done without losing accuracy.

Thus it was possible to achieve a stable control for single-tone measurements. For broadband measurements it was not possible to find an appropriate setting which allowed a control of the third harmonic. The cycle times for the required measurement accuracy were too long and resulted in a too large phase drift of the third harmonic RF source within one control cycle (see section 5.8.8 for details).

5.8.7 Measurement Results (Single-Tone)

To verify the correct operation of the setup, a single-tone measurement was performed. Because the measurement setup provided exactly the same terminations for higher order harmonics (fourth order and higher), the results should match perfectly with the ones from section 5.7. The same bias point ($V_G = -0.85$ V, $V_D = 6$ V) and the default input power level of +15 dBm were used. Also the input matching was left unchanged. The center frequency needed to be reduced to $f_0 = 2.133$ GHz (see section 5.8.1). Since this is a change of $\approx 0.5\%$ in frequency the transistors behavior is almost the same. The higher insertion loss of the unchanged triplexer is entirely compensated by the active loads.

Figures 5.52 and 5.53 show the single-tone results for a two-dimensional sweep over both harmonic phases but for different magnitudes of the reflection coefficient. The ideal case $|\Gamma| = 1$ is depicted in Figure 5.52.

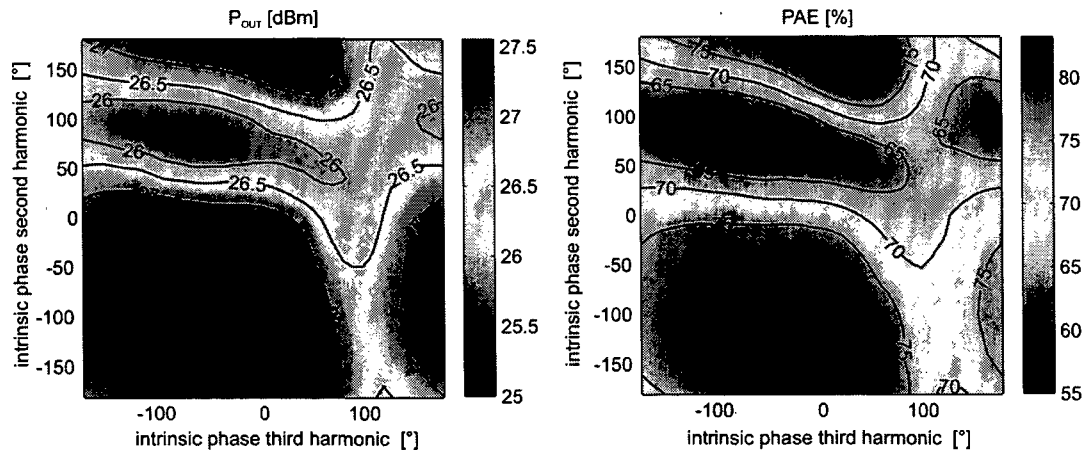


Figure 5.52: Singleton P_{OUT} and PAE dependence on harmonic phases, $|\Gamma_{2f_0,3f_0}| = 1$

As expected, the result gives a very good match to the one of the previous realization.

For comparison the measurement was repeated but with exactly those magnitudes which could be realized with the passive harmonic tuner (compare section 5.6). The data

from the characterization of the harmonic tuner was taken to intentionally set lower Γ -magnitudes. The result is shown in figure 5.53. It can be observed that both measurements

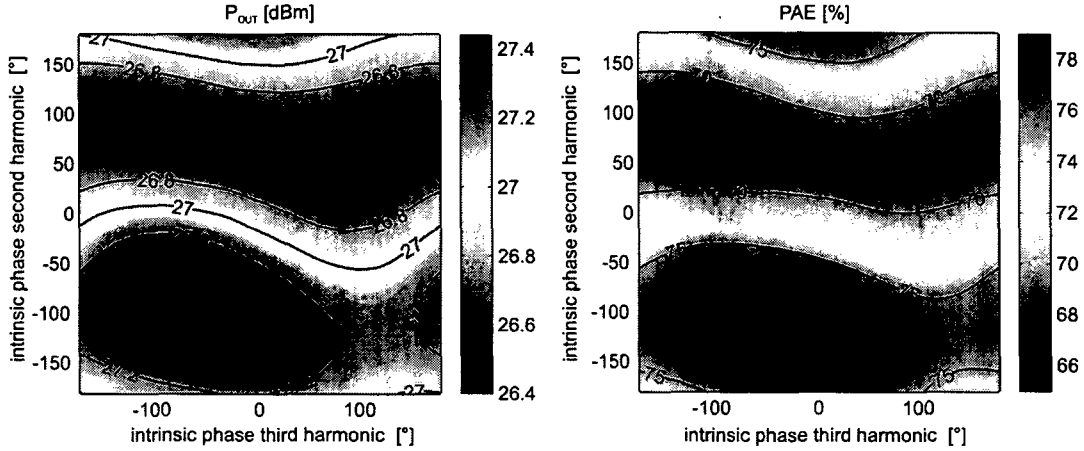


Figure 5.53: Singletone P_{OUT} and PAE dependence on harmonic phases, $|\Gamma_{2f_0,3f_0}| < 1$

look different now. Due to the decreased tuning range the variation of the results also becomes smaller (illustrated in table 5.9). This is exactly what to expect: due to the

reflection coefficient	P_{out} [dBm]	PAE [%]
ideal, $ \Gamma = 1$	25.5...27.5	55...83
equivalent to harmonic tuner, $ \Gamma < 1$	26.4...27.4	66...79

Table 5.9: Result variation for different Γ -magnitudes

reduced reflection of the harmonic terminations the class F case is achieved approximately, resulting in lower output power and efficiency. Phase conditions which gave very poor performance for $|\Gamma| = 1$ leads now to better result. Even those cases can now be realized approximately only.

The result should be seen in this way: starting from an average value for P_{out} and PAE (reached when both harmonics are nonreflective, $\Gamma_{2f_0,3f_0} = 0$) the result can be pulled away from the average as higher the reflection becomes. This can be seen quite well in table 5.9. The second measurement's result-range is a subset of the first measurement.

It is also important to note that both maxima are found at different positions separated up to 40° distance of the first measurement. Thus a termination based on non-ideally ($|\Gamma| < 1$) load-pull measurements would not reside in the correct maximum.

5.8.8 Measurement Results (Broadband)

The use of broadband signals turned out not to be restricted to the fundamental and the second harmonic frequency. The drifting phase difference between the third harmonic generator and the fundamental generator was an unsolvable problem with standard measurement equipment. Due to the transformation of the extrinsic elements a small variation at the test fixture's reference plane results in a much larger variation at the intrinsic

transistor. A phase variation of 90° of the third harmonic in the $50\ \Omega$ -system (fixture or coupler reference plane) results in a maximum phase variation of up to 230° at the intrinsic transistor. Hence, a drifting phase was very critical at the $3f_0$ harmonic frequency due to the strongest transformation of extrinsic elements. This could be kept under control for single-tone signals because much less samples were needed for the reflection coefficient calculation. The algorithm for broadband signals would have required a cycle time of about 10 s. Because forward and backward wave were measured sequentially, the estimator's accuracy was limited due to the phase variation in between. So it was not possible to find a combination which gave a stable result. It was only possible to have a very coarse tracking of the third harmonic.

The results of this measurements (figure 5.54), therefore, show a high dependency on the phase of the second harmonic but a very low on the third harmonic (much too low if compared to the passive harmonic tuner measurement). For the setting of the third

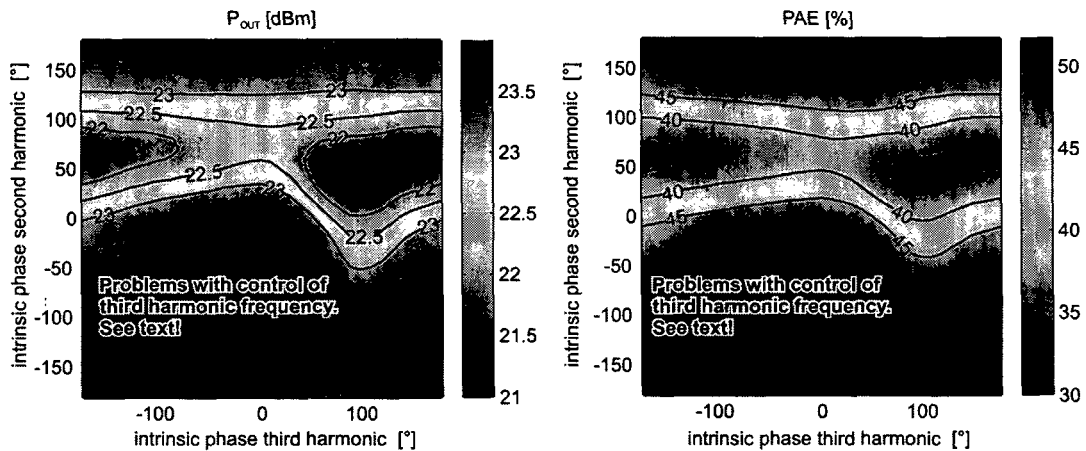


Figure 5.54: Broadband P_{OUT} and PAE dependence on harmonic phases ($3f_0$ erroneous)

harmonic phase a smaller set of values was chosen which was multiple set and results were averaged. Comparing the $2f_0$ -phase of the P_{out} and PAE maxima gives a very good match with the results of the harmonic tuner setup presented in section 5.6.

To be sure that the problems at the third harmonic frequency are not introduced by non-matching forward and backward waves the equivalent baseband signals were measured for different settings of the $2f_0$ - and $3f_0$ -phase. All measurements showed a similar behavior to the result presented in figure 5.55.

The real part of the complex baseband signal at the third harmonic frequency is shown. It can be seen that the forward wave (generated by the transistor) matches the reverse travelling wave (generated by a baseband modulated RF source) quite good. The error signal is 9.8 dB smaller than the signals themselves (measured at a phase setting which gave and $ACPR_1 = -33$ dBc). This indicates that the $3f_0$ -control problem is not caused by non-matching waves. The error signal in figure 5.55 further shows that it is not white noise. Its trace clearly indicates the presence of higher order nonlinearities which were not taken into account for the analytical generation of the equivalent harmonic baseband signals.

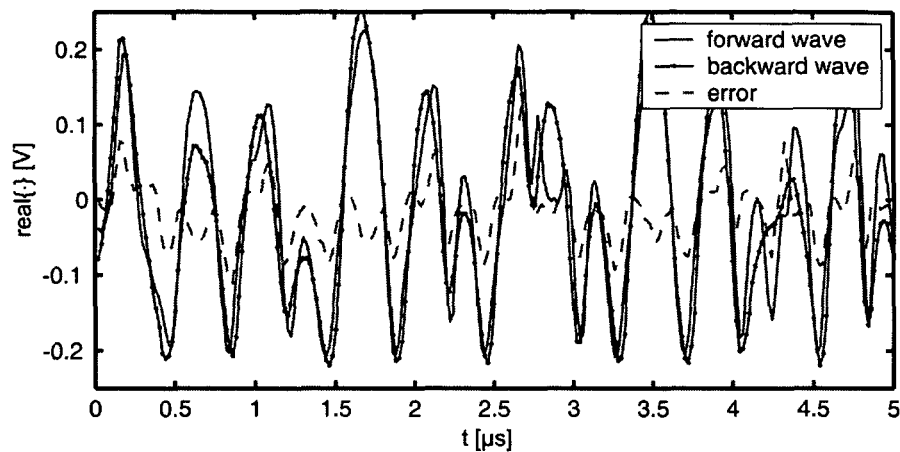


Figure 5.55: Comparison of forward and backward waves of active load

5.8.9 Summary

The proposed setup indicates that the idea of using open loop active terminations for broadband applications is possible in principle. The measurement setup gave the same $2f_0$ -phases for the maximum P_{out} and PAE. The use of the third harmonic was not possible because of the phase drift of the third harmonic generator during the 'long' measurement periods. Nevertheless it was shown that the required baseband signals can be calculated very simply. The difference to the physically generated signals was -9.8 dB.

To implement a stable control it is required to derive all frequencies by frequency doublers and triplers. So, all phase instabilities are eliminated and allow even long cycle times for the control algorithm.

Chapter 6

Summary

Within this thesis four harmonic load-pull setups were realized in order to compare them in terms of tuning range of the reflection coefficient, power handling, usable bandwidth, . . . A microwave power pHEMT served as a device under test. Its extrinsic parameters were taken into account for all measurements. This allowed the calculation of the reflection coefficients which are seen by the intrinsic transistor. A class F amplifier was realized with the GaAs pHEMT and measured with all four harmonic load-pull setups.

The *passive harmonic load-pull setup with a triplexer* was realized of commercially available components. It turned out that the triplexer limits the tuning range due to its insertion loss and such is the key-component of the system. It was also shown that the insertion loss of the entire harmonic load-pull setup exceeds by far the sum of the used component's single insertion losses due to resonance effects.

The measurement of the chosen device under test showed that the tuning range was reduced that much by the triplexer, that a variation of the third harmonic tuner neither influenced output power nor efficiency. Such a system absolutely requires a prematching at the testfixture for successful operation.

To overcome this limitation, a *harmonic load-pull system with a harmonic tuner* was realized. It was shown that it is possible to set up such a tuner very easily. The fabrication was done with off the shelf components and metal-cutting manufacturing without the need for tight tolerances. The realized system showed a high repeatability as well as a much wider tuning range and a simpler setup than the triplexer-system. The measurements further revealed that the optimum terminations for single-tone and broadband excitation are not the same.

Both passive harmonic load-pull systems were not capable of producing reflection coefficients as high as necessary for matching a highly reflecting power amplifier circuit. Hence, the information gained from the passive load-pull measurements does not allow the correct prediction of the full capabilities of the device. The solution for increasing the tuning range is given by means of active harmonic load-pull.

Therefore, an *active harmonic load-pull system for single-tone signals* was set up. To get rid of stability problems a loop-free design was selected. In order to avoid components which are limited to a certain frequency range it was chosen to use standard RF measurement equipment only. The harmonic frequencies, therefore, were not generated by frequency doublers or triplers; synchronized RF sources were used. This, of course, introduced a phase drift which had to be compensated by the control system. A simple

algorithm was used to track the phase drift as well as to set the desired reflection coefficients. The built in capabilities of the RF generators were used to vary their output signal in phase and amplitude.

Furthermore it was possible to reconstruct the intrinsic voltages and currents by using a time domain measurement of the forward and backward travelling waves. Thus, the dynamic load line could be calculated which allows to detect critical voltage overshoots for example. The time domain waveforms can further be used for model verification as it was shown in this thesis.

The last setup was an attempt to set up an *active harmonic load-pull system for broadband signals*. This system used modulated RF sources at the harmonic frequencies in order to produce the required reflection signals. Because loops were avoided, the system is unconditionally stable. This thesis gives equations to relate the equivalent baseband signals of different frequencies to each other as needed for such a setup. The setup was set into operation but it turned out that the phase drift was too high in order to achieve a stable control of the third harmonic frequency. Nevertheless, it is clearly shown that it is possible to realize a system which allows active load-pulling with broadband signals which does not suffer from instable loads. Using specialized hardware would allow to control the third harmonic as well.

Finally, the most important findings of this thesis for harmonic load-pull setups are summarized in the following list:

- Small losses of the components result in a multiple loss of the entire setup. Hence, high quality elements and a compact setup with short cables are required. An alternative would be the use of impedance transformers inside the testfixture.
- A small deviation from $|\Gamma| = 1$ of the tuner system leads to a severe reduction of the intrinsic tuning range because of the transformation applied by the extrinsic elements.
- The largest tuning range is needed for the highest harmonic frequency: This is because of the stronger transformation by the extrinsic elements at higher frequencies and the 10 times larger/smaller impedances which are required to realize an open or a short circuit.
- Passive harmonic load-pull either makes use of a triplexer or resonant tuners. Changing the center frequency requires a change of these components. More flexibility can be achieved with active systems where it is possible to use broadband combiners/couplers.
- Harmonic tuners seem to be the better choice when compared to a triplexer system. They achieve a higher tuning range for the harmonic frequencies. A change in the center frequency can be accomplished much faster also. Whereas a triplexer system requires a new design of the triplexer, the length of a harmonic tuner's resonator stub can be changed within minutes.
- A harmonic tuner can be realized without special materials or tools as it was shown in this thesis. Also the automation of the tuning by off the shelf components shows sufficient accuracy.

- An increased tuning range expands the range of achievable output power and efficiency to higher as well as to lower values. The measurements revealed, that the power and efficiency maxima found by a passive system with $|\Gamma| < 1$ are separated by up to 40° from those determined by an active system with $|\Gamma| = 1$.
- The optimum termination in terms of output power and efficiency for single-tone signals does not need to be the same as for broadband signals
- The use of synchronized generators instead of frequency doublers and triplers is not favorable due to the phase drift. Nevertheless, this allows to set up a harmonic load-pull system by standard measurement equipment. The system shown in this thesis showed proper operation and additionally allowed the display of the intrinsic dynamic load-line.
- Using modulated generators at the harmonic frequencies extends the use of active harmonic load-pull systems to higher bandwidths. The problematic delays can be perfectly compensated.
- The importance of the input matching for class F amplifiers was also shown within this thesis. Depending on the input termination the transistor showed optimum performance for class F or for inverted class F operation.
- Results gained by different tuner systems are hard to compare. Their different tuning ranges as well as their undefined termination of higher order harmonics leads to incompatible results.

Appendix A

Equipment Used

input signal source f_0 (CW / IQ-mod.)	Rohde & Schwarz SMIQ03B
active load source $2f_0$ (CW / IQ-mod.)	Rohde & Schwarz SMIQ06B
active load source $3f_0$ (CW)	Agilent E8244A
active load source $3f_0$ (IQ-mod)	Rohde & Schwarz SMIQ06B
baseband IQ-source for f_0	Rohde & Schwarz AMIQ02
baseband IQ-source for $2f_0$	Rohde & Schwarz AMIQ03
baseband IQ-source for $3f_0$	Rohde & Schwarz AMIQ04
input pre-amplifier f_0	Mini Circuits ZHL-42W
active load power amplifier $2f_0$	Mini Circuits ZVE-8G
active load power amplifier $3f_0$	Mini Circuits ZVE-8G
tuner system control software	Maury Microwave MT993A
automatic tuner f_0	Maury Microwave MT982A02
automatic tuner $2f_0$	Maury Microwave MT982A02
automatic tuner $3f_0$	Maury Microwave MT982A02
tuner controller	Maury Microwave MT986C
input fixed tuner	Microloab/FXR SF-31F
triplexer	realized within this thesis
harmonic tuner	realized within this thesis
input power meters	Agilent E4417A with E9327A sensors
output power meter	Agilent 437B with 8482A sensor
DC power source gate	Keithley 2400 sourcemeter
DC power source drain	Keithley 2400 sourcemeter
current meter drain	Agilent 34401A
bias-tee gate	Agilent 11612B
bias-tee drain	Agilent 11612B
spectrum analyzer	Agilent E4446A
vector network analyzer	Agilent 8364A
IQ demodulator	Pulsar IDO-07-412
baseband lowpass filters	KR Electronics 2515

sampling (RF) oscilloscope	Tektronix 11801A with SD-26 sample head
baseband oscilloscope	Lecroy LC-684DXL
test fixture	Connexion Rosenberger
calibration substrate	realized within this thesis
transistor	IAF Freiburg, Germany, research device
3D field simulator	Ansoft HFSS
RF simulator	AWR Microwave Office
general programming platform	The Mathworks MATLAB

Bibliography

- [1] Frederick H. Raab, "Maximum efficiency and output of class-F power amplifiers", *IEEE Transactions on Microwave Theory and Techniques*, vol. 49, no. 6, pp. 1162–1166, June 2001.
- [2] Steve C. Cripps, *RF Power Amplifiers for Wireless Communications*, Artech House, Inc., Norwood, MA, 1999.
- [3] Peter B. Kenington, *High-Linearity RF Amplifier Design*, Artech House, Inc., Norwood, MA, 2000.
- [4] Frederick H. Raab, "Class-F power amplifiers with maximally flat waveforms", *IEEE Transactions on Microwave Theory and Techniques*, vol. 45, no. 11, pp. 2007–2012, November 1997.
- [5] A. V. Grebennikov, "Circuit design technique for high efficiency class f amplifiers", in *Digest IEEE MTT-S International Microwave Symposium*, 2000, pp. 771–774.
- [6] A. Mallet, D. Floriot, J.P. Viaud, F. Blache, J.M. Nebus, and S. Delage, "A 90 % power-added-efficiency GaInP/GaAs HBT for L-band radar and mobile communication systems", *IEEE Microwave and Guided Wave Letters*, vol. 6, no. 3, pp. 132–134, March 1996.
- [7] D. Barataud, F. Blache, A. Mallet, P.P. Bouysse, J.-M. Nebus, J.P. Villotte, J. Obregon, J. Verspecht, and P. Auxemery, "Measurement and control of current/voltage waveforms of microwave transistors using a harmonic load-pull system for the optimum design of high efficiency power amplifiers", *IEEE Transactions on Instrumentation and Measurement*, vol. 48, no. 4, pp. 835–842, August 1999.
- [8] C. Duvaud, S. Dietsche, G. Pataut, and J. Obregon, "High-efficient class F GaAs FET amplifiers operating with very low bias voltages for use in mobile telephones at 1.75 GHz", *IEEE Microwave and Guided Wave Letters*, vol. 3, no. 8, pp. 268–270, August 1993.
- [9] P. Saunier, W. S. Kopp, H. Q. Tserng, Y. C. Kao, and D. D. Heston, "A heterostructure FET with 75.8GHz", in *Digest of Papers IEEE MTT-S International Microwave Symposium*, June 1992, pp. 51–54.
- [10] P. Colantonio, F. Giannini, E. Limiti, and V. Teppati, "An approach to harmonic load- and source-pull measurements for high-efficiency PA design", *IEEE Transactions on Microwave Theory and Techniques*, vol. 52, no. 1, pp. 191–198, January 2004.

- [11] S. Goto, T. Kunii, A. Ohta, A. Inoue, Y. Hosokawa, R. Hattori, and Y. Mitsui, "Effect of bias condition and input harmonic termination on high efficiency inverse class-f amplifiers", in *Proceedings of the European Conference on Wireless Technology*, 2001, pp. 31–34.
- [12] P.M. White, "Effect of input harmonic terminations on high efficiency class-B and class-F operation of PHEMT devices", in *MTT-S International Microwave Symposium Digest*, 1998, pp. 1611–1614.
- [13] Markus L. Mayer, *Solid State Power Amplifier for DAB in L-Band*, PhD thesis, Vienna University of Technology, December 2003.
- [14] J. Staudinger, "Large signal GaAs MESFET model validation for wireless power amplification", in *Proceedings Wireless-Communications-Conference 1996*, 1996, pp. 57–60.
- [15] S. A. Maas and T. Miracco, "Using load pull analysis and device model validation to improve MMIC power amplifier design methodologies", *Microwave Journal, Euro-Global Edition*, vol. 45, no. 11, pp. 20–33, November 2002.
- [16] C. J. Wei, Y. A. Tkachenko, and D. Bartle, "Alpha owned PHEMT model and its verification by load-pull and waveform measurements", in *IEEE Asia-Pacific Microwave Conference Proceedings*, 2000, pp. 871–874.
- [17] "Maury microwave corporation", <http://www.maurymw.com>, 2900 Inland Empire Blvd., Ontario, California 91764, USA.
- [18] "Focus microwave", <http://www.focus-microwaves.com>, 1603 St. Regis, Dollard-des-Ormeaux, Quebec H9B 3H7, Canada.
- [19] "Athena microwaves", <http://www.athenamw.com>, 6980 Lacroix, Montreal H4E 2V3, Canada.
- [20] "Mircolab/FXR", <http://www.microlab.fxr.com>, Ten Microlab Road, Livingston, NJ 07039-1602, USA.
- [21] Focus Microwaves, "Electronic tuners (ETS) and electro-mechanical tuners (EMT), a critical comparison", product information material.
- [22] Roger B. Stancliff and Dennis D. Poulin, "Harmonic load-pull", in *Proceedings IEEE Microwave Theory and Techniques Symposium MTT-S*, May 1979, pp. 185–187.
- [23] Christos Tsironis, Algis Juenas, and Chris Wei Liu, "Highly accurate harmonic tuners for load pull testing", in *Proceedings of the IEEE Asia-Pacific Microwave Conference*, Taipei, Taiwan, 2001, pp. 1311–1314.
- [24] Andrea Ferrero, GianLuigi Madonna, and Umberto Pisani, "Recent technological advances for modular active harmonic load-pull measurement systems", 1999.
- [25] Johannes Benedikt, Roberto Gaddi, Paul J. Tasker, and Martin Goss, "High-power time-domain measurement system with active harmonic load-pull for high-efficiency base-station amplifier design", *IEEE Transactions on Microwave Theory and Techniques*, vol. 48, no. 12, pp. 2617–2624, December 2000.

- [26] Holger Arthaber, Markus L. Mayer, Amnon Gafni, Michael Gadringer, and Gottfried Magerl, "A time domain large signal measurement setup", *International Journal of RF and Microwave Computer-Aided Engineering*, vol. 14, no. 2, March 2004, in press.
- [27] David J. Williams and Paul J. Tasker, "An automated active source and load pull measurement system", *6th IEEE High Frequency Postgraduate Colloquium*, pp. 7–12, 2001.
- [28] J. M. Nebus, P. Bouysse, J. M. Coupat, and J. P. Villotte, "An active load-pull set-up for the large signal characterization of highly mismatched microwave power transistors", *Conference Record IMTC/93*, pp. 2–5, May 1993.
- [29] K. M. Keen, "Characteristic impedance of dielectric-filled slotted coaxial transmission line", *Proceedings of the IEEE*, vol. 123, no. 10, pp. 981–983, October 1976.
- [30] Harold A. Wheeler, "Transmission-line properties of a strip line between parallel planes", *IEEE Transactions on Microwave Theory and Techniques*, vol. 25, no. 8, pp. 631–647, August 1978.
- [31] Thomas G. Bryant and Jerald A. Weiss, "Parameters of microstrip transmission lines and of coupled pairs of microstrip lines", *IEEE Transactions on Microwave Theory and Techniques*, vol. 16, no. 12, pp. 1021–1027, December 1968.
- [32] R. Jansen and M. Kirschnig, "Arguments and an accurate model for the power-current formulation of microstrip characteristic impedance", *AEU*, vol. 37, no. 3/4, pp. 108–112, 1983.
- [33] Harold A. Wheeler, "Transmission-line properties of a strip on a dielectric sheet on a plane", *IEEE Transactions on Microwave Theory and Techniques*, vol. 25, no. 8, pp. 631–647, August 1977.
- [34] S. Frankel, "Characteristic impedance of parallel wires in rectangular troughs", *Proceedings IRE*, vol. 30, pp. 182–190, April 1942.
- [35] Robin M. Chrisholm, "The characteristic impedance of trough and slab lines", *IRE Transactions on Microwave Theory and Techniques*, vol. 4, no. 3, pp. 166–172, July 1956.
- [36] Ansoft Corporation, "HFSS", <http://www.ansoft.com>, Four Station Square, Suite 200 / Pittsburgh, PA 15219-1119, USA.
- [37] Rosenberger Hochfrequenztechnik, "RPC-7 steckerkopf 07p121-000 mechanische zeichnung", <http://www.rosenberger.de>, Postfach 1260, D-84526 Tittmoning, Germany.
- [38] Rogers Corporation, "RT/duroid 5880 High frequency laminate", <http://www.rogerscorporation.com>, Advanced Circuit Materials, 100 S. Roosevelt Avenue, Chandler, AZ 85226, USA.
- [39] Glenn F. Engen and Cletus A. Hoer, "Thru-reflect-line: An improved technique for calibrating the dual six-port automatic network analyzer", *IEEE Transactions Microwave Theory and Techniques*, vol. 27, no. 12, pp. 987–993, December 1979.

- [40] Agilent Technologies, "Agilent network analysis, applying the 8510 TRL calibration for non-coaxial measurements", *Agilent Product Notes*, May 2001.
- [41] R. Tayrani, J.E. Gerber, T. Daniel, R.S. Pengelly, and U.L. Rhode, "A new and reliable direct parasitic extraction method for MESFETs and HEMTs", in *23rd European Microwave Conference Proceedings*, September 1993, pp. 451–453.
- [42] R. Gaddi, P.J. Tasker, and J.A. Pla, "Direct extraction of LDMOS small signal parameters from offstate measurements", *Electronics Letters*, vol. 36, no. 23, pp. 1964–1966, November 2000.
- [43] Vicentiu I. Cojocaru and Thomas J. Brazil, "A scalable general-purpose model for microwave FETs including DC/AC dispersion effects", *IEEE Transactions on Microwave Theory and Techniques*, vol. 45, no. 12, pp. 2248–2255, December 1997.
- [44] Markus Mayer and Dieter Smely, "Development of a Linear and Efficient 5 W SSPA: Phase 2 Final Design and Test Report, Contract No.: 10779/94/NL/JV-CCN No. 2", Tech. Rep., ESA/ESTEC, 2000.
- [45] Volker Neubauer, Markus Mayer, and Gottfried Magerl, "A Novel Low Loss Microwave Multiplexer Design Based on Directional Filters", in *IEEE Radio and Wireless Conference RAWCON 2002*, Boston, USA, August 2002, pp. 257–260.
- [46] Volker Neubauer, *Low Loss Microwave Triplexer*, diploma thesis, Vienna University of Technology, March 2002.
- [47] 3GPP, "TS 25.101: Technical specification group radio access network: User equipment (UE) radio transmission and reception(FDD), V6.3.0", 2003.
- [48] Applied Wave Research, "Microwave office", <http://www.mwoffice.com>, 1960 E. Grand Avenue, Suite 430 El Segundo, CA 90245, USA.

Curriculum Vitae

Name: Dipl.-Ing. Holger Arthaber

Date of Birth: September 15, 1975

Place of Birth: Vienna, Austria

Parents: Hermann Leopold Arthaber
Heidemaria Arthaber

Degrees: Dipl.-Ing. in Electrical Engineering (summa cum laude), March 2000
Vienna University of Technology
Diploma thesis: "Algorithmen zur Kombination von Diversitätssignalen
in GSM", (Algorithms for Combining GSM Diversity Signals)

Positions: March 1999 – February 2000
Research Scientist, Institute of Communications and Radio-
Frequency Engineering, Vienna University of Technology

since April 2000
Assistant Professor, Institute of Electrical Measurements and
Circuit Design, Vienna University of Technology

Interests: Highly efficient and linear amplifiers
Harmonic load pull, dynamic loadline analysis
Digital predistortion linearization

Affiliations: since 1998
Institute of Electrical and Electronics Engineers (IEEE)